NUSC Report No. 4097

Estimating Ocean Wind Wave Spectra By Means of Underwater Sound

ROBERT G. WILLIAMS
Ocean Science Department
Science and Technology Directorate

15 June 1971

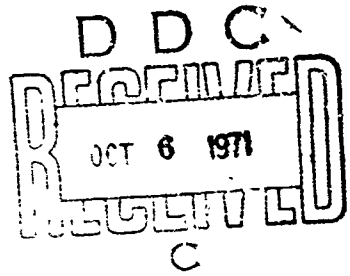

NAVAL UNDERWATER SYSTEMS CENTER

UNCLASSIFIED

Security Classification

DOCUMENT CONTROL DATA - R & D

Security classification of title, body of abstract and indexing annotation must be entered when the overall report is classified)

1 ORIGINATING ACTIVITY (Corporate author)
Naval Underwater Systems Center
Newport, Rhode Island 02840

2a. REPORT SECURITY CLASSIFICATION
UNCLASSIFIED

2b GROUP

3 REPORT TITLE

ESTIMATING OCEAN WIND WAVE SPECTRA BY MEANS OF UNDERWATER SOUND

4 DESCRIPTIVE NOTES (Type of report and inclusive dates)
Research Report

5 AUTHOR(S) (First name, middle initial, last name)

Robert G. Williams

6 REPORT DATE	7a TOTAL NO OF PAGES	7b NO OF REFS
15 June 1971	206	73

8a CONTRACT OR GRANT NO	9a. ORIGINATOR'S REPORT NUMBER(S)
b. PROJECT NO A 400-05-00 A 072-00-00 SF 11 522 101-12858 ZR 011-01-01-61101N	4097
c	9b OTHER REPORT NO(S) (Any other numbers that may be assigned this report)
d.	

10 DISTRIBUTION STATEMENT

Approved for public release; distribution unlimited.

11 SUPPLEMENTARY NOTES	12 SPONSORING MILITARY ACTIVITY
	Department of the Navy

13 ABSTRACT

Measurements of the spectrum of ocean surface reradiated acoustic signals generated by an omnidirectional, sinusoidal source are used to estimate the ocean surface wave-height spectrum. Plane-wave physical optics theory is applied to a long-crested sea surface model to verify Marsh's hypothesis that, for low sea states, the spectrum of acoustic waves reradiated by the rough moving sea surface consists of a specular component at the transmitted frequency and a scattered component which is the weighted surface wave-height spectrum. The approach employs theories by Parkins, Clay and Medwin, and Pierson. The weighting function applied to the surface spectrum depends on signal frequency, experimental geometry, and mean-square wave height. CW signals at 127 Hz and 1702 Hz were transmitted from fixed, omnidirectional sources to receivers 4.5 km and 41 km downrange. Additionally, wave height was monitored continuously by resistance wave staff. The time series records of sound pressure level and ocean wave height were analyzed for spectral content. Agreement between theory and experiment is good when the acoustic sideband levels are not more than 25 dB below the peak level of the specular component.

DD FORM 1 NOV 65 1473 (PAGE 1)

S/N 0102-014-6600

UNCLASSIFIED

Security Classification

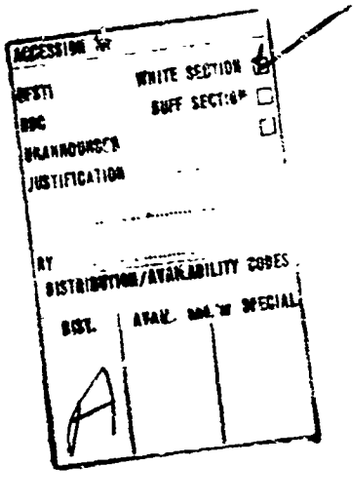

REVIEWED AND APPROVED: 15 June 1971

W. A. Von Winkle

W. A. Von Winkle
Director of Science and Technology
Naval Underwater Systems Center

NOTE

This manuscript was originally prepared by the author as a dissertation for the Department of Meteorology and Oceanography. In April 1971, the dissertation was submitted to the faculty of the Graduate School of Arts and Science in partial fulfillment of the requirements for the degree of Doctor of Philosophy at New York University.

Inquiries concerning this report may be addressed to the author via Officer in Charge, New London Laboratory, Naval Underwater Systems Center, New London, Connecticut 06320

14 KEY WORDS	LINK A		LINK B		LINK C	
	ROLE	WT	ROLE	WT	ROLE	WT
Underwater Sound						
Ocean Wind Wave Spectra						
Acoustic Spectra						

ABSTRACT

An experimental and theoretical study demonstrated that measurements of forward-scattered underwater acoustic waves can be used to estimate the ocean surface wave-height frequency spectrum, under surface duct propagation conditions.

The experimental phase of the investigation consisted of transmitting 127-Hz and 1702-Hz continuous wave acoustic signals from fixed, omnidirectional sources in the BIFI acoustic range in Block Island Sound to receivers 4.5 km and 41 km downrange. During the acoustic transmissions, ocean wave height was monitored continuously by means of a resistance wave staff. The time series records of sound pressure level and ocean wave height were analyzed by digital computer to determine spectral content. Careful consideration was given to optimizing signal processing to achieve maximum resolution and stability. The results showed that the surface reradiated signal spectrum is spread in frequency and consists of (1) a broadened specular component around the transmitted frequency and (2) sidebands. The sidebands resemble the surface height spectrum over typical bandwidths of 0.2 Hz and 1.0 Hz for the 127-Hz and 1702-Hz signals, respectively.

In the theoretical phase of the investigation, generalized physical optics theory was used to predict the spectrum of a sinusoidal signal transmitted by an omnidirectional source and reradiated by the rough, moving sea surface. This generalization, which is based on theories by Parkins and Clay and Medwin, was accomplished by subdividing a large illuminated area on the sea surface and

applying the plane wave Helmholtz integral theory to each subsection. The individual autocovariances were evaluated, summed, and Fourier transformed to obtain the farfield acoustic spectrum. The employment of the linear, long-crested model of random gravity waves, due to Pierson, facilitated the integration of the scattering equations for low sea state conditions. The long-crested waves are assumed to propagate in a direction parallel to the source-receiver line.

The farfield acoustic spectrum is shown to consist of a specular component that is free from Doppler at the transmitted frequency and a scattered component that appears as sidebands. The sidebands are symmetrical about the carrier. The distribution of the variance in the sidebands is given by the weighted surface height spectrum. The weighting function depends on the signal frequency, the experimental geometry, and the mean-square wave height. The weighting function behaves like a low-pass filter that is relatively flat out to some frequency, f_1, and then slopes down to a "cutoff" frequency, f_2. Information about the sea surface wave-height spectrum can be obtained only between these two frequencies. The effective bandwidth of the model at 127 Hz and 1702 Hz is 0.15 Hz and 0.5 Hz, respectively.

Agreement between theory and experiment was good when the acoustic sidebands were not more than 25 dB below the peak level of the coherent component. The bandwidth of the theoretical weighting function was seen to be less than the bandwidth of the weighting function computed from field data. This discrepancy can be explained by noting that the long-crested sea surface model is deficient at the high frequencies when the sea surface is really short-crested. It appears that, when the short-crested character of the sea surface is included in the scattering model using methods due to Pierson, the results will approach Marsh's prediction

that the first-order acoustic sidebands are equal to the uniformly weighted surface height spectrum for unrestricted geometry.

ACKNOWLEDGMENT

I am grateful to the faculty and staff of the Department of Meteorology and Oceanography at New York University for their continuing inspiration and guidance. In particular, I would like to thank my advisor, Dr. Gerhard Neumann, and the members of my dissertation committee, Drs. Willard J. Pierson, Jr., and Eric S. Posmentier. I would also like to thank the fourth member of my dissertation committee, Dr. David F. Paskausky, of the University of Connecticut.

This research would not have been possible without the support of my colleagues at the Naval Underwater Systems Center. Many helpful discussions were held with Drs. H. Wysor Marsh, Albert H. Nuttall, and Robert H. Mellen. The instrumentation was designed by Messrs. Kirk Patton, George F. Battista, John M. Gorman, and Louis F. DiRienzo. The high quality of signal processing required by this study was achieved by Messrs. Thomas R. Finnegan, Peter B. Stahl, and John C. Sikorski. The computer programs for the analysis of the data were written by Messrs. Charles R. Arnold, James F. Ferrie, and G. Clifford Carter. The theoretical equations were programmed by Mr. Robert C. Jennings, who also provided many helpful comments.

The field work was made possible by Dr. Andrew J. Nalwalk, of the University of Connecticut, and Mr. Oram A. Campbell, Master of the R/V UCONN, and his excellent crew.

I am thankful for the support I received from the Naval Underwater Systems Center under the Advanced Professional Development Program. Support for the research was furnished by NUSC Project A-400-05-00, Navy Subproject and Task SF 11 522 101-12858, under Mr. B. King Couper (NAVSHIPS 00V1), and by NUSC Project No. A-072-00-00, Subproject and Task No. ZR 011-01-01-61101N, under Dr. J. H. Huth (DLP/MAT 03L4).

Finally, special thanks are given to my wife Barbara, for her understanding, encouragement, and patience throughout this long endeavor.

TABLE OF CONTENTS

	Page
ABSTRACT	i
ACKNOWLEDGMENT	iv
LIST OF ILLUSTRATIONS	ix
LIST OF TABLES	xiv
LIST OF SYMBOLS AND NOTATIONS	xv
1.0 INTRODUCTION	1
2.0 CHARACTERISTICS OF UNDERWATER ACOUSTIC TRANSMISSIONS IN THE SEA	8
2.1 THE VELOCITY OF SOUND IN THE OCEAN AND ITS EFFECTS ON ACOUSTIC TRANSMISSION	8
2.2 ACOUSTIC PROPAGATION MODELS	11
2.3 REFLECTIONS OF ACOUSTIC WAVES FROM THE SEA SURFACE	12
3.0 THEORY	20
3.1 SYNOPSIS OF THE PHYSICAL OPTICS METHOD	22
3.2 DERIVATION OF THE ACOUSTIC SURFACE RERADIATED SPECTRUM	23
3.3 THE OCEAN WAVE-HEIGHT SPECTRUM IN TERMS OF THE ACOUSTIC SCATTERED SPECTRUM	51
4.0 FIELD EXPERIMENTS AND RESULTS	53
4.1 AREA OF STUDY	54

TABLE OF CONTENTS (Cont'd)

	Page
4.2 EXPERIMENTAL SETUP AND INSTRUMENTATION . . .	57
4.3 PRELIMINARY EXPERIMENTS	61
4.4 ACOUSTIC AND OCEAN WIND WAVE MEASUREMENTS IN BLOCK ISLAND SOUND	62
4.5 OPERATIONAL RESULTS	65
4.6 DATA PROCESSING AND ANALYSIS.	66
4.7 RESULTS OF THE BLOCK ISLAND SOUND EXPERIMENTS	71
4.8 CORRELATION ANALYSIS OF THE SPECTRA	89
5.0 COMPARISON OF THEORY AND EXPERIMENT	91
5.1 THE SUITABILITY OF THE PHYSICAL OPTICS, LONG-CRESTED MODEL TO THE BIFI SCATTERING GEOMETRY	91
5.2 THE NUMERICAL EVALUATION OF THE ACOUSTIC AND SEA SURFACE SPECTRA	98
5.3 DISCUSSION	110
5.4 PHYSICAL OPTICS THEORY AS AN AID TO OCEAN WAVE STUDIES	117
5.5 SPECIAL PRECAUTIONS	118
6.0 CONCLUSIONS	120
7.0 SUGGESTIONS FOR FURTHER STUDY	124
7.1 THE IDEAL OCEAN WAVE/ACOUSTIC SCATTERING EXPERIMENT	124
7.2 ADDITIONAL THEORETICAL STUDY	126

TABLE OF CONTENTS (Cont'd)

	Page
APPENDIX A — THE ILLUMINATION FUNCTION	127
APPENDIX B — OCEANOGRAPHIC OBSERVATIONS DURING THE BLOCK ISLAND SOUND TESTS . .	133
APPENDIX C — INSTRUMENTATION	142
APPENDIX D — DATA PROCESSING AND ANALYSIS	153
APPENDIX E — COMPUTER PROGRAM FOR CALCULATING THE SPECTRA FROM THE PHYSICAL OPTICS MODEL .	162
REFERENCES	180

LIST OF ILLUSTRATIONS

Figure		Page
1	"Single-reflection" surface wave experiment	5
2	Received spectrum of a surface-reradiated, single-frequency acoustic signal	6
3	Derivation of the Rayleigh Criterion	14
4	Experimental geometry for the highly directional source .	26
5	Scattering geometry for the omnidirectional source . . .	30
6	Bottom topography and location of projectors and receivers in Block Island Sound	55
7	Sound speed profiles along the source-receiver line in Block Island Sound (January 1968)	56
8	Surface isotherms contoured from aerial radiometer data taken by the Sandy Hook Marine Laboratory	58
9	Block diagram of the signal transmitting equipment on Block Island	59
10	Block diagram of the signal receiving equipment on Fishers Island	60
11	Spar buoy supporting resistance wave staff and hydrophone .	63
12	Spar buoy on position for measurements off Block Island .	64
13A	Spectrum level of 1702-Hz signal transmitted from Block Island to R/V UCONN via RF link	69
13B	Spectrum level of 127-Hz signal transmitted from Block Island to R/V UCONN via RF link	69
14A	Spectrum level of ocean wave height at Position C for Run I	72

LIST OF ILLUSTRATIONS (Cont'd)

Figure		Page
14B	Spectrum level of acoustic signal at Position C for Run I .	72
15A	Spectrum level of ocean wave height at Position C for Run II	74
15B	Spectrum level of acoustic signal at Position C for Run II .	74
16	Spectrum level of acoustic signal at Fishers Island for Run II	75
17A	Spectrum level of ocean wave height at Position C for Run III	77
17B	Spectrum level of acoustic signal at Position C for Run III .	77
18	Spectrum level of acoustic signal at Fishers Island for Run III	78
19A	Spectrum level of ocean wave height at Position C for Run IV	79
19B	Spectrum level of acoustic signal at Position C for Run IV	79
20	Spectrum level of acoustic signal at Fishers Island for Run IV	80
21	Sample record of ocean wave height and acoustic signal at Position C for Run IV	81
22A	Spectrum level of ocean wave height at Postion C for Run V	82
22B	Spectrum level of acoustic signal at Position C for Run V .	82
23A	Spectral density of ocean wave height at Position C for Run V	83
23B	Acoustic intensity per unit band at Position C for Run V	83
24	Spectrum level of acoustic signal at Fishers Island for Run V	84

LIST OF ILLUSTRATIONS (Cont'd)

Figure		Page
25	Sample record of ocean wave height and acoustic signal at Position C for Run V	85
26A	Spectrum level of ocean wave height at Position C for Run VI	86
26B	Spectrum level of acoustic signal at Position C for Run VI	86
27	Spectrum level of acoustic signal at Fishers Island for Run VI	87
28A	Spectrum level of ocean wave height at Position A for Run VII	88
28B	Spectrum level of acoustic signal at Position A for Run VII	88
29	Spectrum level of acoustic signal at Fishers Island for Run VII	89
30	Frequency versus wavelength for ocean gravity (Airy) waves determined from the relation $4\pi^2 f2 = g K \tanh (Kh)$	94
31	Water wave phase speed squared versus wavelength for ocean gravity (Airy) waves determined from the relation $v^2 = (g/K) \tanh (Kh)$	96
32	Frequency versus wavelength computed from the classic dispersion relation for deep water (Airy) gravity waves, $4\pi^2 f2 = gK$	97
33	Normalized B function for acoustic wave number k = 7.38/m; Block Island Sound. This function was computed using data from Run III	103
34	Normalized average measured B function for acoustic wave number k = 7.38/m; Block Island Sound	104
35A	Normalized acoustic spectra for Run II, 1702 Hz	105
35B	Normalized ocean wave-height spectra for Run II	105

LIST OF ILLUSTRATIONS (Cont'd)

Figure		Page
36A	Normalized acoustic spectra for Run III, 1702 Hz . . .	106
36B	Normalized ocean wave-height spectra for Run III . . .	106
37A	Normalized acoustic spectra for Run IV, 1702 Hz . . .	108
37B	Normalized ocean wave-height spectra for Run IV . . .	108
38A	Normalized acoustic spectra for Run V, 1702 Hz . . .	109
38B	Normalized ocean wave-height spectra for Run V . . .	109
39	Normalized B function for acoustic wave number k = 0.55/m; Block Island Sound. This function was computed using data from Run VI	110
40	Normalized average measured B function for acoustic wave number k = 0.55/m; Block Island Sound	111
41A	Normalized acoustic spectra for Run I, 127 Hz	112
41B	Normalized ocean wave-height spectra for Run I . . .	112
42A	Normalized acoustic spectra for Run VI, 127 Hz	113
42B	Normalized ocean wave-height spectra for Run VI . . .	113
43A	Normalized acoustic spectra for Run VII, 127 Hz . . .	114
43B	Normalized ocean wave-height spectra for Run VII . . .	114
	Appendix B	
B-1	Hourly weather observations at the Block Island Airport .	137
	Appendix C	
C-1	Wave staff calibration at Millstone Pond	148
C-2	Recording electronics for the accelerometer buoy experiment	149
C-3	Receiving and recording electronics aboard R/V UCONN .	150

LIST OF ILLUSTRATIONS (Cont'd)

Figure		Page
C-4	Recording electronics at the Naval Underwater Systems Center (29 December - 30 January 1970)	151
C-5	Modified receiving and recording electronics aboard R/V UCONN (26 January - 30 January 1970)	152
	Appendix D	
D-1	Spectrum level of acoustic signal at Position C (resolution = 0.0056 Hz, EDF = 10)	158
D-2	Spectrum level of acoustic signal at Position C (resolution = 0.0112 Hz, EDF = 21)	159
D-3	Spectrum level of acoustic signal at Position C (resolution = 0.0225 Hz, EDF = 45)	160
D-4	Spectrum level of acoustic signal at Position C (resolution = 0.0550 Hz, EDF = 91)	161

LIST OF TABLES

Table		Page
1	Operational data	67
2	Variances in the ocean wave-height spectra, Runs I - VII . .	70
3	Correlation of acoustic and ocean wave-height spectra between frequency intervals	90
	Appendix B	
B-1	Sound speed versus depth	134

LIST OF SYMBOLS AND NOTATIONS

A	acoustic receiver
$A(\omega)$	received acoustic signal spectrum (microbar^2/Hertz)
$A_{mn}(\omega)$	elementary contribution to the spectrum at the acoustic receiver from subsections m and n (microbar^2/Hertz)
$A_1(\omega)$	positive frequency component of SCAT$\{A(\omega)\}$(microbar^2/Hertz)
$A_{-1}(\omega)$	negative frequency component of SCAT$\{A(\omega)\}$(microbar^2/Hertz)
$B(\omega)$	weighting function that determines how the ocean surface wave-height spectrum is weighted by the parameters of the acoustic experiment to produce first-order sidebands in the acoustic signal spectrum
C	sound speed (meters/second)
$C(\tau)$	received acoustic signal covariance (microbar^2)
$C_{mn}(\tau)$	elementary contribution to the autocovariance at the acoustic receiver from subsections m and n (microbar^2)
$COH\{A(\omega)\}$	coherent (specular) component of $A(\omega)$ (microbar^2)
$COH\{A_{mn}(\omega)\}$	coherent (specular) component of $A_{mn}(\omega)$ (microbar^2)
$COH\{C(\tau)\}$	coherent component of $C(\tau)$ (microbar^2)
$COH\{C_{mn}(\tau)\}$	coherent (specular) component of $C_{mn}(\tau)$ (microbar^2)
D_1	acoustic source depth (meters)
D_2	acoustic receiver depth (meters)
E	$[\Pi \rho C/2\pi]^{1/2}$

$F_i(\omega)$	frequency-dependent geometric term relating the acoustic spectrum to the ocean wave-height spectrum
G_{mn}	phase-dependent geometric term relating the acoustic auto-covariance to the ocean wave-height covariance
$H(\beta, u)$	Fourier transform of the product of illumination functions
$\bar{H}\left(\beta, \alpha \pm \frac{\Omega^2}{g}\right)$	Fourier transform of $H(\beta, u)$
$I(x, y)$	acoustic illumination function
$I(x)$	acoustic illumination function for the long-crested sea surface
$\mathcal{I}$	Fourier transform of the acoustic illumination function
K	ocean surface wave number (meters^{-1})
$\bar{K}$	equivalent surface wave number (meters^{-1})
L	length of subsections on the scattering surface (meters)
M	total number of subsections on the scattering surface
P	parameter to control the shape of the illumination functions
P_r	relative power in the acoustic spectrum
$\hat{P}_m$	geometric term that also depends on the mean-square wave height
R	reflectivity coefficient
R	distance from the acoustic source (meters)
R_{SO}	distance from the acoustic source to the origin of coordinates (meters)
R_{AO}	distance from the origin of coordinates to the acoustic receiver (meters)
R_S	distance from the acoustic source S to $d\bar{S}$ (meters)
R_A	distance from $d\bar{S}$ to the receiver A (meters)

S	acoustic source
S_a	salinity (parts/thousand)
$\bar{S}$	scattering area on the surface of the ocean (meters^2)
$S(\Omega)$	ocean surface wave-height frequency spectrum (meters^2/Hertz)
$SCAT\{A(\omega)\}$	scattered component of $A(\omega)$ (microbars^2/Hertz)
$SCAT\{A_{mn}(\omega)\}$	scattered component of $A_{mn}(\omega)$ (microbars^2/Hertz)
$SCAT\{C(\tau)\}$	scattered component of $C(\tau)$ (microbars^2)
$SCAT\{C_{mn}(\tau)\}$	scattered component of $C_{mn}(\tau)$(microbars^2)
T	temperature (degrees Celsius)
$U(\omega)$	unit step function
$W(\alpha, \beta, \omega)$	spectrum function
X	Cartesian coordinate axis
$\bar{X}$	horizontal distance of the source and the receiver from the origin
X_m	coordinate of the center of m^{th} subsection
Y	Cartesian coordinate axis
Z	Cartesian coordinate axis
a'	arbitrary variable
a_1	X direction cosine of incident plane acoustic wave
$\bar{a}$	$h_r/\sin X$
a	$k(\sin\theta - \sin\psi\cos\psi_1)$, the sum of the X direction cosines of the source and receiver distances R_{S0} and R_{A0} multiplied by the acoustic radiation wave number k (meters^{-1})
b_1	constant
b'	arbitrary variable

b	$-k(\sin\psi \sin\psi_1)$, the sum of the Y direction cosines of the source and receiver distances R_{S0} and R_{A0} multiplied by the acoustic radiation wave number k (meters^{-1})
$\bar{b}$	$\bar{a} \cos(\pi - 2X)$ (meters)
b_1	Y direction cosine of incident plane acoustic wave
c	$-k(\cos\theta + \cos\psi)$, the sum of the Z direction cosines of the source and receiver distances R_{S0} and R_{A0} multiplied by the acoustic radiation wave number k (meters^{-1})
c_1	Z direction cosine of incident plane acoustic wave
$f(\theta)$	geometric function relating the secondary acoustic pressure to the angles of incidence and scatter
f	frequency (Hertz)
f_b	bandshifted carrier frequency (Hertz)
f_0	transmitted frequency of a sinusoidal source (Hertz)
g	acceleration due to gravity (meters/second^2)
h	water depth (meters)
h_r	height of roughness elements (meters)
i	$\sqrt{-1}$
$\vec{i}$	unit vector in the X direction
i	integer
$\vec{i}$	unit vector in the Y direction
k	acoustic radiation wave number (meters^{-1})
$\hat{k}$	integer
$\vec{k}_2$	scattered propagation vector (meters^{-1})
m	integer designating a subsection on the scattering surface
n	integer designating a subsection on the scattering surface
$\vec{n}$	unit normal to the rough surface (positive down)

p	integer
$\vec{q}$	unit vector in the Z direction
r	arbitrary variable
$\vec{r}$	position vector from the origin of coordinates to an elemental area on the surface $d\vec{S}$ (meters)
t	time (seconds)
υ	space lag $x - x'$ (meters)
v	water wave phase speed (meters/second)
x	Cartesian coordinate (meters)
x'	Cartesian coordinate (meters)
y	Cartesian coordinate (meters)
z	Cartesian coordinate (meters)
z'	Cartesian coordinate (meters)
Δf	frequency shift (Hertz)
Δr	path difference of reflected rays (meters)
$\Phi(\alpha, \beta, \tau)$	autocorrelation function
Λ	ocean surface wavelength (meters)
X	grazing angle of acoustic waves (radians)
Π	acoustic source power (watts)
T	record length (seconds)
Φ	acoustic pressure (microbars)
$\Phi(A, t)$	secondary acoustic field observed at the receiver A at time t (microbars)
Ψ	Green's function for the scattered field
Ω	ocean surface wave radian frequency (radians/second)

α	$(a_m + a_n)/2$ (meters^{-1})
β	$a_m - a_n$ (meters^{-1})
δ	Dirac delta function
$\delta_{m,\ n}$	Kronecker delta
ϵ_i	ocean surface wave random phase angle (radians)
$\zeta(x, y, t)$	ocean surface elevation (meters)
$\zeta(x, t)$	surface elevation of the long-crested sea (meters)
θ	angle of incidence (radians)
θ_s	azimuthal angle of ocean waves with the acoustic source-receiver line (radians)
$\bar{\theta}$	$\cos^{-1}(\bar{b}/\bar{a})$
λ	acoustic wavelength (meters)
$\hat{\rho}$	coefficient of correlation between the acoustic scattered spectrum (down-Doppler) and the ocean wave-height spectrum
ρ	autocorrelation function of surface wave heights
$\rho(u, \tau)$	autocorrelation function of surface wave heights for the long-crested sea surface
ρ'	density (kilogram/meter^3)
σ^2	mean-square wave height (meter^2)
τ	time lag (seconds)
ϕ	ocean surface wave phase angle (radians)
ψ	angle of scatter (radians)
ψ_1	angle of scatter out of the plane of incidence (radians)
ω	acoustic radian frequency $= 2\pi f$ (radians/second)
ω_0	$2\pi f_0$

SUBSCRIPTS

A	air
b	bandshifted
c	coherent component of the secondary acoustic field
d	directional
i	integer (generally used as an index of summation)
$\hat{k}$	integer
m	m^{th} subsection on the scattering surface
n	n^{th} subsection on the scattering surface
p	number of averages in FFT spectrum analysis
r	roughness element
s	scattered component of the secondary acoustic field
W	water

NOTATION

*	complex conjugate
$\langle\ \rangle$	ensemble average
$\lvert\ \rvert$	absolute value
•	multiplication

1.0 INTRODUCTION

Remote sensing of the environment offers many exciting possibilities for discovery in the field of geophysics. Aerial radiometer flights to determine sea surface temperature are now a standard technique of physical oceanography and marine meteorology. Chia[1] and Pierson and Moore[2] have shown that it is possible to obtain detailed information about the ocean surface wave spectrum and other characteristics of the air-sea boundary layer by means of radar waves transmitted and received by an orbiting space vehicle. Underwater sound waves have been used since the 1920's to map the ocean floor and to chart the sublayering of the sediments. Vigoureux and Hersey,[3] however, have noted that it is unfortunate that few applications of underwater sound have been made in physical oceanography. Clark and Yarnall[4] have used underwater acoustics to study experimentally the tides, currents, and internal waves in the Straits of Florida. They have suggested that the underwater acoustic range, consisting of a fixed source and fixed receivers, could be made into an effective remote probe to study the marine environment.

This investigation attempts to stimulate the interest of physical oceanographers in underwater acoustics by demonstrating, both theoretically and experimentally, that the low-frequency end of the ocean surface height spectrum can be estimated from the time history of received sound pressure levels. The general problem of using underwater sound to obtain information about the geometry and kinematics of the sea surface was probably first considered seriously by Eckart[5] in 1953. He

studied the case of a highly directional, single-frequency, acoustic projector transmitting in the direction of the stochastic sea surface. The transmitter induces secondary sources on the surface that determine the nature of the scattered field in the water. The acoustic field at a subsurface receiver is then represented by means of the Helmholtz[6] integral, which is evaluated over the insonified area on the surface in terms of the boundary values of the pressure field and its normal derivative. (This approach is often referred to as the "physical optics" method). Eckart determined the scattering coefficient for low surface roughness in terms of the directional surface wave spectrum. He concluded that it would be necessary to vary the direction and frequency of the acoustic waves to obtain an estimate of the surface height spectrum.

Eckart's paper stimulated interest in the acoustic community, and a number of papers followed in which the basic physical optics theory was modified and extended in order to make application to more general situations possible. Proud, Beyer, and Tamarkin[7] used Eckart's theory to estimate the spatial correlation function of a rough, reflecting surface in the laboratory. Clay[8] extended the theory to include omnidirectional sources by subdividing the insonified area on the surface and applying the Helmholtz integral to each subdivision and summing the contributions. He compared his theory with sea data taken by Brown and Ricard[9] and attempted to estimate the correlation distance on the ocean surface. Medwin[10] showed that the mean-square wave height for cases of small surface roughness can be determined from measurements of specularly reflected acoustic intensity.

Other important contributions were made by Liebermann,[11] who introduced the analogy between the reflection of sound waves at the sea surface and the

reflection of plane waves by a diffraction grating, and by Marsh,[12] who formulated the scattering problem in a way completely different from that of Eckart and obtained an exact solution to the scattered field by using Wiener's[13] theory of generalized harmonic analysis. Marsh's approach was basically a randomization of Rayleigh's[14] solution to the scattering problem by Fourier series methods.

Marsh and Mellen[15] predicted that the first-order spectrum of single-frequency acoustic waves reflected from a rough, moving, isotropic sea surface should consist of two distinct parts, i.e., to first order. The first part, or coherent component, is a line at the transmitted frequency, or "carrier," that corresponds to a specular reflection from the mean sea surface. The second part is a continuous spectrum produced by incoherent scattering that is symmetric about the carrier and is a uniformly weighted reproduction of the sea surface height spectrum.

Parkins[16] applied physical optics theory to determine the spectrum of the far-field acoustic pressure due to an incident, highly directional, single-frequency signal reradiated from a rough, moving surface described by the Neumann-Pierson directional wave spectrum. The received signal spectrum is shown to consist of a line component at the carrier frequency (the coherent component) and two delta functions positioned at frequencies equidistant from the carrier. The location of the delta functions depends on the angles of incidence and reception relative to the wind direction and on the frequency of the transmitted signal. The magnitude of the delta functions is determined by the surface wave-height spectrum. This result does not necessarily contradict the predictions of Marsh and Mellen, because Parkins considers a highly directional source, whereas they allow for a wide range of angles of incidence and reflection. Gulin[17] and Roderick and Cron[18] adopted

physical optics theory to explain scattering from moving, sinusoidal surfaces.

Nuttall and Cron[19] used physical optics theory to derive the spectrum for highly directional signals reradiated from narrow-band, time-varying surfaces described by particular correlation functions.

Clay and Medwin[20] extended Clay's earlier theory to determine the covariance of signals reradiated from a slightly rough, moving water surface described by a traveling correlation function.

Experimental verification of these theories has been extensive in the laboratory, but relatively few comparisons have been made with data taken at sea, especially for the case of forward scattering.

Mackenzie[21] reported on a series of experiments in which pure tones of frequencies 350 Hz to 2400 Hz were transmitted across a shallow water area and detected at ranges of up to 27 km. The received signal spectrum was spread in frequency in such a manner that the relative power (P_r) was related to the half-width of the spectrum $|f - f_0|$ by $P_r = b_1 f_0 |f - f_0|^{-3}$, where b is a constant, f_0 is the transmitted frequency, and f is the measured frequency at the receiver.

Scrimger[22] measured the phase and amplitude fluctuations produced by waves generated by a boat running between a source and receiver separated by a distance of 100 m. He found that, for slightly rough surfaces, the frequency spectrum of the acoustic fluctuations was the same as the frequency spectrum of the water surface. For rough water surfaces, the signal spectrum was broader and exhibited second and third harmonics.

Gulin and Malyeshev[23] measured the spatial correlations of the amplitude and phase fluctuations of signals reflected from the surface of a fresh water reservoir.

They found that "the signal amplitude spatial correlation coefficients in the case of small values for the Rayleigh parameter usually take the form of damped-oscillation functions. . . . The oscillation period is related to the average wavelength of these water waves on the sea surface. In the case of . . . (large Rayleigh parameter) a more abrupt drop in the correlation coefficient is observed and the quasiperiodic behavior disappears."

Clark and Yarnall[4] discussed an experiment performed at Fowey Rocks Lighthouse, Miami, in which an acoustic continuous wave (CW) signal was reflected from the sea surface and received by a hydrophone 137 m away in 18 m of water (Figure 1). The resemblance between the wave-height power spectral density (PSD)

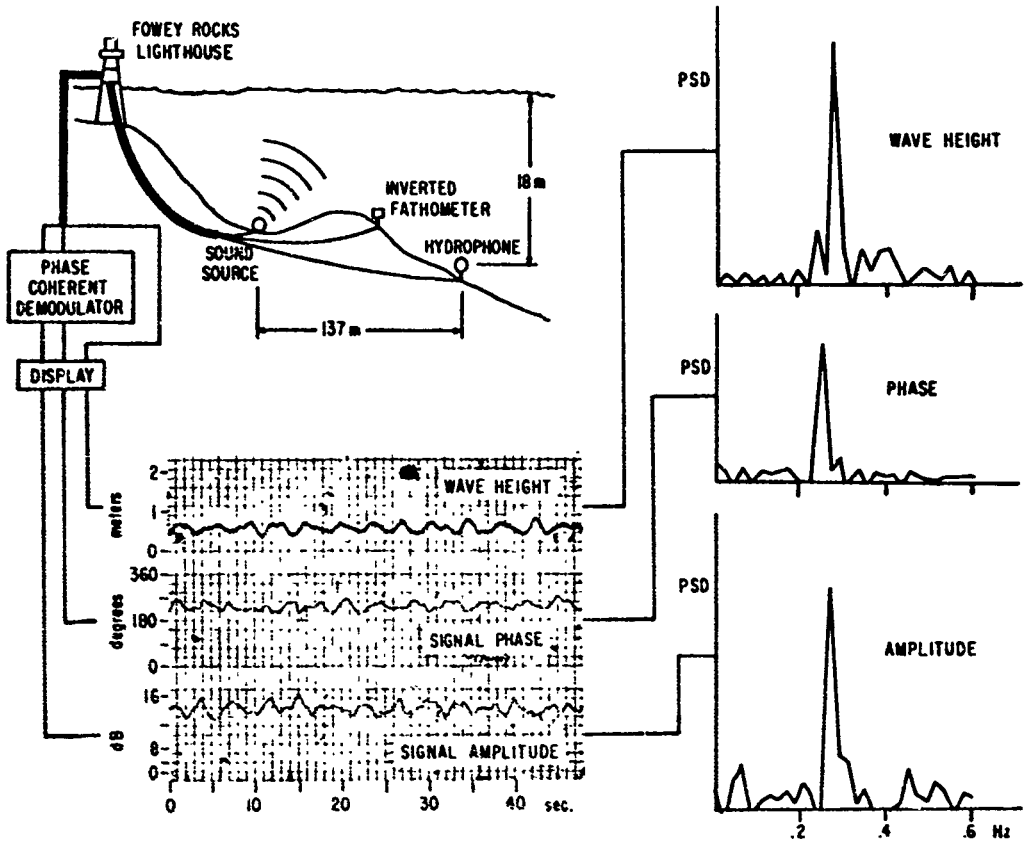

Figure 1. "Single-reflection" surface wave experiment
(From Clark and Yarnall.[4])

and the phase and amplitude PSD is evident.

Ellinthorpe[24] transmitted low-frequency signals from a fixed source to a fixed receiver located in the Sargasso Sea. He observed that "the spectra (Figure 2) all show deep nulls on either side of the transmitted frequency and a pair of relatively broad sidelobes centered at approximately 0.1 Hz away from the central peak. ... These results are consistent in several respects with what would be expected if the underlying physical process were a phase modulation imposed on the acoustic wave by reflection from the moving ocean surface."

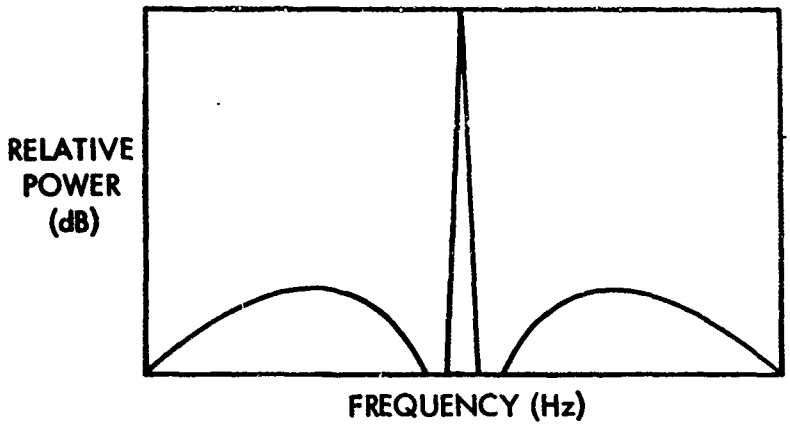

Figure 2. Received spectrum of a surface-reradiated, single-frequency acoustic signal

Roderick and Cron[18] measured surface reflected sound in the deep ocean near Bermuda and compared the spectral content of the received signals with the surface wave-height amplitude spectrum measured 25 nmi away at Argus Island. The results showed that new frequency components in the acoustic signal were generated by the sea surface reflection process and that these components were displaced

from the carrier at multiples of the peak frequency in the surface height spectrum.

The experiments cited above are of considerable value because they show that single-frequency acoustic signals reradiated from a rough, moving water surface are spread in frequency and that this spread is closely related to the properties of the surface. It therefore seems reasonable that the ocean wave-height frequency spectrum can be inferred from the acoustic measurements. The purpose of this thesis is to show by theory and experiments that the ocean wave-height spectrum can be determined explicitly from the acoustic forward-scattered spectrum. The theoretical method used is a combination of the theories of Parkins[16] and Clay and Medwin.[20] The theoretical predictions are then compared with spectra estimated from field measurements of sound pressure level and ocean wave height taken in Block Island Sound. Hopefully, methods similar to those developed here could be applied to obtain information on ocean currents, internal waves, and turbulence. Before considering a particular theoretical formulation of the scattering problem, however, a brief review of pertinent underwater sound transmission characteristics is presented.

2.0 CHARACTERISTICS OF UNDERWATER ACOUSTIC TRANSMISSIONS IN THE SEA

The science of ocean acoustics deals with the effects of the ocean environment on underwater sound propagation. The sources of sound in the sea are either natural or man-made. Examples of natural sounds are the cracking of shrimp, the communications of porpoises and whales, the action of the wind on the waves, and seismic disturbances. Examples of man-made sounds are the explosions used in seismic studies, signals from underwater communication systems and sound detection and ranging systems (sonar), and cavitation from the propellers of ships. In this study, only sinusoidal signals between 100 and 2000 Hz will be considered.

2.1 THE VELOCITY OF SOUND IN THE OCEAN AND ITS EFFECTS ON ACOUSTIC TRANSMISSION

The propagation of sound waves is described to a high order of approximation by the scalar wave equation:

$$\nabla^2\Phi = \frac{1}{C^2}\frac{\partial^2\Phi}{\partial t^2} \quad , \tag{1}$$

where

Φ = acoustic pressure

C = speed of sound expressed in Cartesian coordinates x, y, and z.

When the variations in $C(x, y, z)$ are known, the acoustic field intensity can be determined, in principle, by means of Eq. (1). In most studies of sound

propagation over relatively short ranges, only vertical variations in $C(x, y, z)$ have been considered (i.e., $C(x, y, z) \approx C(z)$). The speed of sound in sea water is a function of the density and the isentropic bulk modulus; it can be determined from routinely measured oceanographic quantities, i.e., temperature, salinity, and depth. Several theoretical and empirical relationships have been derived that give C as a function of these variables. The most generally accepted equation was obtained by Wilson[25] as a polynomial best fit to experimental data measured in the laboratory. This equation is given by Kinsler and Frey[26] as follows:

$$C = 1449 + 4.6T - 0.055T^2 + 0.0003T^3 + (1.39 - 0.012T)(S_a - 35) + 0.017h, \quad (2)$$

where

C = speed of sound in meters per second

T = temperature in degrees Celsius

S_a = salinity in parts per thousand

h = depth in meters.

From typical oceanographic data, this equation shows that a 1° C rise in temperature increases the sound speed by about 3 m/sec, a 1‰ increase in salinity increases the sound speed by 1.3 m/sec, and 10 m increase in depth increases the sound speed by 0.17 m/sec.

Since the ocean is, in general, stratified rather than homogeneous, the speed of sound is a function of depth. This results in acoustic energy being refracted toward regions of minimum velocity as a consequence of Fermat's principle, which reduces to Snell's Law for $C(x, y, z) \approx C(z)$. The speed of sound increases with

increasing depth in the near-surface layer of the Arctic and Antarctic oceans, in the mixed layer of moderate latitudes, and in the coastal waters of temperate zones in winter. Within the near surface layer, propagating sound waves are refracted upward toward the region of lower sound speed near the sea surface. At the sea surface, the large acoustic impedance mismatch between water and air causes a nearly complete reflection of acoustic waves. The reflected waves are bent by refraction toward the sea surface, and the process is repeated again and again, thus fulfilling the condition for a surface channel or duct. The duct affords a means of long-range acoustic signal transmission with small associated energy loss. The important features of these ducts are discussed by Schulkin.[27]

Acoustic signals reflected one or more times from the ocean surface experience energy loss as well as amplitude and phase variations. This total energy loss is the result of the divergence of the acoustic waves from the source (spreading loss), the reflection loss at the sea surface, and the absorption within the water column due to viscosity, thermal conduction, and relaxation. Interference, as well as diffractive leakage out of the duct, results in additional attenuation. The amplitude and phase fluctuations can be caused by the rough, moving surface of the sea, variable currents, internal waves, and turbulence. In this study, only the fluctuations caused by the moving sea surface will be considered. Signal fluctuations induced by the other dynamic processes in the ocean medium are assumed to be either small in comparison to the surface wave effects or of a different temporal character, both of which would result in spectral signatures readily distinguishable from the sea surface effects. Clark and Yarnall[4] and Huff[28] have demonstrated that the various effects of the processes in the ocean can be distinguished from each

other by time-series analysis.

2.2 ACOUSTIC PROPAGATION MODELS

Ray theory, normal mode theory, and empirical methods are generally used for the purpose of constructing models to predict acoustic field intensity. Ray theory is analagous to ray optics and, as such, is intuitively appealing. Rays are used to show the direction of propagation of acoustic energy. If the change in slope of the sound velocity profile is not too large over a distance of 1 wavelength, the ray solution is usually good.

In the normal mode theory, the acoustic field is expressed as the sum of the characteristic functions that satisfy the wave equation and the boundary conditions. The formulas generated are usually quite complicated and must be evaluated numerically on a digital computer. The solution may be difficult to interpret if more than a few modes are present in the channel. However, in shallow water and at long range, the normal mode theory is generally superior to ray theory.

The empirical method utilizes large numbers of measurements of transmission loss versus factors pertaining to the test geometry and the ocean medium. Some features of the models obtained by empirical methods, particularly the Acoustic Meteorological and Oceanographic Survey (AMOS) model, are discussed by Schulkin.[27]

The best choice for an acoustic model is highly dependent on local conditions, as well as on what the investigator hopes to learn from the model. In this study, the emphasis is on the reflection of acoustic waves at the sea surface without regard to any particular propagation model, since the purpose is to show that the

reflected signal spectrum contains information about the surface height spectrum. However, results from both ray theory and normal mode theory will be referred to in the interpretation of experimental data, as required.

2.3 REFLECTIONS OF ACOUSTIC WAVES FROM THE SEA SURFACE

Let us assume a unit amplitude plane wave in the water:

$$\Phi = \exp i(a_1 x + b_1 y - c_1 z - \omega t) , \tag{3}$$

where

a_1, b_1, c_1 = direction cosines

x, y, z = Cartesian coordinates

ω = radian frequency = $2\pi f$

t = time .

If this plane wave is incident on a flat air-sea interface $z = 0$, then the following boundary conditions must be satisfied:

1. The acoustic pressure must be continuous across the boundary.
2. The vertical particle velocity must be continuous across the boundary.

These conditions are expressed as

$$\left(\rho' \frac{\partial \Phi}{\partial t}\right)_W = \left(\rho' \frac{\partial \Phi}{\partial t}\right)_A \tag{4}$$

and

$$\left(\frac{\partial \Phi}{\partial z}\right)_W = \left(\frac{\partial \Phi}{\partial z}\right)_A , \tag{5}$$

where

A, W refer to air and water, respectively

ρ' refers to density.

When these boundary conditions are applied to the incident wave, the angle of incidence is equal to the angle of reflection, and the angle of the refracted ray can be determined from Snell's Law. In addition, the frequencies of the reflected and refracted waves are the same as the frequency of the incident wave. Because of the large acoustic impedance mismatch between water and air ($(\rho'C)_W >> (\rho'C)_A$), almost all the acoustic energy is reflected back into the water. Thus, to a high level of approximation the reflection coefficient is -1, which means that the reflected wave has undergone a phase change of π radians relative to the incident wave. A surface for which $(\rho'C)_W >> (\rho'C)_A$ is called a "pressure release" surface. Thus, the sum of the incident and reflected pressures is zero:

$$\Phi_{\text{incident}} + \Phi_{\text{reflected}} = 0 \ . \tag{6}$$

Hence, a perfectly calm sea surface is an almost perfect reflector of sound.

The problem of determining the reflected field for a rough sea surface is much more complicated than it is for a flat sea surface. In general, an exact solution is not possible. Physically, acoustic energy is scattered in directions other than the specular direction. When the energy scattered by the rough, moving surface is added to the specularly reflected component of the field (the coherent component), amplitude and phase fluctuations are introduced into the secondary acoustic field. This has the effect of broadening the spectrum of the received signal, which is called "Doppler broadening" or "surface wave modulation."

One of the first considerations in any study of scattering from rough surfaces is to obtain an adequate definition of a rough surface. Perhaps the most common definition of surface roughness is the Rayleigh "roughness criterion," which states that a surface is rough if the height of the roughness elements $h \geq \frac{\lambda}{8 \sin X}$, where X is the grazing angle and λ is the wavelength of the incident radiation. The Rayleigh criterion for incident rays on a rough surface will now be derived. From Figure 3, it is seen that

$$\bar{a} = h_r / \sin X$$

$$\bar{b} = \bar{a} \cos \bar{\theta} = \bar{a} \cos (\pi - 2X) \quad . \tag{7}$$

The path difference of rays reflected at Q and at A, $\Delta r = \bar{a} + \bar{b}$, is

$$\Delta r = \frac{h_r}{\sin X} + \frac{h_r}{\sin X} \cos (\pi - 2X)$$

or

$$\Delta r = \frac{h_r}{\sin X} \left[1 + 2 \sin^2 X - 1 \right] = 2 h_r \sin X \quad . \tag{8}$$

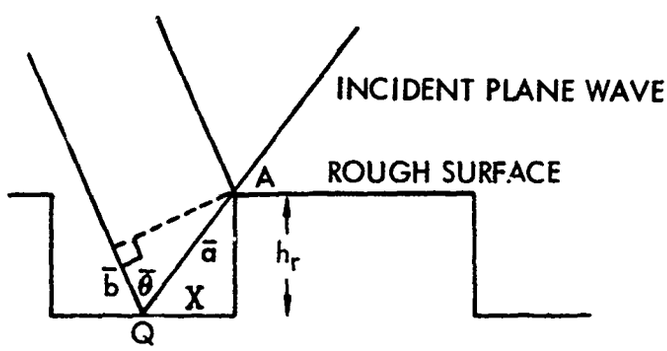

Figure 3. Derivation of the Rayleigh Criterion

Hence, when the phase difference $\left(\frac{2\pi}{\lambda}\ \Delta r\right)$ is near zero, the rays will be almost in phase; however, if it is near π, there will be maximum destructive interference. Arbitrarily choosing a value for the phase difference that is halfway between rough (π) and smooth (0), i.e., $\pi/2$, yields the Rayleigh criterion. Contemporary authors have suggested other criteria, but Beckmann[29] states that, rather than develop a precise definition of roughness in this way, it makes more sense to observe that a surface will be smooth only if $\frac{h_r}{\lambda} \to 0$ or $X \to 0$. The meaning of the Rayleigh criterion for underwater acoustics is that, as the grazing angle decreases and the wavelength increases, the sea surface behaves more and more like a smooth surface.

Another basic problem is to determine how the scattered intensity at the receiver varies as a function of position on the rough surface. In the case of Eckart's[5] physical optics theory, a highly directional transmitter insonifies a relatively small region on the surface around the specular point. However, in the case of an omnidirectional source, a very large area on the surface is insonified and regions far from the specular point may contribute significantly to the scattered field. Beckmann[29] has examined this problem in the case of electromagnetic waves. He regarded the reflecting surface as an aperture that diffracts incident waves propagating from a point source to a point receiver. The diffraction pattern observed at the receiver can be obtained by constructing Fresnel zones on the reflecting surface. (These are zones where the phase difference of the radiation arriving at the receiver from a given zone is one-half a wavelength different from the radiation arriving from the adjacent zones.) In classical optics, where one is concerned with the diffraction of light from an aperture, it is shown that waves

from each zone interfere destructively with those from the two adjacent zones. Consequently, the wave amplitudes from all zones, except the first and the last, nearly cancel each other. The total amplitude is then, to a high order of approximation, the average contribution from the first and last zones. However, since the variation of the obliquity factor reduces the contribution of the last zone to almost zero, the result is half the value of the first zone. (The obliquity factor determines how the amplitudes of the secondary waves vary with direction.) Beckmann[29] has pointed out that caution must be used in applying the results of classical optics directly to radio propagation problems. He has, however, derived formulas to describe the diffraction by the earth of obliquely incident radio waves and has reached the following conclusions:

1. The first Fresnel zone is the most important region on the scattering surface in contributing to the total field received at a given point.

2. Other important contributions come from areas on the surface above the transmitter and receiver. These areas are not included in any Fresnel zone.

3. The Fresnel zones on the surface are ellipses and, for small grazing angles, are very long and narrow.

There is every reason to believe that these conclusions are valid for underwater acoustics. Scrimger[22] found that water waves immediately above the transmitter and receiver cause amplitude and phase fluctuations in the received signal. Clay[8] and Medwin and Clay[30] found that the areas far from the specular point must be considered to correctly predict the scattered field intensity.

An important conclusion that has emerged from many of the theoretical and experimental investigations on scattering from rough surfaces is that periodic, rough surfaces tend to behave as diffraction gratings and thus scatter sound into discrete directions corresponding to the orders of the grating (Bragg scattering). This means that the directions of maximum intensity of the field scattered by a periodic surface are given by

$$\sin \psi_p = \sin \theta + p \frac{\lambda}{\Lambda} \quad (p = 0, \pm 1, \pm 2, \ldots) , \tag{9}$$

where

ψ_p = angle of scatter

θ = angle of incidence

λ = acoustic wavelength

Λ = surface wavelength

p = integer mode index .

This aspect of scattering has been treated in detail by Beckmann,[29] who presents scattering diagrams as a function of angle of incidence. In reality, of course, other directions of scattering are possible, but the maxima of the scattered field are given by the Bragg relation. Beckmann has handled this situation by removing the constraint of the integer mode index p .

Liebermann[11] asserted that a random surface, which is presumably composed of elementary sinusoidal waves, behaves like a diffraction grating in the sense that single-frequency radiation will be preferentially scattered according to the wavelengths present in the surface. He demonstrated experimentally that, for sinusoidal

radiation, a very narrow band of frequencies in the rough surface produces the scattering. Therefore, "a spectrum analysis of surface roughness can be obtained by slowly varying the frequency of the incident radiation and observing the magnitude of the scattered radiation."[11] Marsh et al.,[12, 15, 31] in a series of papers, further developed this concept and referred to an "equivalent surface wave number":

$$\bar{K} = k(\cos X_{in} + \cos X_{re}) \quad , \tag{10}$$

where

k = radiation wave number

X_{in} = incident grazing angle

X_{re} = reflected grazing angle .

Wright[32] employed this concept in connection with the scattering of radar waves from the sea surface. Recent evidence for the validity of Bragg scattering has come from model tank experiments by Kingsbury.[33]

The concept of Bragg scattering can also be applied to explain the Doppler broadening observed when a signal is reflected from a rough, moving surface. The signal is scattered into discrete orders by elements of the rough surface. Since these elements are in motion, the frequencies of the scattered orders are shifted away from the carrier. Gulin[17] determined that the frequency shift is

$$\Delta f = p \frac{v}{\Lambda} \quad , \tag{11}$$

where

v = phase speed of the surface irregularities

Λ = wavelength of the surface

p = the scattered order .

Hence, there is no Doppler shift in the specular direction where order $p = 0$. Kingsbury[33] has experimentally verified this relationship for water surfaces characterized by a sharply peaked spectrum.

3.0 THEORY

The purpose of this chapter is to provide a theoretical basis for estimating the ocean wave-height spectrum by means of the acoustic forward-scattered spectrum. There are many possible theoretical approaches to the general problem of determining the field scattered by the rough sea surface. Fortuin[34] has recently provided a fairly complete summary of the better known methods. The majority of these methods lead to solutions that are not exact and involve a large number of simplifying assumptions.

Perhaps the most nearly complete theory of scattering of acoustic waves in the ocean is that of Marsh et al.[12,35,36,37] Without considering the time variation of the ocean surface, Marsh demonstrated by means of a randomized Rayleigh-type solution that, for small surface roughness, the received acoustic intensity consists of a specular reflection term and a nonspecular scattered term. Rayleigh-based methods are frequently referred to as "wave expansion methods." The wave expansion method is used to derive expressions for the magnitude of the specular and nonspecular terms. These terms are used in the prediction of the acoustic surface loss per bounce in cases of surface duct propagation.

Marsh et al.,[15,31] through keen physical insight, have heuristically extended their mathematical model to predict the effects of acoustic reflections from the time-varying surface of the ocean. They assert that the first-order, near-specular scattered spectrum in the frequency domain will be equal to the uniformly weighted sea

surface spectrum (for low surface roughness). This conclusion was reached by considering the constraints placed on acoustic propagation via surfaced reflected paths, i.e., Bragg scattering, Doppler shifts, the dispersion relation for deep water gravity waves, and the requirements for the conservation of energy. Results from simulations of scattering problems on the computer have supported the hypothesis that the weighting is, in fact, uniform when all possible angles of scatter are considered.

In the present study, Marsh's predictions of the forward-scattered spectrum in the frequency domain will be examined quantitatively by means of a simpler theory; i.e., the "physical optics" theory developed by Eckart[5] in 1953. (Tolstoy and Clay[38] develop this theory from basic principles.) Parkins[16] has used physical optics theory to determine the spectrum of a sinusoidal acoustic signal reradiated from a rough, moving sea surface characterized by the Neumann-Pierson directional wave spectrum. He found that the received acoustic signal spectrum consists of three delta functions. This result would follow for any directional wave spectrum as long as the dispersion relation holds.

Parkins' result cannot be compared with Marsh's predictions, because Parkins used a highly directional source and receiver and, thus, obtained a very restrictive relationship between the ocean wave-height spectrum and the acoustic frequency and geometry of the experiment, as did Eckart. However, it is shown here that, if Parkins' theory is generalized to allow for wide-beam sources, the reradiated acoustic spectrum is equal to the weighted ocean surface wave-height spectrum and that the weighting depends upon the source frequency and the experimental geometry. Parkins' theory is generalized for the long-crested sea surface

(Pierson[39,40]) by using methods developed by Clay and Medwin[20] and Nuttall and Cron.[19] When the model is extended to the short-crested sea surface (Pierson[39,40]), the weighting will probably be more nearly uniform and, hence, will approach Marsh's prediction.

3.1 SYNOPSIS OF THE PHYSICAL OPTICS METHOD

The acoustical pressure due to a sinusoidal, narrow-beam signal reradiated from a rough, moving sea surface is derived by using the Helmholtz[6] integral and the Kirchoff[29] approximation. This solution can be generalized to describe an omnidirectional source by using Clay's[8] method of subdividing the total insonified area on the surface and applying Helmholtz-Kirchoff[38] theory to each subarea. The total field can then be obtained by summing the contributions from each subarea, but the coherent and incoherent components of the field must be summed separately. It is assumed that the surface is rough in only one dimension (long-crested), so that only variations parallel to the source-receiver line are considered.

Since the received signal spectrum is the desired result of this analysis, the autocovariance function at a single receiver due to any two subareas (subsections) m and n is formed from the expressions for the received pressure by using methods developed by Clay and Medwin.[20] The ensemble average is taken by using the method of characteristic functions.[16] When the distribution of surface heights is Gaussian, the ensemble average is an exponential expression containing the space-time correlation function of the sea surface. This exponential expression is expanded and only the first two terms are retained in order to examine in greater detail the dependence of the acoustic field on the sea surface correlation function.

This procedure limits the subsequent analysis to cases of small surface roughness or long acoustic wavelengths.

The expansion of the exponent also separates the acoustic field contributions into specular (coherent) and scattered components[20] and facilitates the eventual summation over all subsections. The coherent component can be integrated and is shown to depend on the frequency, the geometry of the experiment, and on the mean-square wave height. The scattered component is evaluated by using the long-crested, linear, Gaussian, Eulerian model (Pierson[39,40]), which expresses the space-time correlation function of the sea surface in terms of the ocean surface height spectrum. The resulting expression for the acoustic covariance can then be integrated and Fourier transformed by using methods developed by Parkins[16] to yield the received spectrum. When the spectral contributions resulting from all subsections are combined, the scattered acoustic spectrum is expressed as the product of the ocean wave-height spectrum and a weighting factor that depends on the transmitted frequency, the mean-square wave height, and the source-receiver geometry. It is thus possible, in principle, to apply this weighting factor to the acoustic scattered spectrum to recover the ocean wave-height spectrum if the ocean surface is not too rough and is nearly long-crested.

3.2 DERIVATION OF THE ACOUSTIC SURFACE RERADIATED SPECTRUM

In the subsequent derivation, a number of approximations and assumptions are made. For convenience, they are listed below as follows:

1. The acoustic signal is received in the farfield (Fraunhofer zone) of the source.

2. The plane wave approximation is valid for small sections of the insonified area.

3. The incident signal is a pure tone (sinusoid).

4. The ocean surface is a pressure-release surface.

5. The rough ocean surface is long-crested, has a Gaussian distribution of heights, and has a mean-square height of σ^2 .

6. The surface is homogeneous and stationary over the time of the measurements.

7. The Kirchoff approximation is made locally, i.e., the derivative of the secondary field Φ normal to the surface is given by

$$\frac{\partial \Phi}{\partial n} = - R\left(\frac{\partial \Phi_i}{\partial n}\right) ,$$

where

R = reflectivity coefficient, which is -1 for a pressure-release surface

$\vec{n}$ = unit normal to the rough surface (positive down)

Φ_i = incident acoustic field.

8. The surface is not too rough, and the reradiated field can be separated into a coherent (specular) component and a scattered component.

9. The ocean medium is isovelocity for the depths considered.

A highly directional acoustic transmitter will now be assumed in order to obtain an expression for the surface reradiated acoustic pressure, as was done by Tolstoy and Clay,[38] who based their derivations on the work of Eckart.[5] The

experimental geometry is shown in Figure 4, and the symbols are defined as follows:

S_d = highly directional acoustic source

A = receiver

X, Y, Z = orthogonal Cartesian coordinates specified by unit vectors $\vec{i}, \vec{j}, \vec{q}$

R_{S0} = distance from the source to the origin of the coordinates, which is positioned in the center of the insonified area on the surface $\bar{S}[=\zeta(x, y, t)]$

R_{A0} = distance from the origin to the receiver

$\vec{r} = x\vec{i} + y\vec{j} + z\vec{q}$ = position vector from the origin to an elemental area $d\bar{S}$ on the surface, which has a unit normal $\vec{n}$, (positive down)

R_S and R_A = distances from the source S_d to $d\bar{S}$ and from $d\bar{S}$ to the receiver A, respectively

θ = angle of incidence of the acoustic waves

ψ = angle of scatter

ψ_1 = angle of lateral scattering out of the plane of incidence.

The source S_d is radiating an acoustic field $\Phi(x, y, z, t)$, which is given as

$$\Phi(x, y, z, t) = \frac{1}{R}\sqrt{\frac{\Pi\rho C}{2\pi}}\, I(x, y) \exp i\left\{kR - \omega_0 t\right\}, \qquad (12)$$

where

R = distance from S_d

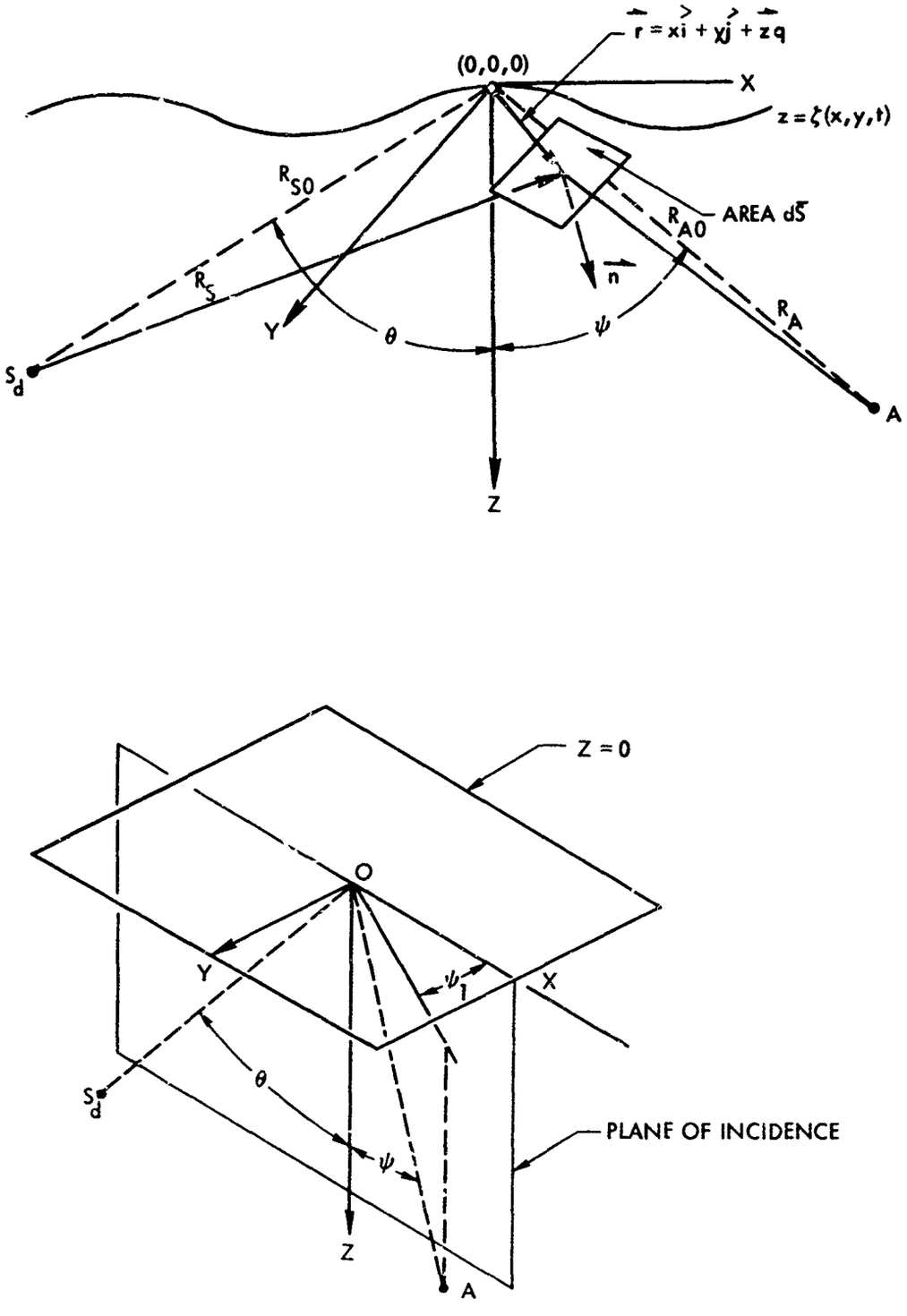

Figure 4. Experimental geometry for the highly directional source

Π = source power

ρ = density of the water

C = speed of sound

$I(x, y)$ = source beam pattern (illumination function)

k = acoustic wave number

ω_0 = source radian frequency

t = time

$i = \sqrt{-1}$.

The reradiated acoustic field at the receiver A, which is produced by reflection and scattering from the rough sea surface $\zeta(x, y, t)$ is given by the Helmholz theorem[6]

$$\Phi(A, t) = -\frac{1}{4\pi} \int_{\bar{S}} \int d\bar{S} \left[\Phi \Big|_{\bar{S}} \frac{\partial \Psi}{\partial n} - \Psi \frac{\partial \Phi}{\partial n} \Big|_{\bar{S}} \right] , \qquad (13)$$

where

$\Phi\big|_{\bar{S}}$ and $\left.\frac{\partial \Phi}{\partial n}\right|_{\bar{S}}$ = values of Φ and its normal derivative on the surface

$\Psi = \exp i \left\{ \vec{k}_2 \bullet (\vec{R}_{AO} - \vec{r}) \right\} / \left| \vec{R}_{AO} \right|$, the Green's function for the scattered field

$\vec{k}_2$ = scattered propagation vector.

The value of $\Phi\big|_{\bar{S}}$ and $\left.\frac{\partial \Phi}{\partial n}\right|_{\bar{S}}$ can be determined by using the pressure release condition and the Kirchoff approximation, i.e.,

$$\Phi\Big|_{\bar{S}} = -\Phi_i \text{ and } \frac{\partial \Phi}{\partial n}\Big|_{\bar{S}} = \frac{\partial \Phi_i}{\partial n}\Big|_{\bar{S}} , \qquad (14)$$

where

Φ_i = incident acoustic field on $\bar{S}$

$\frac{\partial}{\partial n}$ = normal to the plane tangent to the point of evaluation on the rough surface.

Therefore,

$$\Phi(A, t) = -\frac{1}{4\pi} \int_{\bar{S}} \int d\bar{S} \frac{\partial}{\partial n} (\Phi_i \Psi) . \qquad (15)$$

Substituting for Φ_i and Ψ and partially integrating, as in Tolstoy and Clay,[38] results in

$$\Phi(A, t) = \frac{ik E f(\theta) \exp i \left\{k (R_{A0} + R_{S0})\right\}}{2\pi R_{A0} R_{S0}} \exp (i \omega_0 t)$$

$$\cdot \int_{-\infty}^{+\infty} \int dx\, dy\, I(x, y) \exp i \left\{ax + by + c\zeta(x, y, t)\right\} , \qquad (16)$$

where

$$k = \left|\vec{k}\right|$$

$$E = \sqrt{\frac{\Pi \rho C}{2\pi}}$$

$$f(\theta) = \frac{1 + \cos\theta\cos\psi - \sin\theta\sin\psi\cos\psi_1}{\cos\theta + \cos\psi}$$

$$a = k(\sin\theta - \sin\psi\cos\psi_1)$$

$$b = -k(\sin\psi\sin\psi_1)$$

$$c = -k(\cos\theta + \cos\psi) \quad .$$

In the derivation of Eq. (16), the slopes on the rough surface are assumed to be small. The plane wave approximation has also been made, since differences in direction between R_S and R_{S0} and between R_A and R_{A0} are neglected.

Equation (16) cannot be applied to omnidirectional or wide-beam sources, because a, b, and c are treated as constants and, hence, the insonified (illuminated) area on the surface cannot be too large. In addition, the curvature of the incident, spherical wave fronts must be very small so that the plane wave approximation is reasonably good.

Clay,[8] however, has shown that this theory can be applied to the case of wide-beam sources by subdividing the insonified area on the sea surface and applying Eq. (16) to each subarea. The total field is then obtained by summing the contributions from all subareas m and n. The scattering geometry for the long-crested sea surface is shown in Figure 5, where

S = omnidirectional source

(0, 0) = origin of coordinates halfway between the source and the receiver

$(-\bar{X}, D_1)$, $(\bar{X}, D_2)$ = source and receiver coordinates, respectively.

L = length of subsections

$(X_m, 0)$, $(X_n, 0)$ = centers of subsections m and n, respectively

R_{Sm}, R_{Sn} = distances from the source to $(X_m, 0)$ and $(X_n, 0)$, respectively

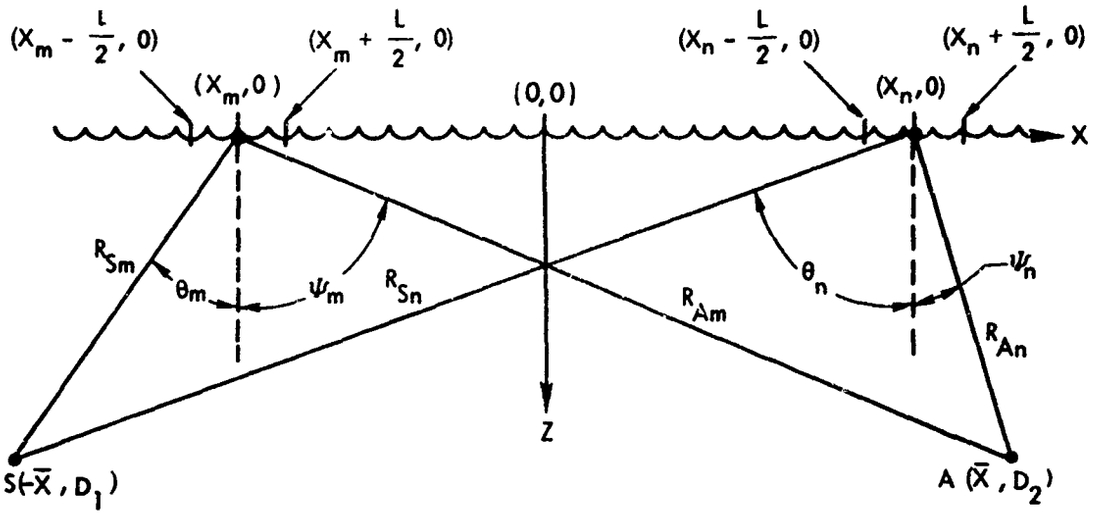

Figure 5. Scattering geometry for the omnidirectional source

R_{Sm}, R_{Sn} = distances from the source to $(X_m, 0)$ and $(X_n, 0)$, respectively

R_{Am}, R_{An} = distances from $(X_m, 0)$ and $(X_n, 0)$, respectively to the receiver A

θ_m, θ_n = angles of incidence to the subsection m and n, respectively

ψ_m, ψ_n = angles of scatter from subsection m and n, respectively, to the receiver A.

When Eq. (16) is applied to individual subsections m or n to obtain the reradiated field, $\Phi_m(A,t)$ or $\Phi_n(A,t)$, the position dependent quantities in Eq. (16) must be appropriately subscripted. For example, when a is applied to subsection m, a becomes $a_m = k(\sin\theta_m - \sin\psi_m)$.

The first step in the summing procedure is to separate the reradiated field into a specular (coherent) component and a scattered (partially coherent) component, since the specular contributions add coherently, whereas the scattered contributions are only partially coherent and must be summed separately.[20] This means that the total acoustic field $\Phi(A, t)$ is given by the sum over all M subsections:

$$\Phi(A, t) = \sum_{m=0}^{M} \left[\Phi_c(A, t) + \Phi_s(A, t) \right], \qquad (17)$$

where

$\Phi_c(A, t)$ = coherent component of the field

$\Phi_s(A, t)$ = scattered component of the field.

The autocovariance at the receiver A due to reflection and scattering from two subsections m and n is given by

$$\left\langle \Phi(A, t)\, \Phi^*(A, t+\tau) \right\rangle = \sum_{m=0}^{M} \sum_{n=0}^{M} \left\langle \Phi_{cm}(A, t) \Phi^*_{cn}(A, t+\tau) \right\rangle + \sum_{m=0}^{M} \sum_{n=0}^{M} \left\langle \Phi_{sm}(A, t)\, \Phi^*_{sn}(A, t+\tau) \right\rangle, \qquad (18)$$

where

$*$ denotes the complex conjugate

$\langle\ \rangle$ denotes the ensemble average.

This result follows from Eq. (17) because the mean of the products of the coherent and scattered components is assumed to be zero.[20] The received signal spectrum can now be obtained by substituting Eq. (16) into Eq. (18) and Fourier transforming the result; the y dependence is suppressed, since the rough surface is long-crested. The contribution to the temporal autocovariance function at the receiver A, $C_{mn}(\tau)$, from all subsections m and n, is the ensemble average of the product of $\Phi_m(A, t)$ with the complex conjugate of $\Phi_n(A, t)$:

$$C_{mn}(\tau) = \left\langle \Phi_m(A, t)\, \Phi_n^*(A, t+\tau) \right\rangle$$

$$= \frac{k^2 E^2 f_m(\theta) f_n(\theta)}{4\pi^2 R_{Sm} R_{Am} R_{Sn} R_{An}} \exp i \left\{ k(R_{Sm} - R_{Sn} + R_{Am} - R_{An}) - \omega_0 \tau) \right\}$$

$$\cdot \int_{-\infty}^{+\infty} \int dx\, dx' \left[I_m(x)\, I_n(x') \exp i\, (a_m x - a_n x') \right.$$

$$\left. \cdot \left\langle \exp i \left\{ c_m \zeta(x, t) - c_n \zeta(x', t+\tau) \right\} \right\rangle \right], \qquad (19)$$

where the primed quantities refer to the nth subsection. The time average has been moved inside the integral, because the time variation of the surface is slow compared with the transmitted signal.

Since, in the subsequent analysis, the only function of the term $\exp(-i\omega_0 \tau)$ is to locate the center frequency (carrier frequency) of the received signal spectrum, ω_0 will be set equal to zero, and the calculated spectrum will be symmetric about zero frequency.

Now, by performing the ensemble average on Eq. (19) and by assuming that the distribution of surface heights is Gaussian, we see that the autocovariance becomes

$$C_{mn}(\tau) = \frac{k^2 E^2 f_m(\theta) f_n(\theta) \exp i \left\{ k(R_{Sm} - R_{Sn} + R_{Am} - R_{An}) \right\}}{4\pi^2 R_{Sm} R_{Am} R_{Sn} R_{An}}$$

$$\cdot \int_{-\infty}^{+\infty} \int dx\, dx' \left[I_m(x)\, I_n(x') \exp i(a_m x - a_n x') \right.$$

$$\left. \cdot \exp \left\{ -\sigma^2 \left[c_m^2 + c_n^2 - 2 c_m c_n \rho(x - x', \tau) \right] \right\} \right] . \qquad (20)$$

Since the illumination functions $I_m(x)$ and $I_n(x')$ must express the fact that the acoustic intensity for each subsection has a nonzero value only within the region -L to L, they must be of the form

$$I_m(x) = I\left(\frac{x - X_m}{PL}\right) \text{ and } I_n(x') = I\left(\frac{x' - X_n}{PL}\right), \tag{21}$$

where

P = parameter included to control the shape of the function

X_m = center of the m^{th} subsection

X_n = center of the n^{th} subsection.

When the individual subsection illumination functions are added together, the result must be a good approximation to the actual source beam pattern on the sea surface.

A change of variables is now made in Eq. (20) in order to express the auto-covariance in terms of space lag u.

Let

$$\begin{cases} x = x'' + X_m - \dfrac{u}{2} \\ x' = x'' + X_n + \dfrac{u}{2} \end{cases} . \tag{22}$$

With this change of variables in the integral, the limits on x'' and u are $-\infty$ to $+\infty$ and the Jacobian of the transformation is one. The result is

$$C_{mn}(\tau) = \frac{k^2 E^2 f_m(\theta)\, f_n(\theta)}{4\pi^2 R_{Sm} R_{Am} R_{Sn} R_{An}} \exp i\left\{k(R_{Sm} - R_{Sn} + R_{Am} - R_{An})\right\}$$

$$\cdot \int_{-\infty}^{+\infty} \int dx'' \, du \, I\left(\frac{x'' - \frac{u}{2}}{PL}\right) I\left(\frac{x'' + \frac{u}{2}}{PL}\right)$$

$$\cdot \exp i \left\{ (a_m - a_n) x'' + (a_m X_m - a_n X_n) - \left(\frac{a_m + a_n}{2}\right) u \right\}$$

$$\cdot \exp \left\{ -\sigma^2 \left[c_m^2 + c_n^2 - 2 c_m c_n \rho(u, \tau) \right] \right\} . \qquad (23)$$

Dropping the primes and factoring out the constant phase term results in

$$C_{mn}(\tau) = \frac{k^2 E^2 f_m(\theta) f_n(\theta)}{4\pi^2 R_{Sm} R_{Am} R_{Sn} R_{An}} \exp i \left\{ k(R_{Sm} - R_{Sn} + R_{Am} - R_{An}) + (a_m X_m - a_n X_n) \right\}$$

$$\cdot \int_{-\infty}^{+\infty} \int dx \, du \left[I\left(\frac{x - \frac{u}{2}}{PL}\right) I\left(\frac{x + \frac{u}{2}}{PL}\right) \exp i \left\{ (a_m - a_n) x - \alpha u \right\} \right.$$

$$\left. \cdot \exp \left\{ -\sigma^2 \left[c_m^2 + c_n^2 - 2 c_m c_n \rho(u, \tau) \right] \right\} \right] . \qquad (24)$$

where

$$\alpha \equiv \left(\frac{a_m + a_n}{2}\right) . \qquad (25)$$

Now an integration over x can be effected by factoring and interchanging the order of integration as follows:

$$C_{mn}(\tau) = G_{mn} \exp\left\{-\sigma^2(c_m - c_n)^2\right\} \int_{-\infty}^{+\infty} du \left[H(\beta, u) \exp(-i\alpha u) \right.$$

$$\left. \cdot \exp\left\{-2c_m c_n \sigma^2 \left[1 - \rho(u, \tau)\right]\right\} \right]. \qquad (31)$$

Equation (31) is analagous to Clay and Medwin's Eq. (16), if a Gaussian illumination function is substituted for I. Within the limits of the Kirchoff approximation, Eq. (31) is the solution for the covariance of the received acoustic field reradiated by subsections m and n on the rough surface. Before the total field can be evaluated by means of Eq. (18), the covariance must be separated into coherent and scattered components. This is done by making the "small roughness" or "long wavelength" approximation[16] and retaining only the first two terms in the resulting power series expansion. The first term is the coherent component, whereas the second term is the first-order scattered component. For larger roughness, one could proceed by retaining higher order terms in the expansion. The small roughness approximation is made as follows:

$$\exp\left\{-2c_m c_n \sigma^2 \left[1 - \rho(u, \tau)\right]\right\} = \exp\left\{-2c_m c_n \sigma^2\right\} \exp\left\{2c_m c_n \sigma^2 \rho(u, \tau)\right\}$$

$$\approx \exp(-2c_m c_n \sigma^2)\left[1 + 2c_m c_n \sigma^2 \rho(u, \tau)\right], \qquad (32)$$

for $2c_m c_n \sigma^2 \rho(u, \tau) << 1$.

$$C_{mn}(\tau) = G_{mn} \int_{-\infty}^{+\infty} du \left[\exp(-i\alpha u) \exp\left\{ -\sigma^2 \left[c_m^2 + c_n^2 - 2c_m c_n \rho(u, \tau) \right] \right\} \right.$$

$$\left. \cdot \int_{-\infty}^{+\infty} dx \exp i(a_m - a_n) x \, I\left(\frac{x - \frac{u}{2}}{PL} \right) I\left(\frac{x + \frac{u}{2}}{PL} \right) \right], \qquad (26)$$

where

$$G_{mn} = \frac{k^2 E^2 f_m(\theta) f_n(\theta)}{4\pi^2 R_{Sm} R_{Am} R_{Sn} R_{An}} \exp i\left\{ k(R_{Sm} - R_{Sn} + R_{Am} - R_{An}) + (a_m X_m - a_n X_n) \right\} . \qquad (27)$$

The integral over x can be defined as

$$H(\beta, u) \equiv \int_{-\infty}^{+\infty} dx \exp(i\beta x) \, I\left(\frac{x - \frac{u}{2}}{PL} \right) I\left(\frac{x + \frac{u}{2}}{PL} \right) , \qquad (28)$$

where

$$\beta \equiv (a_m - a_n) . \qquad (29)$$

After this substitution, Eq. (26) becomes

$$C_{mn}(\tau) = G_{mn} \int_{-\infty}^{+\infty} du \left[H(\beta, u) \exp(-i\alpha u) \right.$$

$$\left. \cdot \exp\left\{ -\sigma^2 \left[c_m^2 + c_n^2 - 2c_m c_n \rho(u, \tau) \right] \right\} \right] . \qquad (30)$$

If the exponential involving $\rho(u, \tau)$ is factored, this expression can be written as

Substituting Eq. (32) into Eq. (31) and performing appropriate factoring results in

$$C_{mn}(\tau) \approx G_{mn} \exp\left\{-\sigma^2\left[c_m^2 + c_n^2\right]\right\} \int_{-\infty}^{+\infty} du\, H(\beta, u) \exp(-i\alpha u)$$

$$+ 2c_m c_n G_{mn} \exp\left\{-\sigma^2\left[c_m^2 + c_n^2\right]\right\}$$

$$\cdot \int_{-\infty}^{+\infty} du\, H(\beta, u) \exp(-i\alpha u)\, \sigma^2 \rho(u, \tau) \quad . \tag{33}$$

The coherent component can be integrated after an appropriate illumination function is chosen. As in Clay and Medwin,[20] the Gaussian illumination function is selected in order to eliminate diffraction sidelobes resulting from the source beam pattern and to facilitate a smooth transition between subsections. The function $H(\beta, u)$ is evaluated in Appendix A and is expressed by

$$H(\beta, u) = PL(\pi/2)^{1/2} \exp\left\{-\beta^2 p^2 L^2/8 - u^2/2P^2 L^2\right\} \quad , \tag{34}$$

which, when substituted into the first term of Eq. (33), results in

$$\left\langle \Phi_{cm}(A, t)\, \Phi^*_{cn}(A, t+\tau) \right\rangle \equiv \mathrm{COH}\left\{C_{mn}(\tau)\right\} = P^2 L^2 \pi G_{mn}$$

$$\cdot \exp\left\{-\sigma^2\left[c_m^2 + c_n^2\right] - (P^2L^2/4)(a_m^2 + a_n^2)\right\} \quad , \tag{35}$$

where $\mathrm{COH}\left\{C_{mn}(\tau)\right\}$ is the coherent component of the acoustic autocovariance at a point receiver due to subsections m and n on the rough surface. From Eq. (18), the total coherent component is

$$\mathrm{COH}\left\{C(\tau)\right\} = P^2 L^2 \pi \sum_{m=0}^{M} \sum_{n=0}^{M} G_{mn} \exp\left\{-\sigma^2\left[\left(c_m^2 + c_n^2\right)\right]\right.$$

$$\left. -(P^2 L^2/4)(a_m^2 + a_n^2)\right\} . \qquad (36)$$

The coherent component is thus seen to be independent of τ and, hence, does not contribute to the signal fading. The spectrum of the coherent component, $\mathrm{COH}\left\{A(\omega)\right\}$, is obtained by taking the Fourier transform of $C(\tau)$:

$$\mathrm{COH}\left\{A(\omega)\right\} = \left[2P^2 L^2 \pi^2 \sum_{m=0}^{M} \sum_{n=0}^{M} G_{mn} \exp\left\{-\sigma^2\left[\left(c_m^2 + c_n^2\right)\right]\right.\right.$$

$$\left.\left. -(P^2 L^2/4)(a_m^2 + a_n^2)\right\}\right] \delta(\omega) , \qquad (37)$$

which shows that the specular (coherent) component is an impulse at the transmitted frequency, for conditions of low surface roughness. The magnitude of this component depends upon the source frequency, the experimental geometry, and the mean-square surface roughness. As the roughness increases, the magnitude of the coherent component decreases.

Application of Eq. (37) to the scattering experiment depicted by Figure 5 shows that further simplification of the expression for the coherent component is possible. The position-dependent phase term,

$$\exp i\left\{k\left[(R_{Sm} + R_{Am}) - (R_{Sn} + R_{An})\right] + (a_m X_m - a_n X_n)\right\},$$

is contained in G_{mn} of Eq. (37). Since there is typically at least some jitter in the hydrophone position in measurements at sea, the R's are not constant but vary randomly. If the hydrophone is fixed to the bottom, the R's again vary randomly because of random variations in the ocean stratification that change effective path lengths. Hence, it is desirable to perform an ensemble average on this term over position. This average is not performed for the R's in the denominator because the variation with change in R is very slow compared with the exponent. Now, if the position dependent variables have a standard deviation such that the phase terms range over many radians, then

$$\left\langle \exp i\left\{k\left[(R_{Sm}+P_{Am}) - (R_{Sn}+R_{An})\right] + (a_m X_m - a_n X_n)\right\}\right\rangle$$

$$= \begin{cases} 0 \text{ if } m \neq n \\ 1 \text{ if } m = n \end{cases} = \delta_{m,n} = \text{Kronecker Delta,} \qquad (38)$$

because the phase is distributed uniformly, and over many radians, the cross-product terms nearly cancel.

Averaging over position-dependent phase and substituting from Eq. (27) for G_{mn} yields

$$\text{COH}\left\{A(\omega)\right\} = \left\{(P^2 L^2 k^2 E^2)/2\right.$$

$$\cdot \sum_{m=0}^{M} \sum_{n=0}^{M} f_m(\theta)\, f_n(\theta) \exp\left\{-\sigma^2\left[(c_m^2 + c_n^2)\right]\right.$$

$$\left. - (P^2 L^2/4)(a_m^2 + a_n^2)\right\} / R_{Sm}\, R_{Am}\, R_{Sn}\, R_{An} \Bigg| \delta(\omega) \ . \qquad (39)$$

Grouping the m and n subscripted expressions results in

$$COH\left\{A(\omega)\right\} = \left\{ (P^2 L^2 k^2 E^2)/2 \right.$$

$$\cdot \sum_{m=0}^{M} \sum_{n=0}^{M} \left\{ \frac{\exp\left\{-\sigma^2 c_m^2 - (P^2 L^2 a_m^2/4)\, f_m(\theta)\right.}{R_{Sm}\, R_{Am}} \right\}$$

$$\left. \left\{ \frac{\exp\left\{-\sigma^2 c_n^2 - (P^2 L^2 a_n^2/4) f_n(\theta)\right.}{R_{Sn}\, R_{An}} \right\} \right\} \delta(\omega) \ . \qquad (40)$$

If the terms in braces are called $\hat{P}_m$ and $\hat{P}_n$, respectively, the summation term in Eq. (39) can be written as a single summation over i:

$$\sum_{m=0}^{M} \sum_{n=0}^{M} \hat{P}_m \hat{P}_n = \sum_{i=0}^{M} \left| \hat{P}_i \right|^2 \ .$$

Now, from the geometry of Figure 5,

$$f_i(\theta) = \frac{1 + \left(\frac{D_1}{R_{Si}}\right)\left(\frac{D_2}{R_{Ai}}\right) - \left(\frac{|\bar{X}| + X_i}{R_{Si}}\right)\left(\frac{|\bar{X}| - X_i}{R_{Ai}}\right)}{\left(\frac{D_1}{R_{Si}}\right) + \left(\frac{D_2}{R_{Ai}}\right)} \ , \qquad (41)$$

and, consequently,

$$\mathrm{COH}\left\{A(\omega)\right\} = \frac{1}{2} P^2 L^2 k^2 E^2 \sum_{i=0}^{M} \left| \frac{1}{R_{Si} R_{Ai}} \left(\frac{R_{Si} R_{Ai} + D_1 D_2 - \left(\left| \bar{X} \right|^2 - X_i^2 \right)}{D_1 R_{Ai} + D_2 R_{Si}} \right) \right.$$

$$\left. \cdot \exp \left\{ -\sigma^2 c_i^2 + (P^2 L^2 a_i^2)/4 \right\} \right|^2 \delta(\omega) \quad . \tag{42}$$

The first-order scattered component of the received acoustic signal spectrum will now be derived. From Eq. (33), the scattered component of the autocovariance due to subsections m and n is

$$\left\langle \Phi_{Sm}(A, t)\, \Phi_{Sn}^{*}(A, t+\tau) \right\rangle \equiv \mathrm{SCAT}\left\{ C_{mn}(\tau) \right\}$$

$$= 2 c_m c_n G_{mn} \exp\left\{ -\sigma^2 \left[c_m^2 + c_n^2 \right] \right\}$$

$$\cdot \int_{-\infty}^{+\infty} du\, H(\beta, u) \exp(-i\alpha u)\, \sigma^2 \rho(u, \tau) \quad . \tag{43}$$

Now, define the integral as

$$\int_{-\infty}^{+\infty} du\, H(\beta, u) \exp(-i\alpha u)\, \sigma^2 \rho(u, \tau) \equiv \sigma^2 \Theta(\alpha, \beta, \tau) \quad , \tag{44}$$

in analogy to Parkins'[16] procedure for the case of single-area scattering. Then, substituting Eq. (44) into Eq. (43), we obtain

$$\text{SCAT}\left\{C_{mn}(\tau)\right\} = 2c_m c_n G_{mn} \exp\left\{-\sigma^2\left[c_m^2 + c_n^2\right]\right\} \sigma^2 \Theta(\alpha, \beta, \tau) \ . \qquad (45)$$

The spectral contribution from the m^{th} and n^{th} subsections, SCAT $\left\{A_{mn}(\omega)\right\}$ is determined by taking the Fourier transform of Eq. (45) with the result that

$$\text{SCAT}\left\{A_{mn}(\omega)\right\} = 2c_m c_n G_{mn} \exp\left\{-\sigma^2\left[c_m^2 + c_n^2\right]\right\} \sigma^2 W(\alpha, \beta, \omega) \ , \qquad (46)$$

where

$$\sigma^2 W(\alpha, \beta, \omega) \equiv \int_{-\infty}^{+\infty} d\tau \exp(i\omega\tau)\, \Theta(\alpha, \beta, \tau) \ . \qquad (47)$$

The long-crested, linear, Eulerian model of random gravity waves (Pierson,[39,40] and Neumann and Pierson[41]) is employed to determine $\rho(u, \tau)$ in order to evaluate $\sigma^2 \Theta(\alpha, \beta, \tau)$.

In this model, long-crested Airy (small amplitude) waves are assumed to be propagating parallel to an acoustic transmitter-receiver line. The sea surface elevation $\zeta(x_i, t_i)$ above some mean level $\zeta = 0$ is

$$\zeta(x_i, t_i) = \int_0^{\infty} \cos\left(\frac{\Omega^2}{g} x_i - \Omega t_i + \epsilon_i\right) \sqrt{2S(\Omega)\, d\Omega} \ , \qquad (48)$$

where

x_i = distance along the source receiver line

t_i = time

Ω = surface wave radian frequency

g = acceleration due to gravity

$S(\Omega)$ = ocean surface frequency spectrum

ϵ_i = random phase .

The general properties of this model, as well as proofs of limit theorems pertaining to the term $\sqrt{2S(\Omega)\, d\Omega}$, are given in Pierson,[40] Neumann and Pierson,[41] and Kinsman.[42] The model includes the following features:

1. It is characterized by an invariant probabilistic structure, i.e., the statistical properties of specific samples never change.

2. The waves are all traveling in the same direction (long-crested).

3. The randomness enters the model through the phase terms ϵ_i . The phase of each (i^{th}) wave is between 0 and 2π , with all values being equally likely, i.e., the probability of occurrence of a phase angle between ϕ and $\phi + d\phi$ is

$$p(\phi < \epsilon_{2j+1} < \phi + d\phi) = \frac{d\phi}{2\pi} \quad . \tag{49}$$

Thus, each surface generated by Eq. (48) is identical except for the phase.

4. The model is strictly valid only for infinitely deep ocean gravity waves, where the frequency Ω and the wave number K are related by the dispersion relation:

$$\Omega^2 = gK \quad . \tag{50}$$

From Eq. (48), the covariance function $\sigma^2_\zeta(u, \tau)$ is then formed by taking the ensemble average of the product of $\zeta(x_{i1}, t_{i1})$ and $\zeta(x_{i2}, t_{i2})$ as follows:

$$\left\langle \zeta(x_{j1}, t_{j1})\, \zeta(x_{j2}, t_{j2}) \right\rangle = \sigma^2 \rho(u, \tau) = \int_0^\infty d\Omega \cos\left(\frac{\Omega^2}{g} u - \Omega \tau\right) S(\Omega) \ , \qquad (51)$$

where

$u = x_{j1} - x_{j2}$

$\tau = t_{j1} - t_{j2}$

Ω = radian frequency

$S(\Omega)$ = surface wave-height frequency spectrum

$$\sigma^2 = \int_0^\infty d\Omega S(\Omega)$$

$\rho(u, \tau)$ = autocorrelation function.

Equation (51) represents the model as it will be used in further applications in this study. This equation represents a traveling wave-like correlation function in space-time. It bears many similarities to the theoretical correlation functions employed in the acoustic studies of Clay and Medwin[20] and the water wave studies of Clay et al.[43]

Now, Eq. (51) can be rewritten as the sum of exponential terms:

$$\sigma^2 \rho(u, \tau) = \frac{1}{2} \int_0^\infty d\Omega S(\Omega) \exp\left\{ i \left(\frac{\Omega^2}{g} u - \Omega \tau \right) \right\}$$

$$+ \frac{1}{2} \int_0^\infty d\Omega S(\Omega) \exp\left\{ -i \left(\frac{\Omega^2}{g} u - \Omega \tau \right) \right\} \ . \qquad (52)$$

When this result is substituted into Eq. (44) and after collecting terms on u, the result is

$$\sigma^2\Theta(\alpha,\beta,\tau)=\frac{1}{2}\int_0^{\infty}d\Omega S(\Omega)\int_{-\infty}^{+\infty}du\left[H(\beta,u)\exp\left\{-i\left(\alpha-\frac{\Omega^2}{g}\right)u\right\}\exp\left\{-i\Omega\tau\right\}\right]$$

$$+\frac{1}{2}\int_0^{\infty}d\Omega S(\Omega)\int_{-\infty}^{+\infty}du\left[H(\beta,u)\exp\left\{-i\left(\alpha+\frac{\Omega^2}{g}\right)u\right\}\right.$$

$$\left.\cdot\exp\left\{i\Omega\tau\right\}\right]. \tag{53}$$

Now, by defining

$$\left.\begin{aligned}\bar{H}\left(\beta,\alpha-\frac{\Omega^2}{g}\right)&\equiv\frac{1}{2\pi}\int_{-\infty}^{+\infty}du\exp\left\{-i\left(\alpha-\frac{\Omega^2}{g}\right)u\right\}H(\beta,u)\\ \bar{H}\left(\beta,\alpha+\frac{\Omega^2}{g}\right)&\equiv\frac{1}{2\pi}\int_{-\infty}^{+\infty}du\exp\left\{-i\left(\alpha+\frac{\Omega^2}{g}\right)u\right\}H(\beta,u)\end{aligned}\right\} \tag{54}$$

and substituting Eq. (54) into Eq. (53), we obtain

$$\sigma^2\Theta(\alpha,\beta,\tau)=\pi\int_0^{\infty}d\Omega S(\Omega)\bar{H}\left(\beta,\alpha-\frac{\Omega^2}{g}\right)\exp(-i\Omega\tau)$$

$$+\pi\int_0^{\infty}d\Omega S(\Omega)\bar{H}\left(\beta,\alpha+\frac{\Omega^2}{g}\right)\exp(i\Omega\tau)\ . \tag{55}$$

The spectrum function $\sigma^2 W(\alpha, \beta, \omega)$ is derived by taking the Fourier transform of Eq. (55):

$$\sigma^2 W(\alpha, \beta, \omega) = \pi \int_{-\infty}^{+\infty} \int_{0}^{\infty} d\tau \, d\Omega \exp\left\{ i(\omega - \Omega)\tau \right\} S(\Omega) \bar{H}\left(\beta, \alpha - \frac{\Omega^2}{g}\right)$$

$$+ \pi \int_{-\infty}^{+\infty} \int_{0}^{\infty} d\tau \, d\Omega \exp\left\{ i(\omega + \Omega)\tau \right\} S(\Omega) \bar{H}\left(\beta, \alpha + \frac{\Omega^2}{g}\right). \quad (56)$$

After interchanging the order of integration and integrating on τ, the result is

$$\sigma^2 W(\alpha, \beta, \omega) = \pi \int_{0}^{\infty} d\Omega \, S(\Omega) \cdot 2\pi\delta[\omega - \Omega] \bar{H}\left(\beta, \alpha - \frac{\Omega^2}{g}\right)$$

$$+ \pi \int_{0}^{\infty} d\Omega \, S(\Omega) \cdot 2\pi\delta[\omega + \Omega] \bar{H}\left(\beta, \alpha + \frac{\Omega^2}{g}\right). \quad (57)$$

Since the delta function "samples" the integral at $\Omega = \omega$ and $\Omega = -\omega$, respectively, it follows that

$$\sigma^2 W(\alpha, \beta, \omega) = 2\pi^2 \bar{H}\left(\beta, \alpha - \frac{\omega^2}{g}\right) S(\omega) U(\omega)$$

$$+ 2\pi^2 \bar{H}\left(\beta, \alpha + \frac{\omega^2}{g}\right) S(-\omega) U(-\omega), \quad (58)$$

where

$U(\omega) = 1$ if $\omega > 0$, and 0 otherwise

$U(-\omega) = 1$ if $\omega < 0$, and 0 otherwise .

Equation (58) can be evaluated by determining the functions $\bar{H}$. This can be done by a method due to Nuttall,[44] the details of which are given in Appendix A. The result is that

$$\bar{H}\left(\beta\,,\ \alpha - \frac{\omega^2}{g}\right) = 4\pi P^2 L^2 \, \mathcal{J}\left[-(PL\beta)/2 - PL\left(\alpha - \frac{\omega^2}{g}\right)\right] \cdot \mathcal{J}\left[-(PL\beta)/2 + PL\left(\alpha - \frac{\omega^2}{g}\right)\right]$$

and

$$\bar{H}\left(\beta\,,\ \alpha + \frac{\omega^2}{g}\right) = 4\pi P^2 L^2 \, \mathcal{J}\left[-(PL\beta)/2 - PL\left(\alpha + \frac{\omega^2}{g}\right)\right] \cdot \mathcal{J}\left[-(PL\beta)/2 + PL\left(\alpha + \frac{\omega^2}{g}\right)\right] , \tag{59}$$

where $\mathcal{J}$ = Fourier transform of the illumination function. For the Gaussian illumination function, Eq. (59) becomes (Appendix A)

$$\bar{H}\left(\beta\,,\ \alpha - \frac{\omega^2}{g}\right) = P^2 L^2 \exp\left\{-\left(P^2 L^2/2\right)\left[\left(\alpha - \frac{\omega^2}{g}\right)^2 + \beta^2/4\right]\right\}$$

and

$$\bar{H}\left(\beta\,,\ \alpha + \frac{\omega^2}{g}\right) = P^2 L^2 \exp\left\{-\left(P^2 L^2/2\right)\left[\left(\alpha + \frac{\omega^2}{g}\right)^2 + \beta^2/4\right]\right\} . \tag{60}$$

Now after substituting Eq. (60) into Eq. (58), applying suitable factoring, and replacing α and β by their defined values $\alpha \equiv \left(\frac{a_m + a_n}{2}\right)$; $\beta \equiv a_m - a_n$, the result is

$$\sigma^2 W(a_m, a_n, \omega) = 2\pi^2 p^2 L^2 \exp\left\{-(p^2L^2/8)(a_m - a_n)^2\right\}$$

$$\cdot \exp\left\{-\left(\frac{p^2L^2}{2}\right)\left[\frac{\omega^2}{g} - \left(\frac{a_m + a_n}{2}\right)\right]^2\right\} S(\omega)\, U(\omega) + 2\pi^2 p^2 L^2 \exp\left\{-(p^2L^2/8)(a_m - a_n)^2\right\}$$

$$\cdot \exp\left\{-\left(\frac{p^2L^2}{2}\right)\left[\frac{\omega^2}{g} + \left(\frac{a_m + a_n}{2}\right)\right]^2\right\} S(-\omega)\, U(-\omega). \qquad (61)$$

After substituting Eq. (61) into Eq. (46) and summing the spectral contributions from all subsections, the scattered received signal spectrum SCAT $A(\omega)$ is seen to be

$$\text{SCAT}\left\{A(\omega)\right\} = 4\pi^2 p^2 L^2 S(\omega)\, U(\omega) \sum_{m=0}^{M} \sum_{n=0}^{M} \left\{ c_m c_n G_{mn} \exp\left\{-\sigma^2\left[c_m^2 + c_n^2\right]\right\}\right.$$

$$\left. \cdot \exp\left\{-\left(\frac{p^2L^2}{8}\right)(a_m - a_n)^2\right\} \exp\left\{-\left(\frac{p^2L^2}{2}\right)\left[\frac{\omega^2}{g} - \left(\frac{a_m + a_n}{2}\right)\right]^2\right\}\right\}$$

$$+ 4\pi^2 p^2 L^2 S(-\omega)\, U(-\omega) \sum_{m=0}^{M} \sum_{n=0}^{M} \left\{ c_m c_n G_{mn} \exp\left\{-\sigma^2\left[c_m^2 + c_n^2\right]\right\}\right.$$

$$\left. \cdot \exp\left\{-\left(\frac{p^2L^2}{8}\right)(a_m - a_n)^2\right\} \exp\left\{-\left(\frac{p^2L^2}{2}\right)\left[\frac{\omega^2}{g} + \left(\frac{a_m + a_n}{2}\right)\right]^2\right\}\right\}, \qquad (62)$$

where appropriate factoring has been performed.

Equation (62), the scattered acoustic spectrum, when combined with Eq. (42), the coherent component, gives the complete signal spectrum. The scattered spectrum is symmetric about the coherent component, with an up-Doppler component given by the first term of Eq. (62) and a down-Doppler component given by the second term of Eq. (62). The spectrum of the scattered component thus depends on the following:

1. The experimental geometry
2. The incident radiation wavelength
3. The rms surface roughness
4. The surface height frequency spectrum.

Frequencies in the received signal spectrum will be emphasized when

$$\frac{\omega^2}{g} = \pm\left(\frac{a_m + a_n}{2}\right) , \tag{63}$$

because the functions

$$\exp\left\{-\frac{p^2L^2}{2}\left[\frac{\omega^2}{g} \pm \left(\frac{a_m + a_n}{2}\right)\right]^2\right\}$$

have maxima at these values. These are the resonance relations connecting the frequency and geometry of the experiment with the component waves of the sea surface. The sums of the direction cosines, $(a_m + a_n)/2$, behave like water wave numbers in determining the possible scattered frequencies in the received acoustic spectrum, through the "dispersion relation" $\frac{\omega^2}{g} = \pm\left(\frac{a_m + a_n}{2}\right)$. However, since the exponential functions do have nonzero values for $\frac{\omega^2}{g} \neq \pm\left(\frac{a_m + a_n}{2}\right)$,

small contributions will enter the sum from these values of ω .

Since the scattered spectrum predicted by this equation is symmetric about the coherent component, it is necessary to consider only one of the terms. The positive term only will be treated in the work that follows. This term will be defined as

$$A_1(\omega) \equiv 4\pi^2 P^2 L^2 S(\omega) \sum_{m=0}^{M} \sum_{n=0}^{M} \left\{ c_m c_n \exp\left\{ -\sigma^2 \left[c_m^2 + c_n^2 \right] \right\} \right.$$

$$\left. \cdot \exp\left\{ -\left(\frac{P^2 L^2}{8} \right) (a_m - a_n)^2 \right\} \exp\left\{ -\left(\frac{P^2 L^2}{2} \right) \left[\frac{\omega^2}{g} - \left(\frac{a_m + a_n}{2} \right) \right]^2 \right\} \right\} . \quad (64)$$

Now, when Eq. (64) is applied to the scattering experiment depicted in Figure 5 and when a procedure similar to that for the coherent component is followed, i.e., Eqs. (37) to (42), the result is

$$A_1(\omega) = (k^4 E^2 P^2 L^2) \exp\left\{ -(p^2 L^2 \omega^4 / 2g^2) \right\} S(\omega) \sum_{i=0}^{M} \left| F_i(\omega) \right|^2 , \quad (65)$$

where

$$F_i(\omega) \equiv \frac{R_{Si} R_{Ai} + D_1 D_2 - (|\bar{X}|^2 - X_i^2))}{R_{Si} R_{Ai}}$$

$$\cdot \exp\left\{ -\sigma^2 c_i^2 - (P^2 L^2 a_i^2)/4 + P^2 \omega^2 a_i / 2g \right\} . \quad (66)$$

Equation (65) represents the positive, first-order sideband of an acoustic signal re-radiated by a rough, moving, long-crested sea surface. It is limited to cases of low

surface roughness in such a manner that the term $2c_m c_n \sigma^2 \rho(v, \tau)$ must be < 1 in Eq. (32). This condition is reasonable for low sea state underwater sound experiments using low-frequency acoustic waves at large angles of incidence relative to the sea surface. Equation (65) will be a better representation of the scattering from the swell rather than a representation of scattering from the locally generated sea, since the swell is more nearly long-crested than is the sea.[45]

Equation (65) represents the scattered acoustic spectrum as the product of the ocean surface wave-height spectrum and a weighting function, i.e.,

$$A_1(\omega) = S(\omega)\ B(\omega)\ , \tag{67}$$

where

$$B(\omega) = B(\omega, a_i, c_i, \sigma^2) = (k^4 E^2 P^2 L^2) \exp\left\{-\left(P^2 L^2 \omega^4 / 2g^2\right)\right\} \left\{\sum_{i=0}^{M} \left| F_i(\omega) \right|^2\right\}, \tag{68}$$

which depends on the acoustic frequency, the experimental geometry, and the mean-square wave height.

3.3 THE OCEAN WAVE-HEIGHT SPECTRUM IN TERMS OF THE ACOUSTIC SCATTERED SPECTRUM

Since the acoustic, first-order, forward-scattered spectrum is the product of the ocean wave-height spectrum $S(\omega)$ and a weighting factor $B(\omega)$, Eq. (67), it is possible, at least in principle, to invert Eq. (67) and solve for $S(\omega)$ when $A(\omega)$ is measured and $B(\omega)$ is known:

$$S(\omega) = A_1(\omega)/B(\omega) \quad . \tag{69}$$

If we think of the acoustic source and receiver setup as an instrument with which to measure properties of the ocean surface, then $B(\omega)$ is the frequency response function of the "instrument." It gives us the frequency band on the surface that can be measured by this means, as well as the gain or weighting over that band.

In the experiments to be discussed in the next chapter, measurements of the acoustic forward-scattered spectrum and the ocean wave-height spectrum made in the BIFI(Block Island-Fishers Island) acoustic range in Block Island Sound will be used to evaluate the usefullness of Eqs. (67) and (69) as analytical tools for studying the sea surface.

4.0 FIELD EXPERIMENTS AND RESULTS

Tolstoy and Clay[38] and Fortuin[34] have summarized the results of the most significant model tank experiments on the scattering of underwater acoustic waves from rough surfaces. The general validity of both the physical optics and the wave expansion theories has been proved for low surface roughness, even under conditions where some of the theoretical assumptions were violated. Thus, sufficient knowledge has been acquired to make experiments at sea both practical and desirable, especially in view of recent advances in signal processing technology.[46,47] However, Marsh and Mellen,[15] Parkins,[16] and Fortuin[34] have noted that few bistatic measurements of surface reflected acoustic signals in the ocean have been reported. In addition, in many of the sea surface scattering experiments described in the literature, measurements of the sea surface were limited to visual observations. Although measurements of ocean wave-height and surface-reflected sound pressure levels have been made,[4,18,48,49,50] a great need still exists for additional scattering measurements at sea under conditions varied enough to test the applicability of existing scattering theory to ocean wave research.

In this chapter, the results from several acoustic surface scattering experiments conducted in Block Island Sound are presented. These experiments involved sinusoidal, omnidirectional acoustic signals transmitted from projectors near Block Island and received by means of two widely separated hydrophones. Ocean wave height was monitored simultaneously by a resistance wave staff, and acoustic and

ocean wave-height data were analyzed for spectral content. Results from the spectral analysis of seven of these experiments are presented with particular attention given to determining relationships between the ocean wave-height spectra and the first-order sidebands in the acoustic spectra. These results will be used to evaluate Eqs. (67) and (69) and to further examine the potential of underwater acoustics as a tool in ocean wind wave studies.

4.1 AREA OF STUDY

The experimental part of this investigation was carried out in the BIFI (Block Island — Fishers Island) acoustic range in Block Island Sound. Block Island Sound (Figure 6) is situated at about latitude 41°10' N and is bounded by Block Island, Fishers Island, Long Island, and the Rhode Island shore line. It is shaped like a parallelepiped and has a surface area of about 400 sq. mi. The mean depth of Block Island Sound is 40 m; the greatest depth is about 100 m, near Fishers Island.

The bottom slopes downward from Fishers Island and the mainland toward Block Island. Near Fishers Island, the bottom is uneven and rocky and has many depressions. Near Block Island, the bottom is quite flat and is composed of sand and mud.

The hydrographic features of Block Island Sound are seasonal and thus result in (1) negative sound speed gradient conditions in summer and early fall and (2) isovelocity or slightly positive sound speed gradient conditions in late autumn, winter, and early spring. These conditions limit surface duct acoustic propagation to the cold season. The results of a velocimeter probe survey made in January 1968 are shown in Figure 7. This section exhibits the slightly positive sound speed gradients

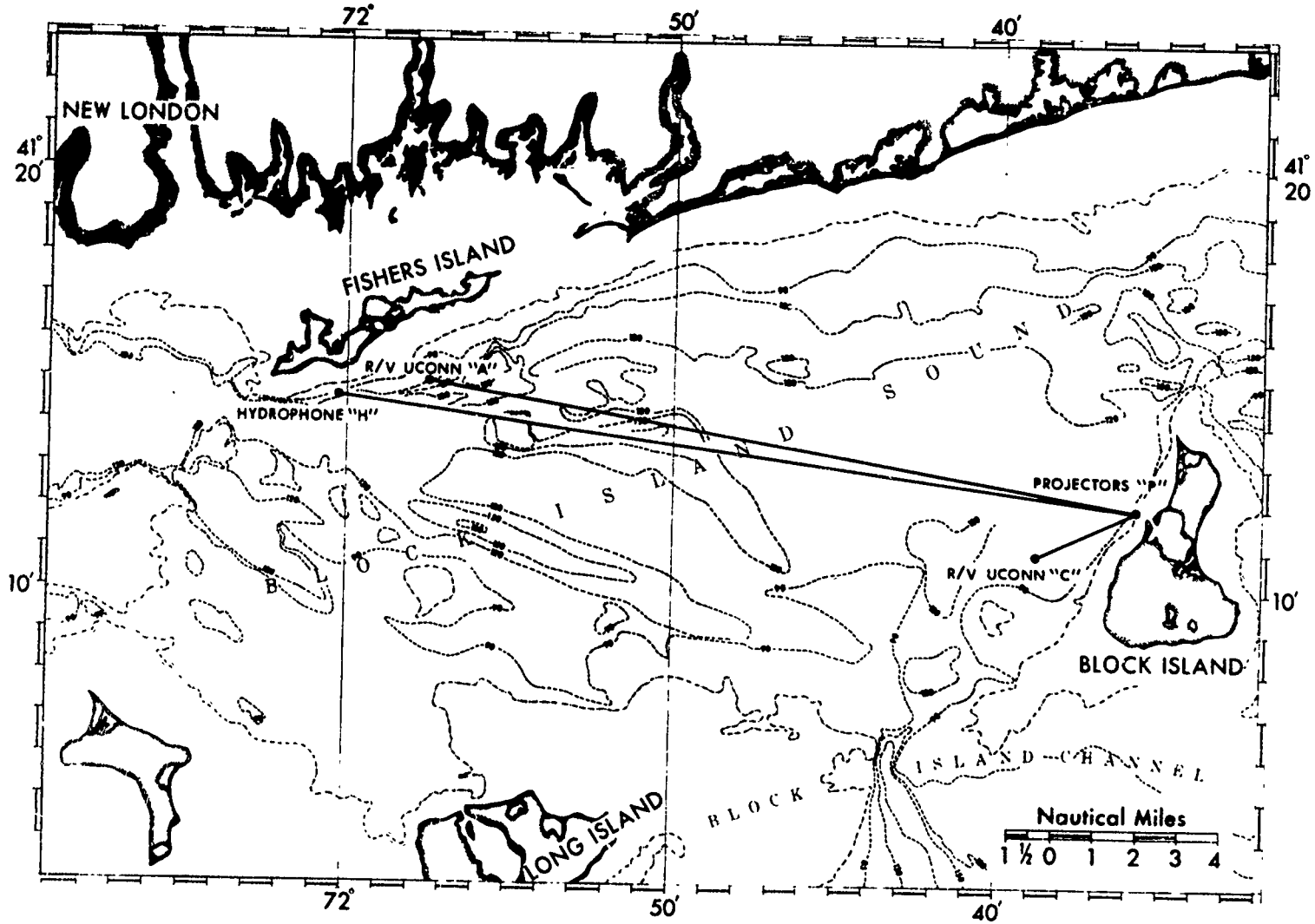

Figure 6. Bottom topography and location of projectors and receivers in Block Island Sound

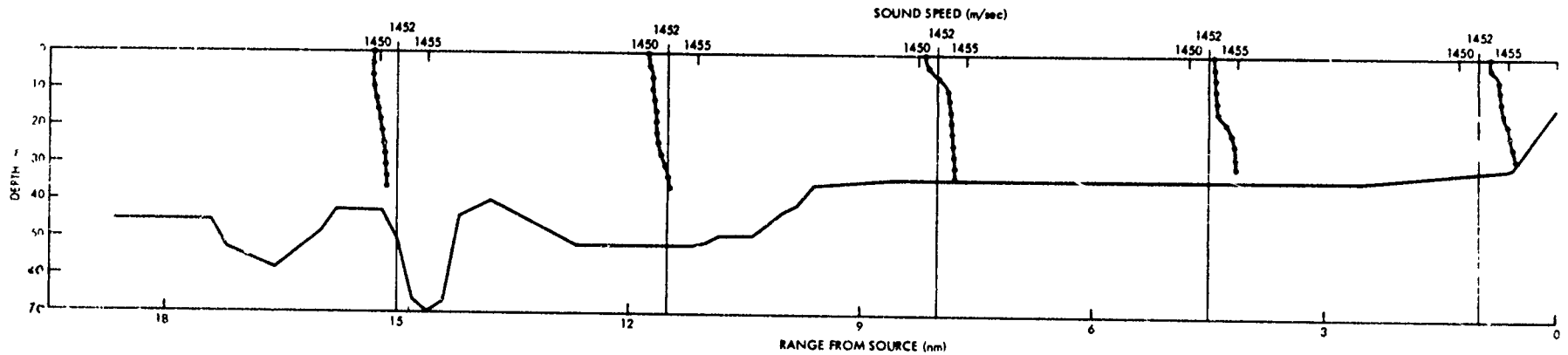

Figure 7. Sound speed profiles along the source-receiver line in Block Island Sound (January 1968)

that are typical in January and February. The horizontal distribution of properties is also characterized by small gradients in winter, as exemplified by Figure 8, which presents isotherms contoured from aerial radiometer data taken in January. A more detailed discussion of the oceanographic features of Block Island Sound is given by Williams,[51] Williams, Azarovitz, and Lamoureaux,[52] and Nalwalk, Rathbun, Robinson, and Riley.[53] Oceanographic and meteorological observations during the time of the measurements are given in Appendix B.

4.2 EXPERIMENTAL SETUP AND INSTRUMENTATION

The facilities of the BIFI Range in Block Island Sound (Figure 6) include three bottom-mounted receiving hydrophones at Fishers Island, three bottom-mounted projectors at Block Island, and various types of oceanographic buoys. A complete description of this range is given by Hasse and Schumacher.[54] The acoustic projectors are operated from a manned field station at Block Island, and receiving hydrophones are connected by cable to an unmanned field station at Fishers Island. Both the Block Island and Fishers Island stations are linked by telephone data transmission lines to the BIFI data acquisition and analysis laboratory at the NUSC laboratory in New London.

Block diagrams showing the arrangement of the transmitting and receiving equipment used in the experiments are shown in Figures 9 and 10. Precise signal frequency control was provided by coherent decade frequency synthesizers at the transmitting and receiving locations. These instruments are equipped with tunable quartz-crystal-controlled oscillators with resolution to nine significant figures. They have rms frequency deviations on the order of 3 parts in 10^9. A description

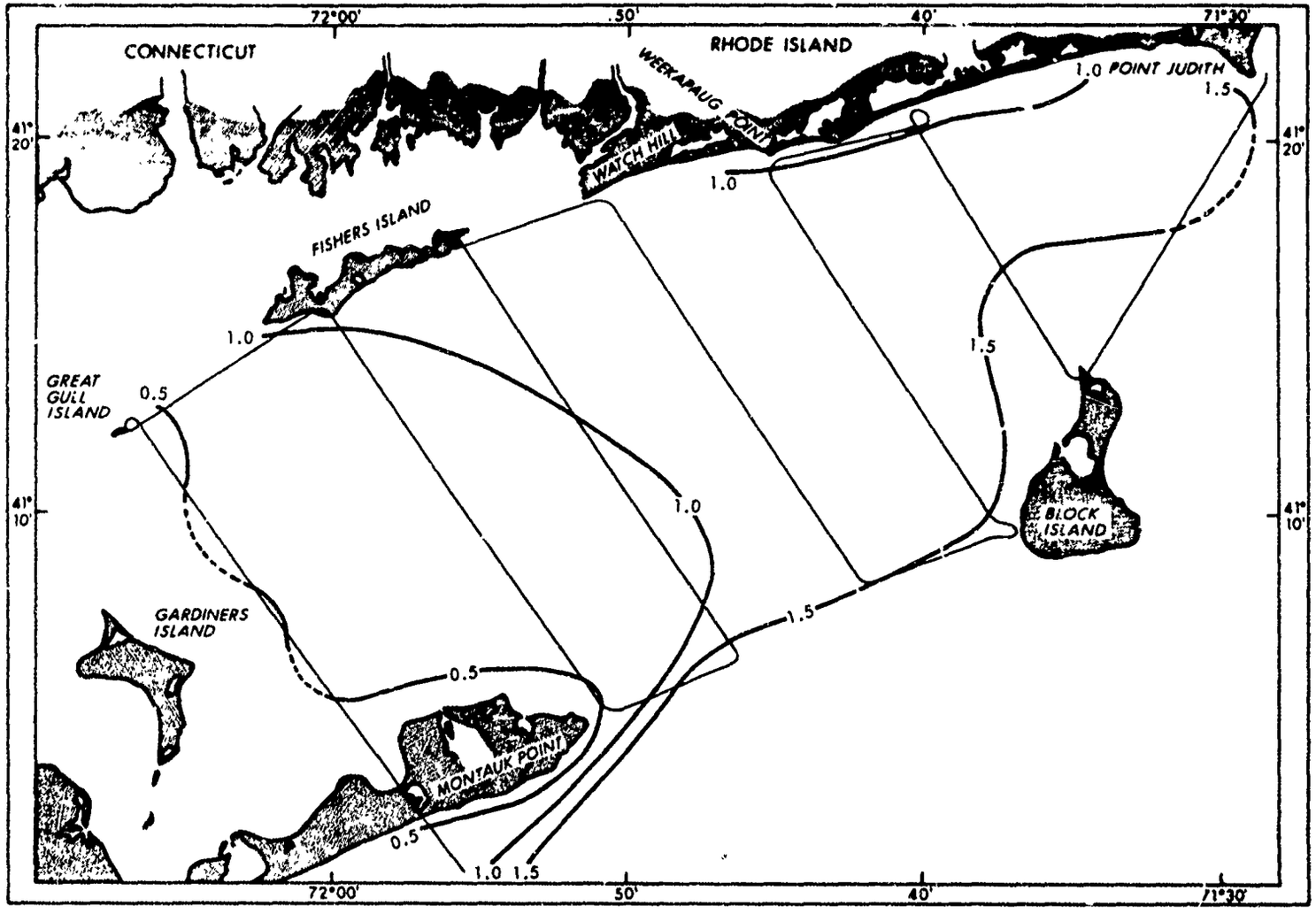

Figure 8. Surface isotherms contoured from aerial radiometer data taken by the Sandy Hook Marine Laboratory (From Williams, Azarovitz, and Lamoureaux.[52])

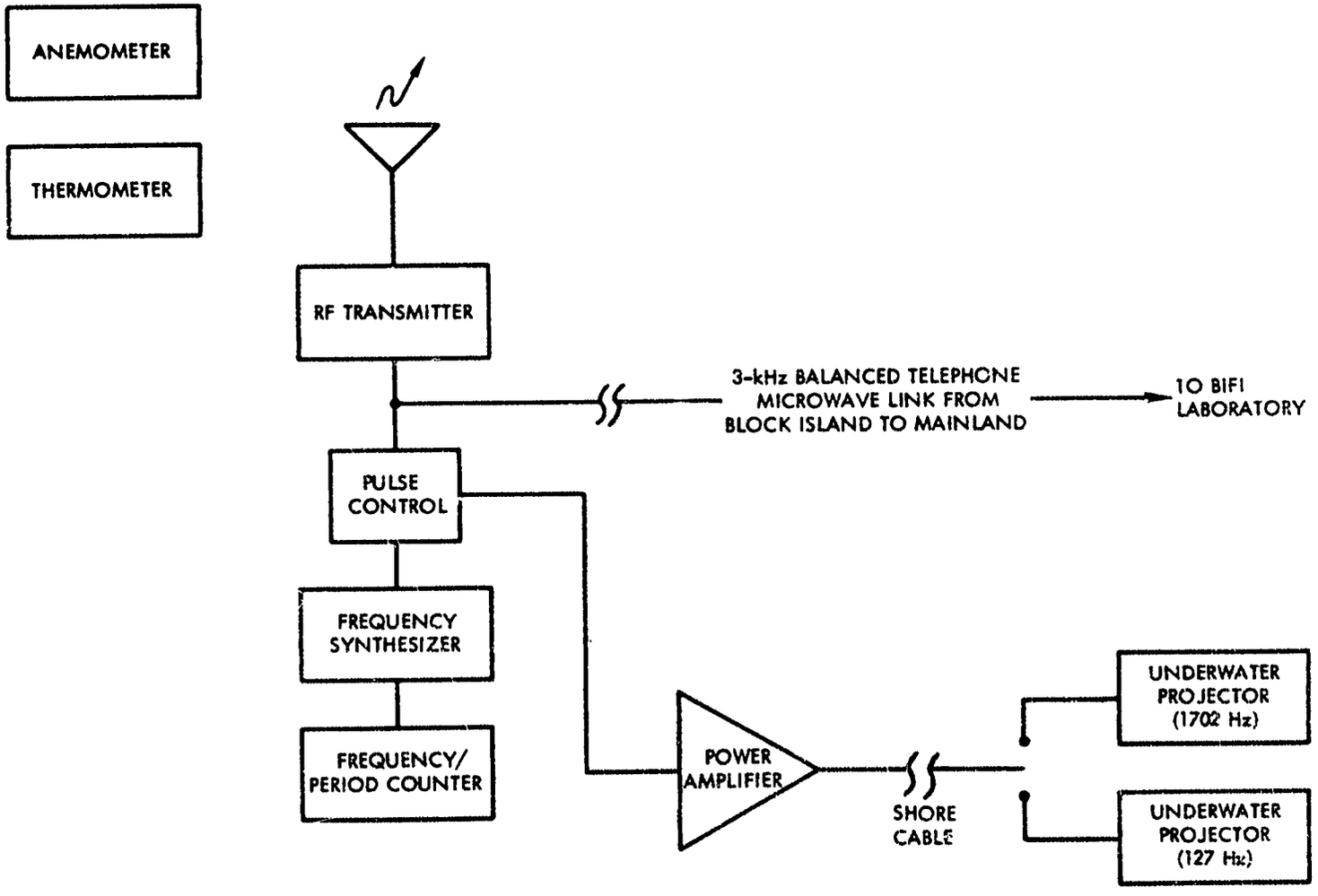

Figure 9. Block diagram of the signal transmitting equipment on Block Island

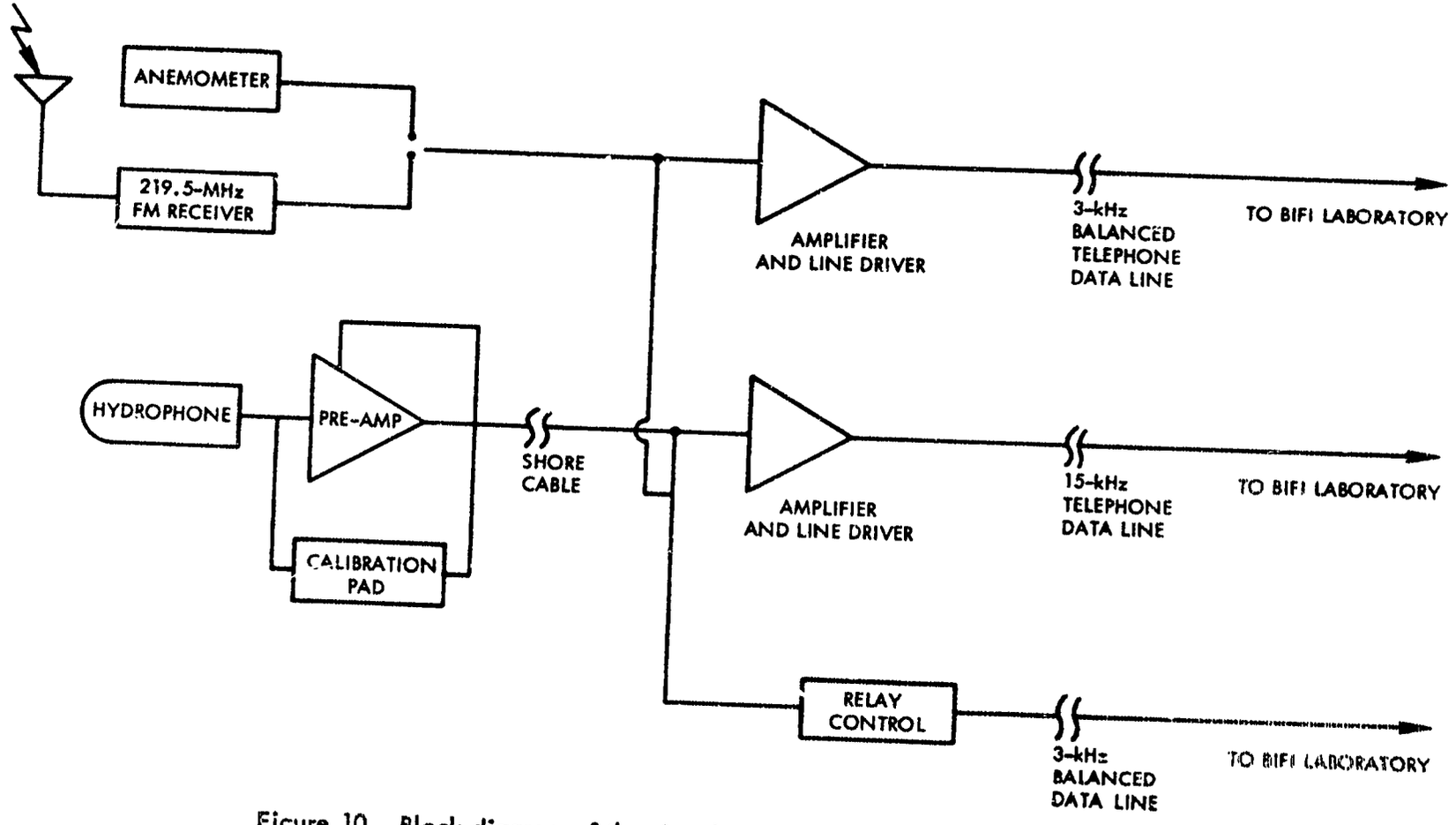

Figure 10. Block diagram of the signal receiving equipment on Fishers Island

of the instrumentation used in this study is given in Appendix C.

4.3 PRELIMINARY EXPERIMENTS

A number of preliminary experiments were performed to determine the feasibility of making a detailed study of the effects of the rough sea surface on sinusoidal signals transmitted across the BIFI range. Although previous studies indicated that surface effects would dominate the short-term signal fading, the multipath and multiple reflection propagation conditions in the BIFI range could mask the surface scattering effect.

In the most significant of these experiments, 1702-Hz tones were transmitted across Block Island Sound, from Block Island to Fishers Island, while ocean surface activity was monitored by an accelerometer wave buoy tethered to a moored buoy equipped with telemetry apparatus. Seventeen runs of 20-min duration each were obtained between 12 April through 30 May 1968. The following conclusions were drawn from these tests[55]:

1. Under calm sea conditions, no frequency spreading occurred above the system noise level.

2. Under negative sound speed gradient conditions (late May), no significant spreading occurred, even though the sea surface was quite rough.

3. During surface duct propagation conditions (early April), when frequent interactions between the acoustic waves and the sea surface occurred, the acoustic signal spectrum obtained from a time history several minutes long exhibited first-order sidebands that were spread in frequency from the carrier by an amount close to the peak frequency in the ocean wind wave spectrum. The level of the sidebands

was about 13 dB below the carrier.

Although these conclusions could be drawn from the 1968 experiments, it was felt that greater experimental accuracy could be obtained in the ocean wave measurements by using a resistance-type wave staff. In oddition, acoustic measurements closer to the transmitter appeared highly desirable, both to compare experimental data with a single-reflection theoretical model and to examine qualitatively the effects of multiple surface reflections. Hence, a series of experiments was planned for the winter of 1969-70.

4.4 ACOUSTIC AND OCEAN WIND WAVE MEASUREMENTS IN BLOCK ISLAND SOUND

Sea surface elevation and underwater surface-reflected sinusoidal signals were obtained simultaneously at both short (4.5 km) and long (31 km) ranges from the acoustic projectors at two different frequencies (127 Hz and 1702 Hz). The wavelengths of these signals were, on the average, 11.4 m and 0.86 m, respectively. Both acoustic projectors are nearly omnidirectional. The short-range measurements were taken from the University of Connecticut's research vessel, the R/V UCONN, a 20-m converted Army T-Boat.

After hydrographic measurements were taken at Positions B and C (Figure 6), a 12-m aluminum spar buoy supporting a 4.6-m resistance wave staff and an omnidirectional, broad-band hydrophone was launched at Position C. The buoy was tethered to the UCONN by means of a 76-m mooring and signal cable with several floats attached. The configuration of the buoy system is shown in Figure 11. Its resonant period of oscillation is over 20 sec, so that it is effectively decoupled from the surface wave motion prevalent in Block Island Sound. After the buoy

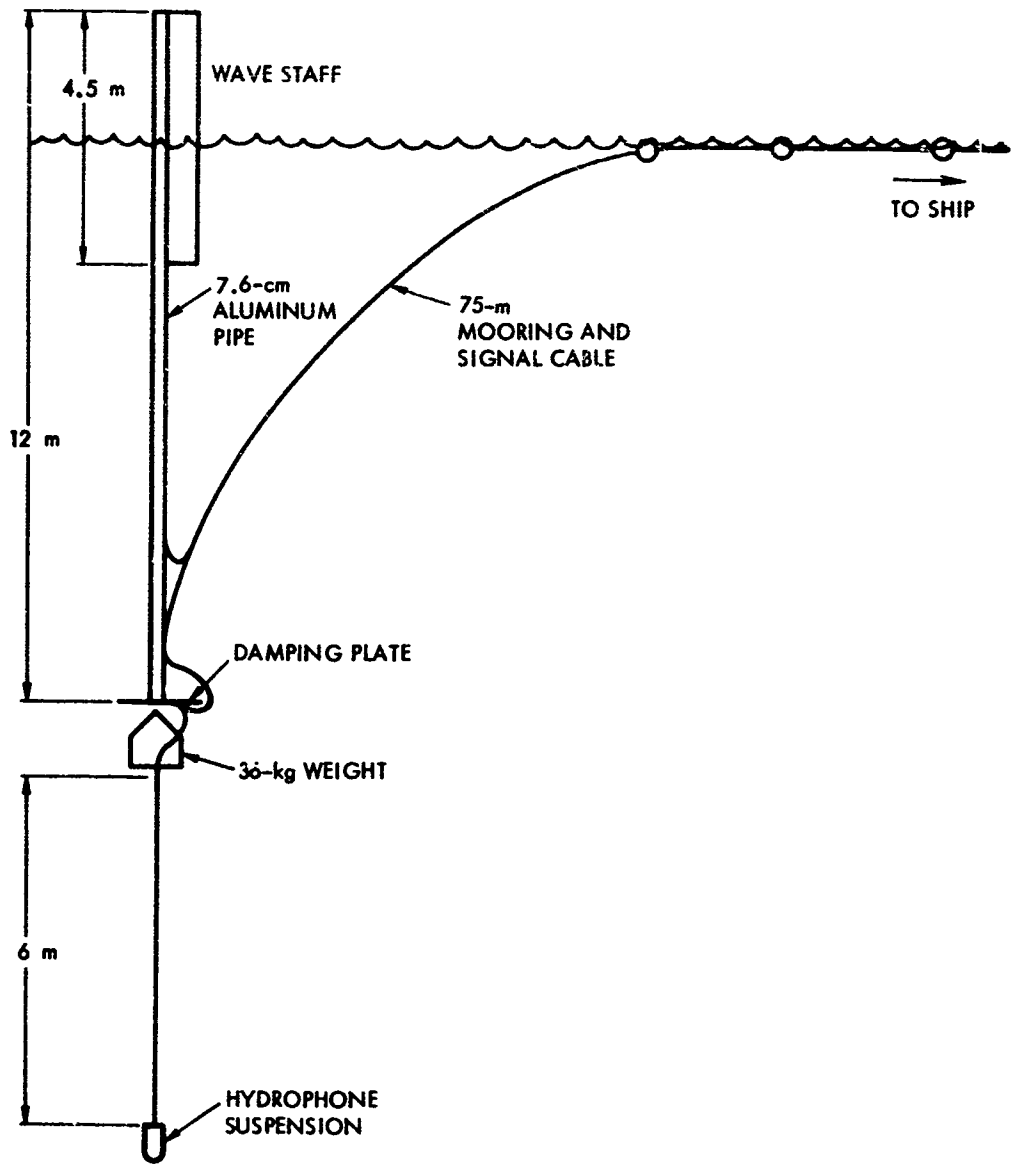

Figure 11. Spar buoy supporting resistance wave staff and hydrophone

position was adjusted (Figure 12), samples of broad-band and narrow-band ambient noise were taken to determine the background noise level. Wind velocity was monitored both onboard the UCONN and at the Block Island field station.

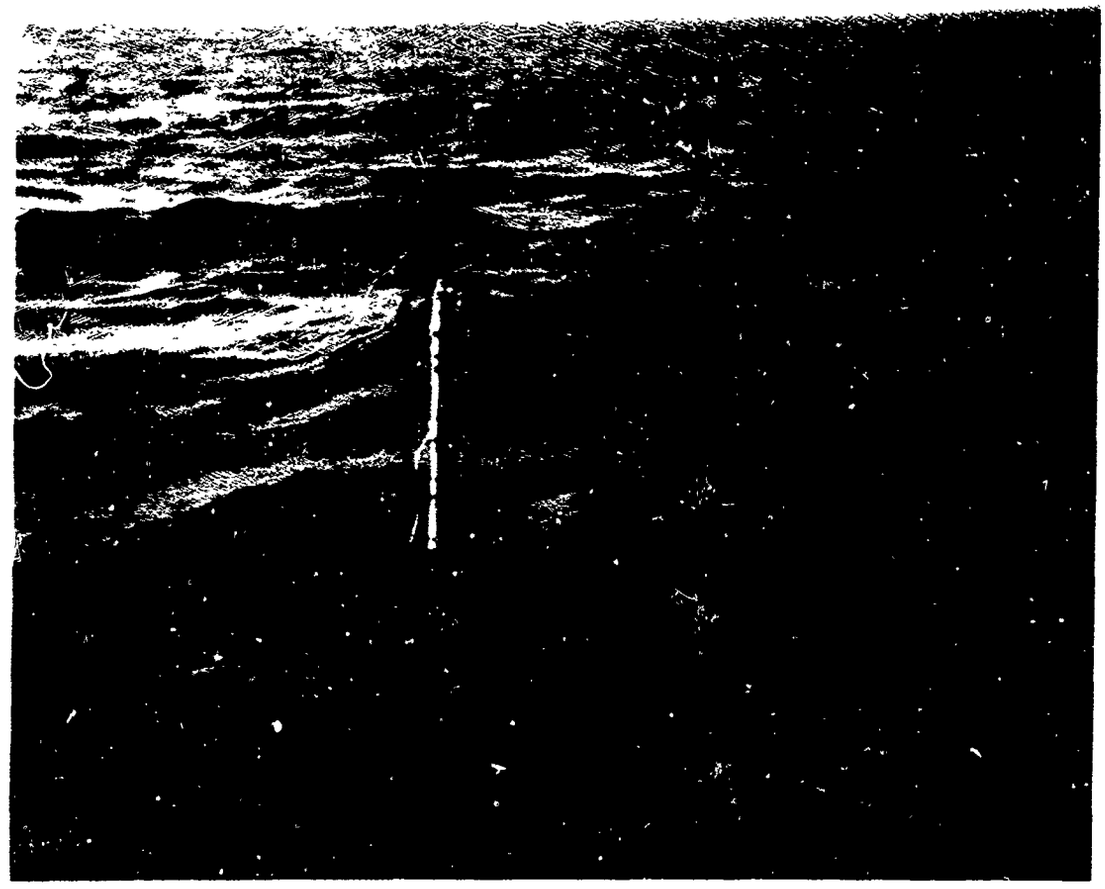

Figure 12. Spar buoy on position for measurements off Block Island (Photograph courtesy Prof. D. Paskausky.)

The wave staff and hydrophone were then calibrated, and a 20-min recording of both the wave height and the transmitted acoustic signal was made. The desire for as high a resolution in the spectrum as possible versus the length of time that the sea surface could reasonably be considered stationary determined the selection of the 20-min time history. Prior to recording, the acoustic signal was amplified,

filtered, and bandshifted to 8 Hz to facilitate analog-to-digital conversion and computer processing. The wave-staff signal was recorded directly on magnetic tape as a varying dc level. During the later experiments in this series, the acoustic signal was transmitted over a radio frequency link and was received, demodulated, bandshifted, and recorded by electronics identical to those used for the underwater signal. This procedure verified that none of the sideband structure in the acoustic signal spectrum was caused by instrumentation. Upon completion of the recording, a second calibration was performed, the second transmitter was switched on, and the procedure was repeated. Other details of the recording, including block diagrams of the electronics, are given in Appendix C.

The acoustic signals from Block Island were received by the Fishers Island hydrophone and transmitted to the BIFI laboratory in New London, where they were recorded on magnetic tape by a procedure similar to that on the UCONN. After the acoustic and ocean wave measurements were completed, the UCONN steamed to Position A and another hydrographic cast was made.

4.5 OPERATIONAL RESULTS

Fifteen runs were made in Block Island Sound between 29 December 1969 and 30 January 1970. During these runs, simultaneous measurements of wave height and sound pressure level were obtained, and the acoustic signal from the Fishers Island hydrophone was recorded at the BIFI laboratory and also aboard the R/V UCONN. Most of the experiments were of 20 min duration, although some were shorter because of operational difficulties, such as ships moving into the area. Although all the experiments produced interesting results, this discussion is limited

to seven cases, which are sufficient to represent a variety of fair weather sea conditions in coastal waters. A summary of the operational data for these experiments is given in Table 1.

It must be pointed out that larger sea states were, of course, encountered during storm conditions, but when such conditions occurred, it was not possible to conduct the experiment because of the difficulty of holding the boat in position and of launching the spar buoy from a pitching deck. In addition, for wind speeds greater than 35 knots, the signal-to-noise ratio for the acoustic signals is normally so low that acoustic reception at Fishers Island is not possible. This is probably the result of high ambient noise levels due to the rough sea, as well as to the formation of a bubble layer near the surface of the water, which greatly increases surface loss on each bounce. Thus, all the data presented in the following sections were acquired during relatively low sea-state conditions.

4.6 DATA PROCESSING AND ANALYSIS

The recorded wave-staff and bandshifted acoustic data were signal-conditioned, low-pass filtered, and digitized simultaneously at a rate of 64 Hz. These procedures were followed in order to prevent aliasing of the computed signal spectra. Details on the techniques used in this study are presented in Appendix D.

Variance spectra were computed by means of the Fast Fourier Transform (FFT) algorithm of Cooley and Tukey (Cooley, Lewis, and Welch[56]). Prior to spectral analysis, the dc component and the linear trend were removed from the data. The time histories were then sectioned into overlapping pieces, which were "windowed" in the time domain to minimize spectral leakage, following the procedures of

Table 1

OPERATIONAL DATA

Date	Run Number	Frequency (Hz)	Wind			Weather		Sea Condition	Remarks
			Speed (knots)	Direction	Duration	Sky	Temperature (°F)		
12/29/69	I	127	15 - 30 gusts to 30	WNW	Constant for past 2 days.	Clear	28	Locally wind-generated sea, no swell. Wind and sea from the same direction. Waves fairly regular at 5 ft.	Extensive whitecaps Ice formed on boat.
1/ 8/70	II	1702	10 - 12	NNW	Relatively constant for past 2 days.	Clear	20	Long, low swell from the S to SE at 2-3 ft. Period about 10 sec. Small wind sea from the NW superimposed on the swell.	Very few whitecaps. Interference effects observed between incoming waves and waves reflected from the mainland.
1/16/70	III	1702	10 - 15	WNW	Relatively constant for past 2 days.	Clear	20	No swell—wind waves relatively constant in direction of the wind. About 3-4 sec in period and 1 - 1 1/2 ft high.	Run taken after 2 days of strong winds due to a high-pressure system. The sea had an extensive capillary wave structure riding on the gravity waves. The small-scale phenomena could be described as "rough."
1/20/70	IV	1702	1 - 5	-	Variable for past 2 days.	8/10 cloud cover.	18	Calm—slight residual swell 1 - 1 1/2 ft.	Closest approximation to a completely flat surface in this series of experiments.
1/26/70	V	1702	5 - 10	-	Variable for past 2 days.	Heavy cloud cover breaking up.	25	4 - 6 ft swell.	Difficult to estimate period because of interference effects.
1/26/70	VI	127	5 - 10	-	Variable for past 2 days.	Heavy cloud cover breaking up.	25	4 - 6 ft swell, predominantly from the S.	Difficult to estimate period because of interference effects.
1/30/70	VII	127	18	NW	Wind backing due to the passage of a cold front.	Heavy clouds had recently broken up due to passage of the front.	38	2 - 3 ft — from NW, with whitecaps; residual swell from SE.	Ship position in lee of Fishers Island. Several hours prior to this run, the swell had been regular from the S; 7 - 10 sec period. After the wind shift the swell was gradually beaten down, but the wind sea increased.

Welch[57] and Bingham, Godfrey, and Tukey.[58] The FFT's were computed (Arnold, Nuttall, Ferrie, and Carter[59]) for each piece, and then the individual estimates were averaged to achieve statistical stability in the sense of Blackmon and Tukey.[60]

In addition, following Jenkins and Watts,[61] window carpentry was applied by trying different windowing functions, and window closing was applied to the time histories by computing average spectra for small transform sizes (large bandwidth) and progressively doubling the transform size until maximum resolution (smallest bandwidth) was achieved. The increased resolution resulted in decreased statistical stability.

By analyzing many samples in this way, it became clear that a transform size of 2,048 data points (resolution of 0.0225 Hz) provided the best trade off between resolution and stability. These considerations are dealt with in greater detail in Appendix D. All spectra presented in this section are resolved to 0.0225 Hz.

The frequency resolution of the electronic system was checked by recording and processing pure tones in the same manner as the data signals. A resolution capability of better than 0.01 Hz was achieved. A field check was obtained by transmitting 127-Hz and 1702-Hz signals from Block Island to the UCONN by means of a radio link. The signals were detected, bandshifted, and recorded by electronics identical to the water path system. Figure 13A shows the spectrum of the 1702 Hz signal, and Figure 13B shows the spectrum of the 127 Hz signal. These tests show that the observed variance in the sidebands of the acoustic signal spectra are a consequence of fluctuations in the ocean medium and are not due to the recording electronics.

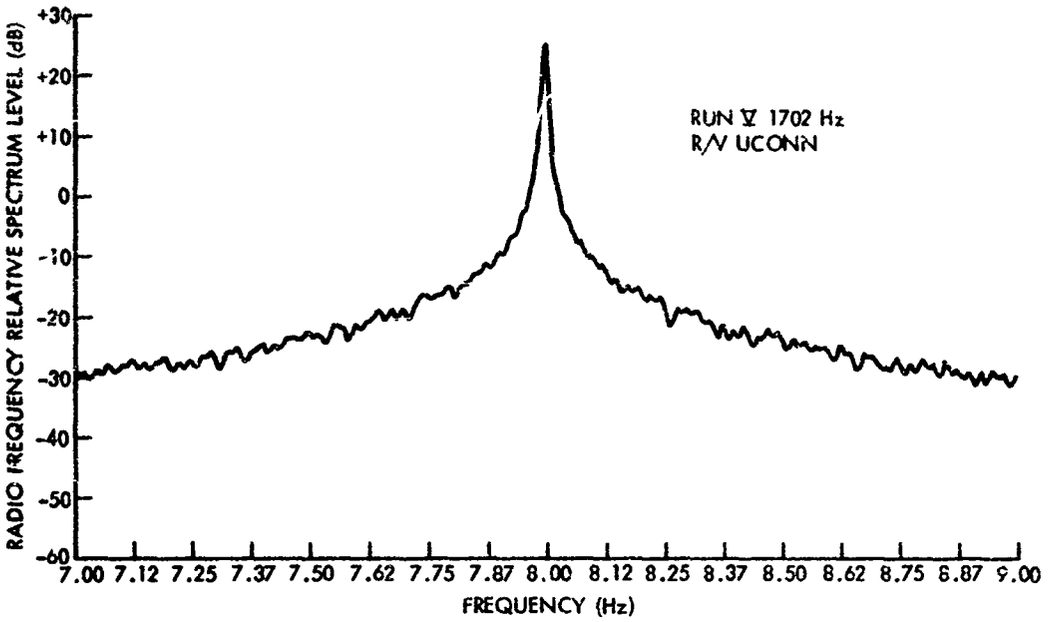

Figure 13 A. Spectrum level of 1702-Hz signal transmitted from Block Island to R/V UCONN via RF link

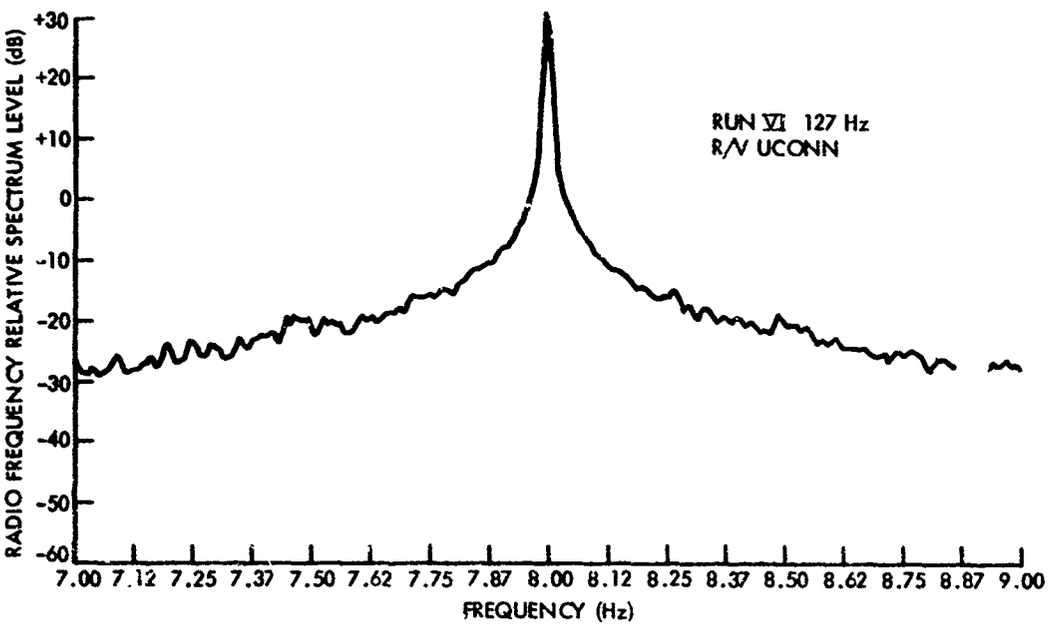

Figure 13 B. Spectrum level of 127-Hz signal transmitted from Block Island to R/V UCONN via RF link

In the presentation of the spectra measured from the UCONN, the ocean wave-height spectrum appears directly above the acoustic signal spectrum. The variance calculated from each wave-height record is presented in Table 2.

Table 2

VARIANCES IN THE OCEAN WAVE-HEIGHT SPECTRA, RUNS I - VII

Run Number	Variance (M^2)
I	0.0591
II	0.0139
III	0.0082
IV	0.0021
V	0.0606
VI	0.0413
VII	0.0132

The center frequency of the acoustic spectra for both the 127-Hz and the 1702-Hz signals is 8 Hz. All acoustic signals were bandshifted to this low frequency in order to facilitate digital analysis of the 20 min data samples required for fine resolution and good statistical stability (Appendix D). In some cases, the peak frequency in the acoustic spectra are not exactly at 8 Hz. This could be the result of three factors: (1) failure to properly tune all frequency synthesizers (Appendix C), (2) nonstationary processes taking place in the ocean, e.g., accelerating currents, (3) drift in the position of the spar buoy supporting the hydrophone. The error in absolute frequency location was corrected by using the peak value in the spectrum as the reference point for determining Doppler shifts (i.e., sideband locations) in the received signal.

Since the sea surface modulates the transmitted signal, the plots of the acoustic spectra are double-sided, i.e., sum and difference frequencies appear about the carrier frequency. On the other hand, the ocean wave-height spectra are most properly presented as single-sided, positive-frequency spectra. However, the acoustic and wave-height spectra can be compared since zero frequency in the wave-height spectrum corresponds to the bandshifted carrier frequency (f_b) in the acoustic spectrum. The acoustic up-Doppler sideband is readily compared with the wave-height spectrum by aligning frequency f_1 in the wave-height spectrum with frequency $f_1 + f_b$ in the acoustic spectrum. The down-Doppler component is compared by taking the mirror image of the wave-height spectrum about zero frequency and aligning frequency $-f_1$ in the wave-height spectrum with frequency $f_b - f_1$ in the acoustic spectrum. In the following section, peak locations and slopes in the acoustic spectra are expressed in terms of the magnitude of the frequency displacement away from the carrier. In cases of asymmetry, the down-Doppler component is used.

4.7 RESULTS OF THE BLOCK ISLAND SOUND EXPERIMENTS

As a first example, consider Run I (Table 1), which was obtained near the end of a period of strong northwesterly winds (Appendix B). The wind-driven sea surface frequency spectrum was single-peaked with maximum energy at about 0.25 Hz, as seen in Figure 14A. No swell components are evident in this spectrum. The sea surface during this run was characterized by a high percentage of foam and whitecaps. The acoustic spectrum shows considerable broadening around the transmitted frequency (the location of the specular component). Nuttall and Cron[19] refer to this as "zeroeth order scattering." A distinct down-Doppler sideband occurs

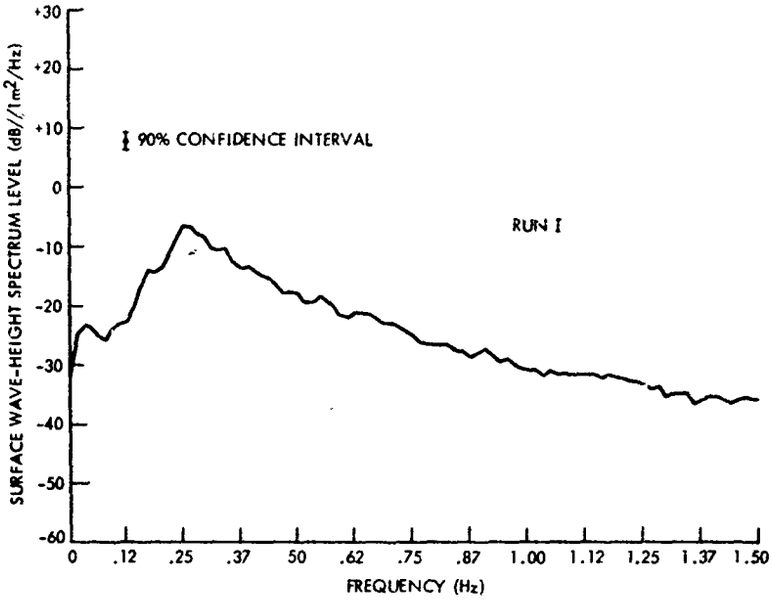

Figure 14A. Spectrum level of ocean wave height at Position C for Run I

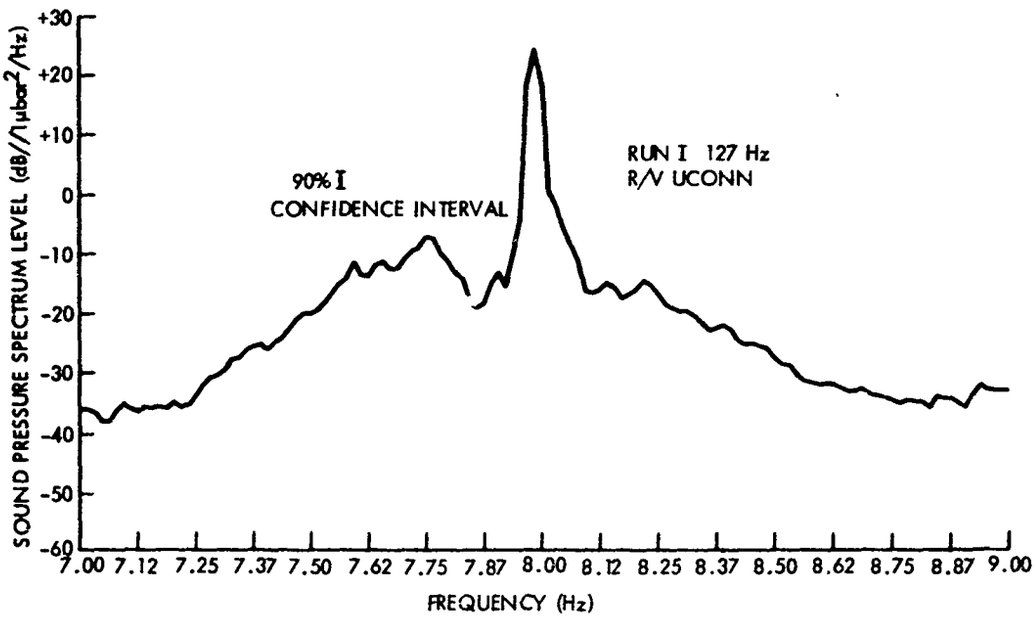

Figure 14B. Spectrum level of acoustic signal at Position C for Run I

33 dB below the peak level of the carrier. The asymmetry in the sidebands is probably due to multipath interference.

A comparison of the down-Doppler scattered spectrum (defined here rather arbitrarily as between 7.87 Hz and 7.25 Hz) with the mirror image of the ocean wave-height spectrum, as described above, shows that the peaks match reasonably well. The acoustic peak is 0.016 Hz (1 frequency bin) closer to the reference or "zero" frequency than is the wave-height spectrum. Since the two spectra represent estimates from random processes, this small difference in location is probably not significant. The mean slopes of the spectra are nearly equal between 0.25 Hz and 0.5 Hz, but between 0.5 Hz and 0.75 Hz the sea surface spectrum slopes down toward higher frequency at about 24 dB/Hz, whereas the acoustic spectrum slopes away from the carrier at about 53 dB/Hz. Frequencies displaced by more than $\pm$0.75 Hz from the carrier, contain no information since the noise floor of the recording and processing systems has been reached.

An example from a sea surface composed of a swell component plus residual wind waves is given by Run II. In this case, the incoming swell was running almost counter to the sea (Table 1). In addition, swell waves that had been reflected from the beach were propagating in the same direction as the wind waves. The swell component is quite possibly the result of a storm that had passed off the Atlantic coast at Norfolk at 0700 hr the previous day.[62]

The spectra at Position C are presented in Figure 15. The ocean wave-height spectrum exhibits the swell peak at 0.09 Hz and the local wind wave peak at 0.34 Hz. The acoustic spectrum exhibits a greatly broadened central peak, i.e., considerable zero-order scattering. First-order sidebands occur at $\pm$.08 Hz from

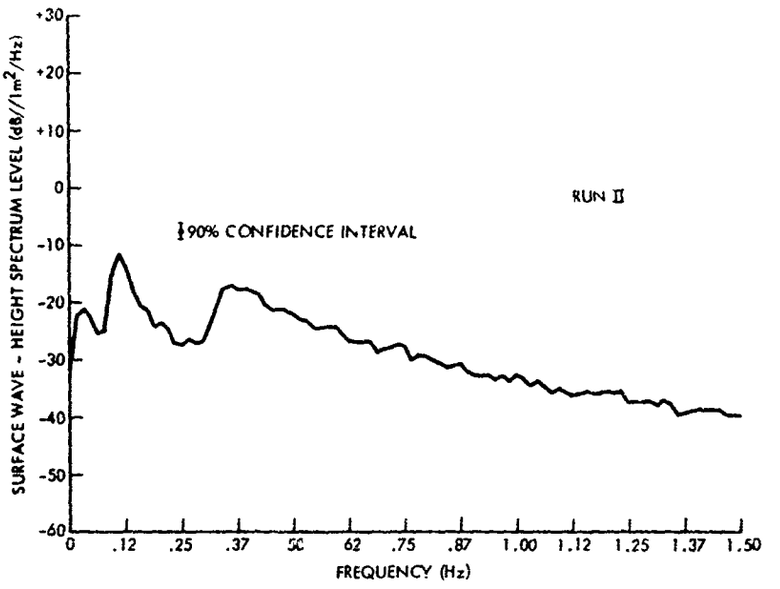

Figure 15A. Spectrum level of ocean wave height at Position _ for Run II

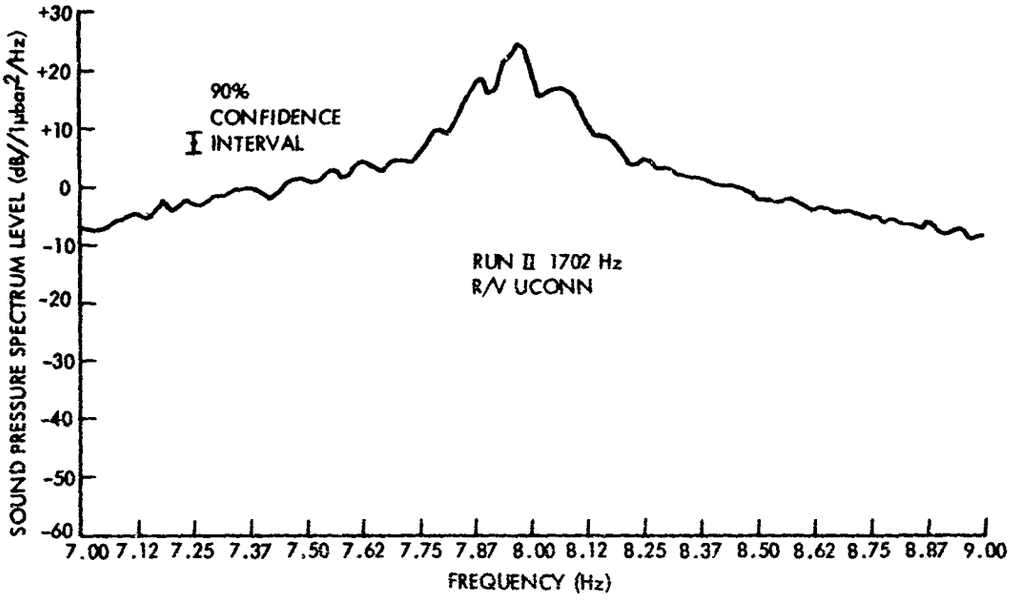

Figure 15B. Spectrum level of acoustic signal at Position C for Run II

the carrier at about 6 dB below the peak level. From the wave-height spectrum, the wind wave peak is 5 dB below the swell peak, whereas the corresponding peaks in the acoustic spectrum differ by 12 dB. This is an indication that the low-frequency wave components present in the sea surface are the primary forward scatterers for the acoustic waves. Between 0.5 Hz and 0.75 Hz, the wave-height spectrum slopes down at 24 dB/Hz, whereas the acoustic spectrum slopes at 18 dB/Hz. Figure 16 shows the acoustic spectrum received at Fishers Island for Run II. This spectrum shows a narrower specular component with first-order sidebands 9 dB and 11 dB below the peak carrier level. Between 0.25 Hz and 0.5 Hz, the slope in the acoustic spectrum at Position C is about 18 dB/Hz, whereas the spectrum at Fishers Island slopes at 36 dB/Hz. Between 0.5 Hz and 0.75 Hz, both spectra slope at 18 dB/Hz.

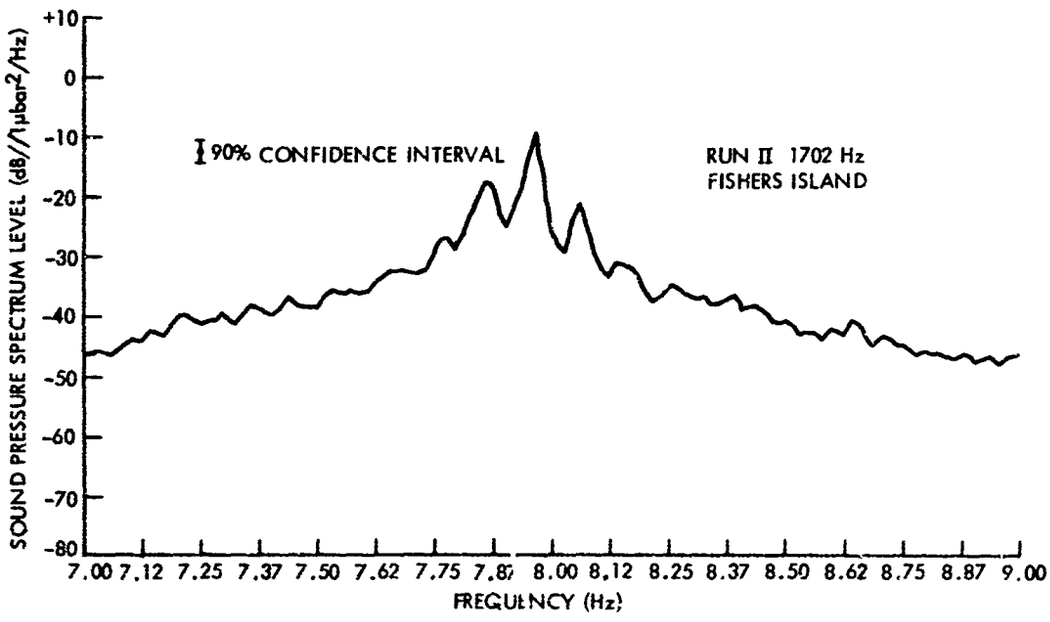

Figure 16. Spectrum level of acoustic signal at Fishers Island for Run II

Run III was made after several days of winds from the west-northwest. Before and during the run, the sea was calming down, with local wind waves and residual wind waves dominating the wave-height spectrum (Figure 17A), which peaks at 0.4 Hz. Again the slope between 0.5 Hz and 0.75 Hz (and beyond to 1 Hz) is 24 dB/Hz. The corresponding acoustic spectrum (Figure 17B) exhibits broad sidebands having a peak value displaced by 0.4 Hz from the carrier. The level of the sidebands is about 17 dB below the peak carrier level. The spectrum at Fishers Island for Run III (Figure 18) exhibits a slightly broadened specular component but no clearly discernible sidebands.

Conditions of a perfectly flat surface would have been desirable as a reference for these experiments, but in the ocean such a surface never exists. The closest approximation to a completely flat surface occurred on 20 January (Run IV), when a very slight residual swell was running but ripples were nearly absent, i.e., the sea was becoming glassy. The spectra at Position C are shown in Figure 19. The wave-height spectrum exhibits the swell peak at about 0.12 Hz. Between 0.5 Hz and 0.75 Hz, the spectrum slopes down at 32 dB/Hz, which is considerably steeper than the slopes for the previous three runs. This is the result of the near-glassy surface conditions. The acoustic spectrum exhibits very weak first-order sidebands at about $\pm$0.1 Hz from the carrier. The level of the sidebands is 25 dB below the carrier. Between 0.5 and 0.75 Hz, the spectrum slopes down at 32 dB/Hz.

The spectrum at Fishers Island (Figure 20) exhibits well-defined first-order sidebands at about $\pm$0.12 Hz from the carrier and 16 dB below the carrier level.

The discrepancy in the location of the sideband peak in the acoustic spectrum at Position C, as compared with the other two spectra, could be due to the fact that

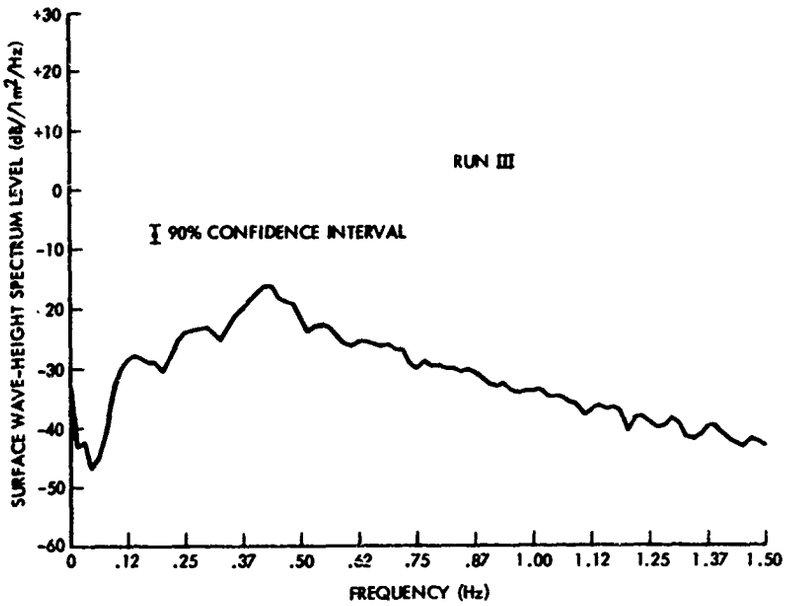

Figure 17A. Spectrum level of ocean wave height at Position C for Run III

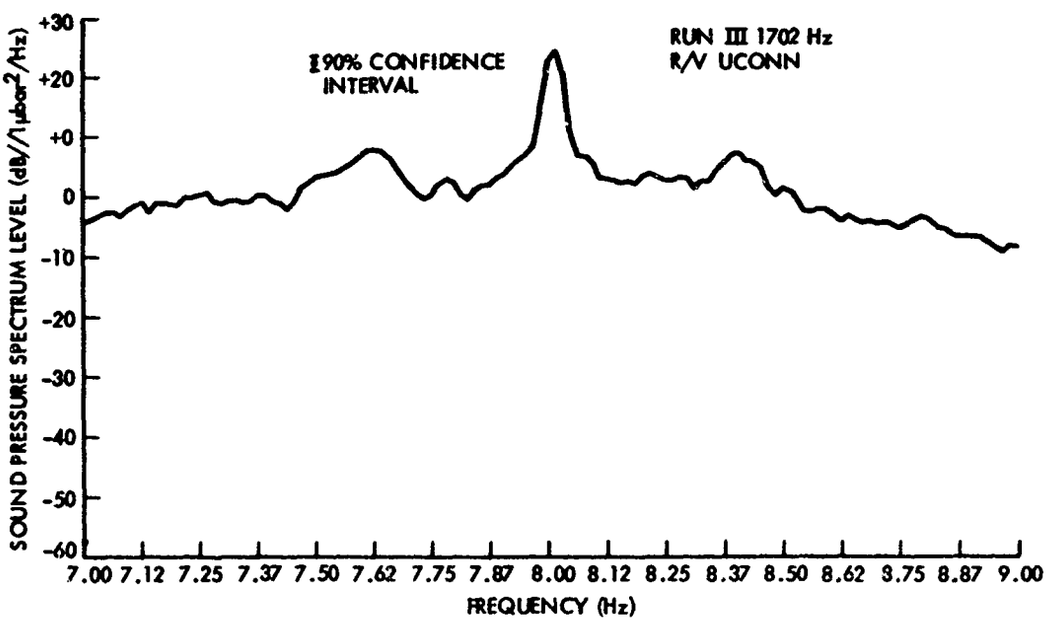

Figure 17B. Spectrum level of acoustic signal at Position C for Run III

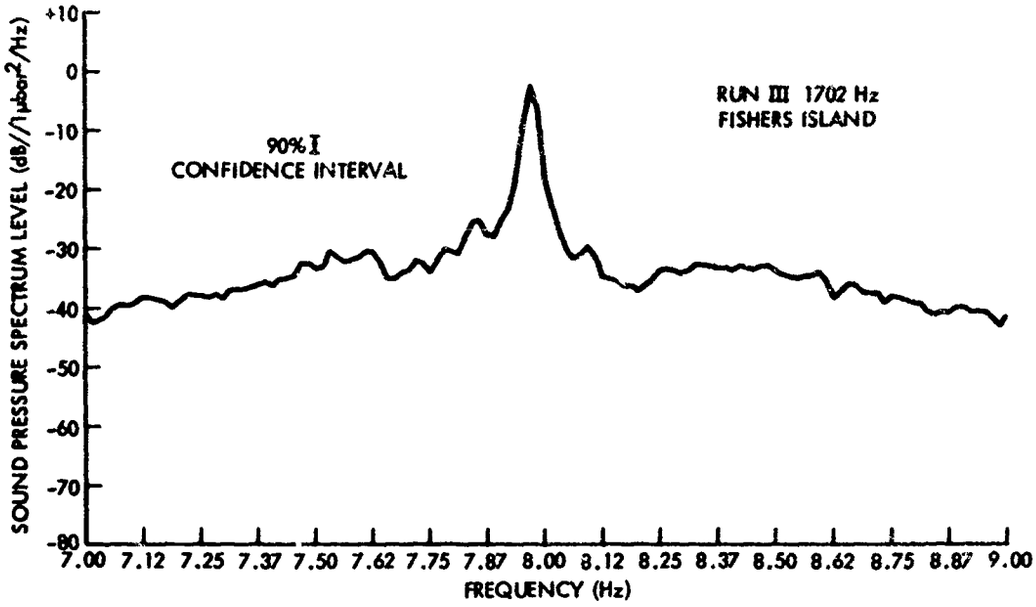

Figure 18. Spectrum level of acoustic signal at Fishers Island for Run III

before and during the run the air temperature was increasing rapidly, while the water surface was nearly calm (Appendix B). This heating could result in a warm surface layer that would refract some of the acoustic energy away from the sea surface. The Fishers Island spectrum could agree with the location of the swell peak since the water column is always well mixed near Fishers Island because of high current speeds. A sample of the actual data recorded aboard the R/V UCONN is presented in Figure 21.

Two of the best runs in this series were made on 26 January: Run V at 1702 Hz and Run VI at 127 Hz. The prevailing weather conditions were the result of a stationary front that had developed during the early morning hours just southeast of Block Island and that covered an area from Atlantic City, N. J., to a low-pressure area centered in the Gulf of Maine.[63] The spectra at Position C for

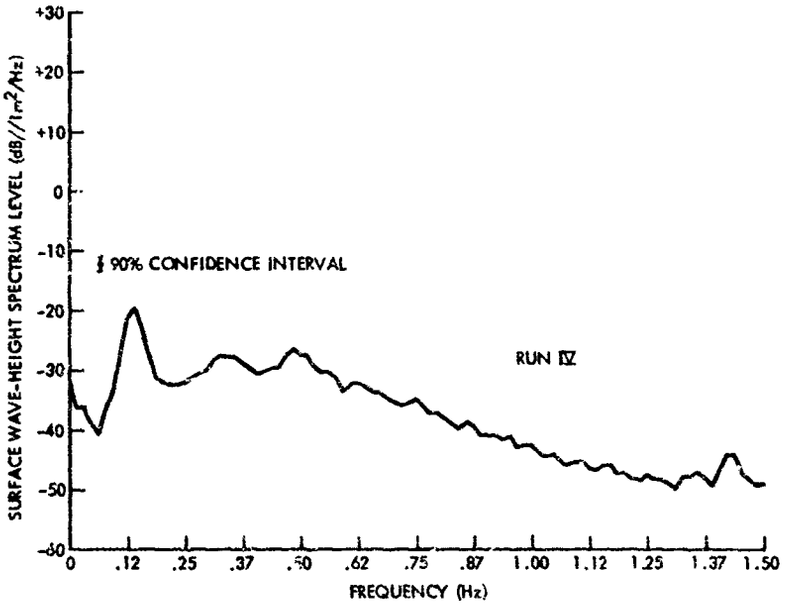

Figure 19A. Spectrum level of ocean wave height at Position C for Run IV

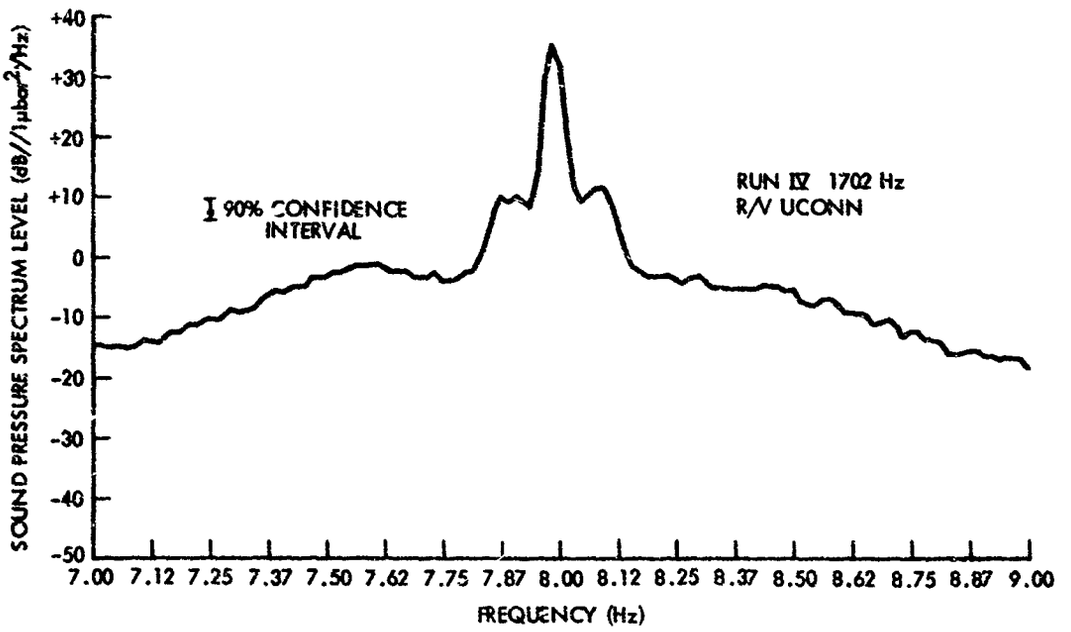

Figure 19B. Spectrum level of acoustic signal at Position C for Run IV

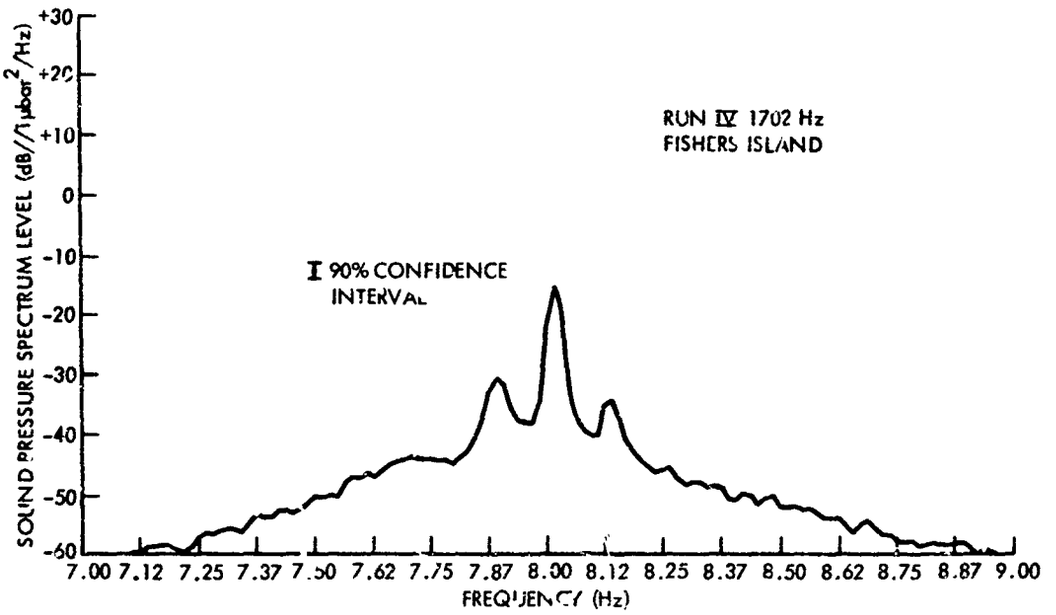

Figure 20. Spectrum level of acoustic signal at Fishers Island for Run IV

Run V are presented in Figure 22. This run represents the heaviest sea conditions in this series of measurements. Since the first-order sidebands at ±.12 Hz from the carrier are only 3 dB below the carrier level, the data can be presented on a linear plot (Figure 23). There is good agreement between the location of the peak in the wave-height spectrum and the first-order sidebands in the acoustic spectrum. From Figure 22, the slopes of both acoustic and wave-height spectra are about 24 dB/Hz between 0.5 and 0.75 Hz. In Figure 23, there are small peaks in the acoustic spectrum at about 0.25 Hz; these peaks are 6 dB below the first-order peaks. These peaks are probably due to second-order scattering since they occur at twice the frequency of the first-order peaks. Evidence of a small amount of higher order scatter can also be found by noticing the broadening of the specular component (although this broadening could also be the result of internal waves). The spectrum at Fishers Island is shown in Figure 24. The specular component and the sidebands are more narrow than in those at Position C, but the possible second-order peaks

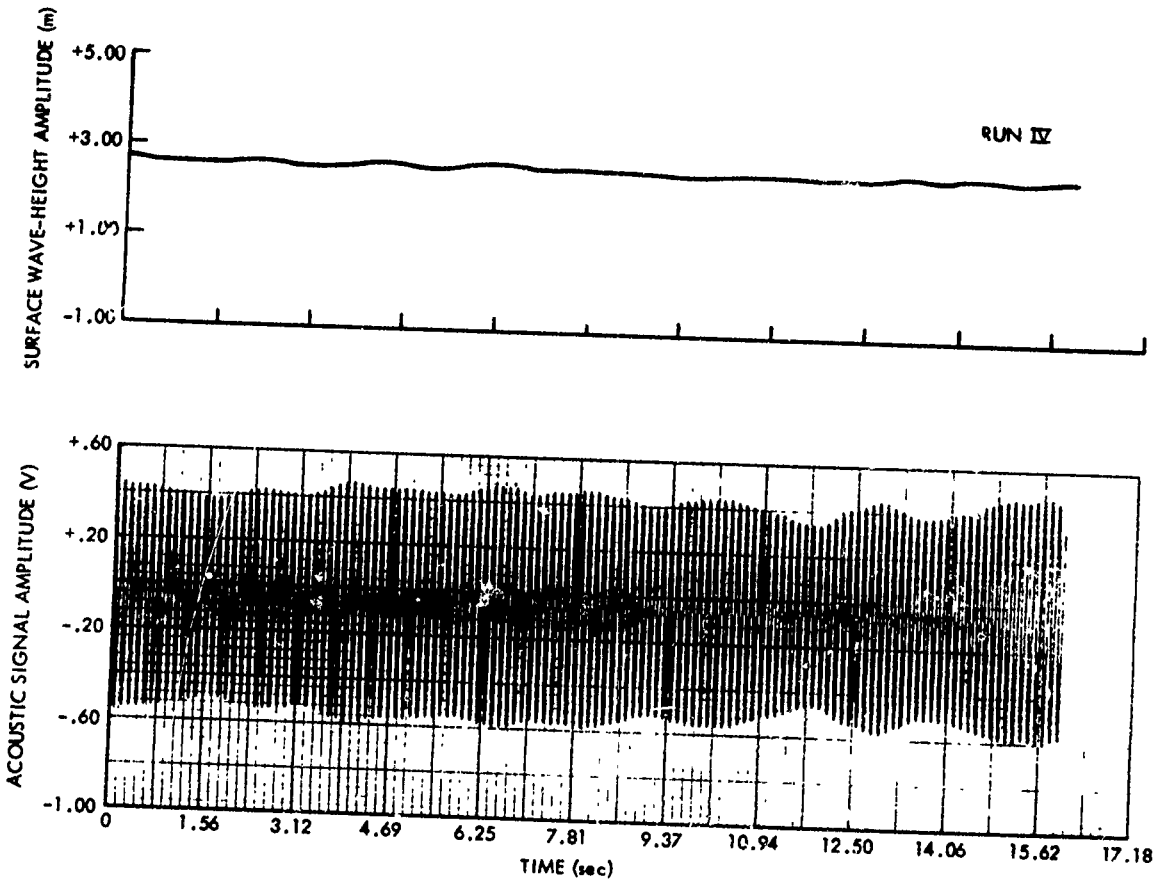

Figure 21. Sample record of ocean wave height and acoustic signal at Position C for Run IV

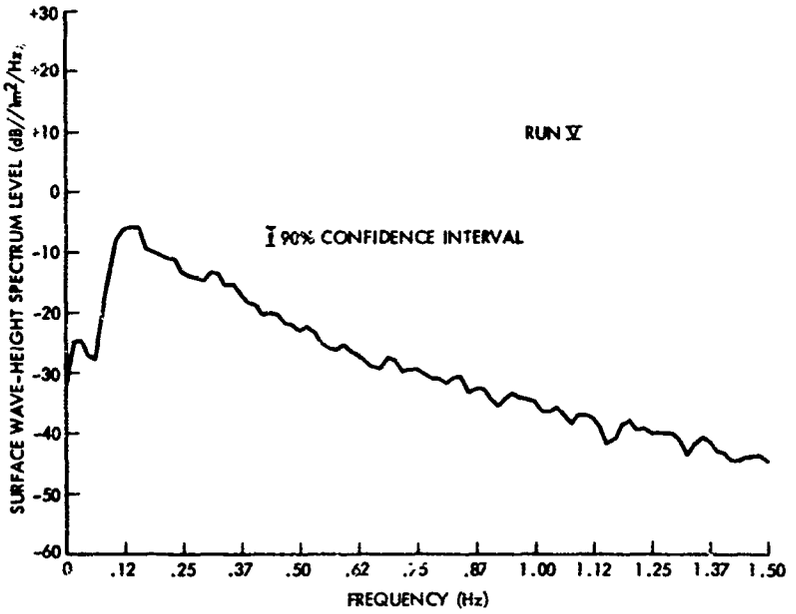

Figure 22A. Spectrum level of ocean wave height at Position C for Run V

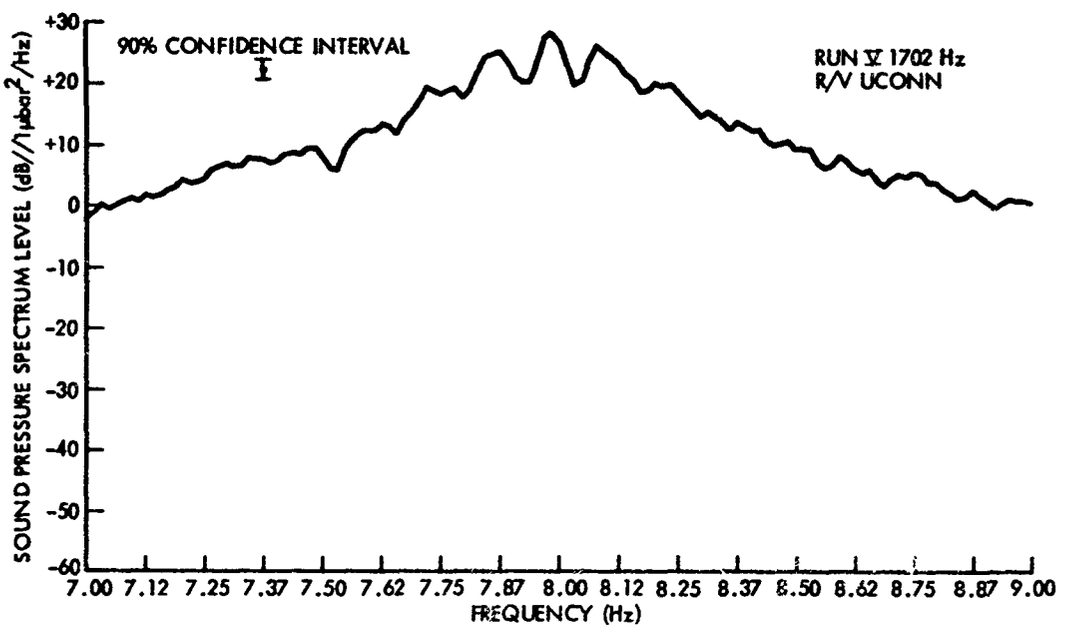

Figure 22B. Spectrum level of acoustic signal at Position C for Run V

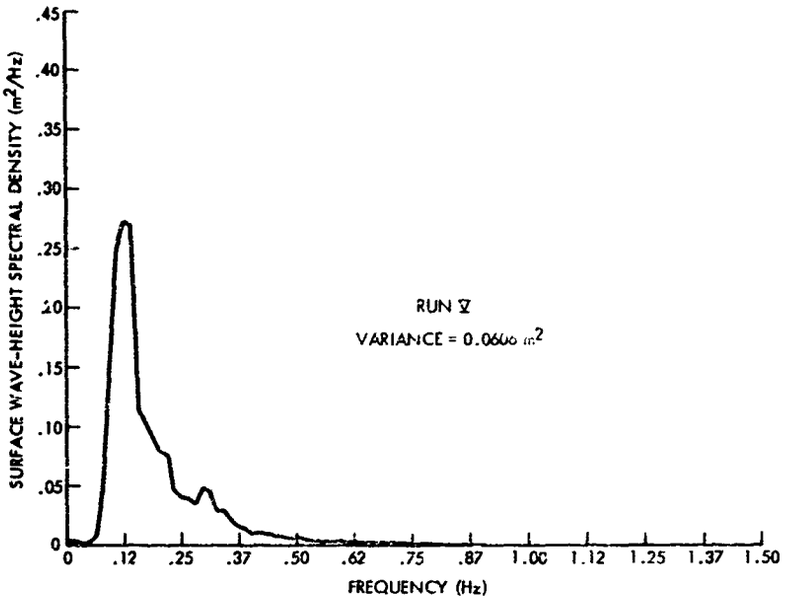

Figure 23A. Spectral density of ocean wave height at Position C for Run V

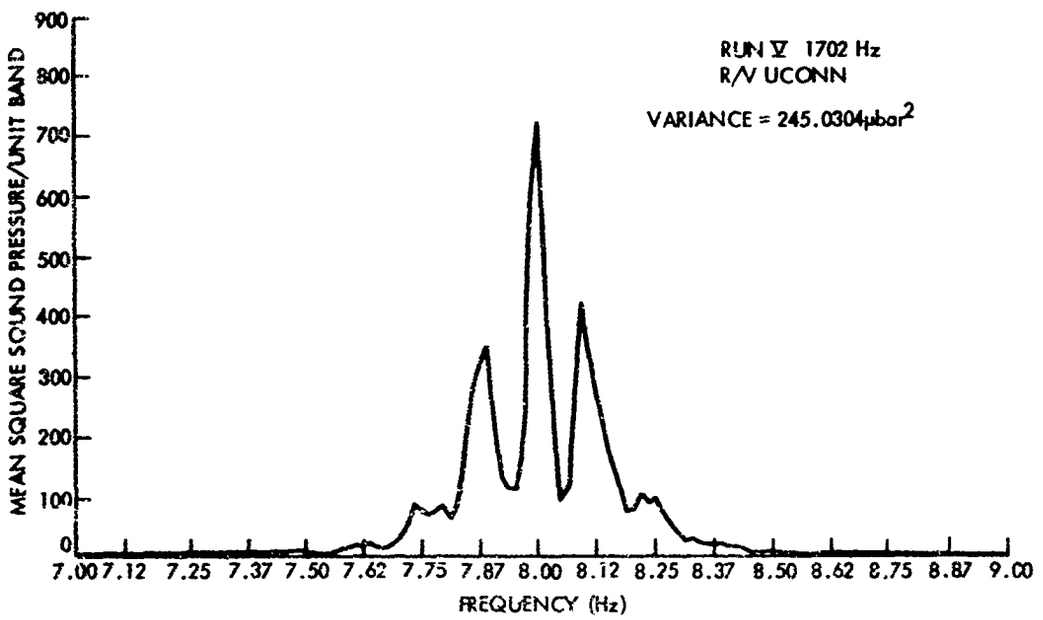

Figure 23B. Acoustic intensity per unit band at Position C for Unit V

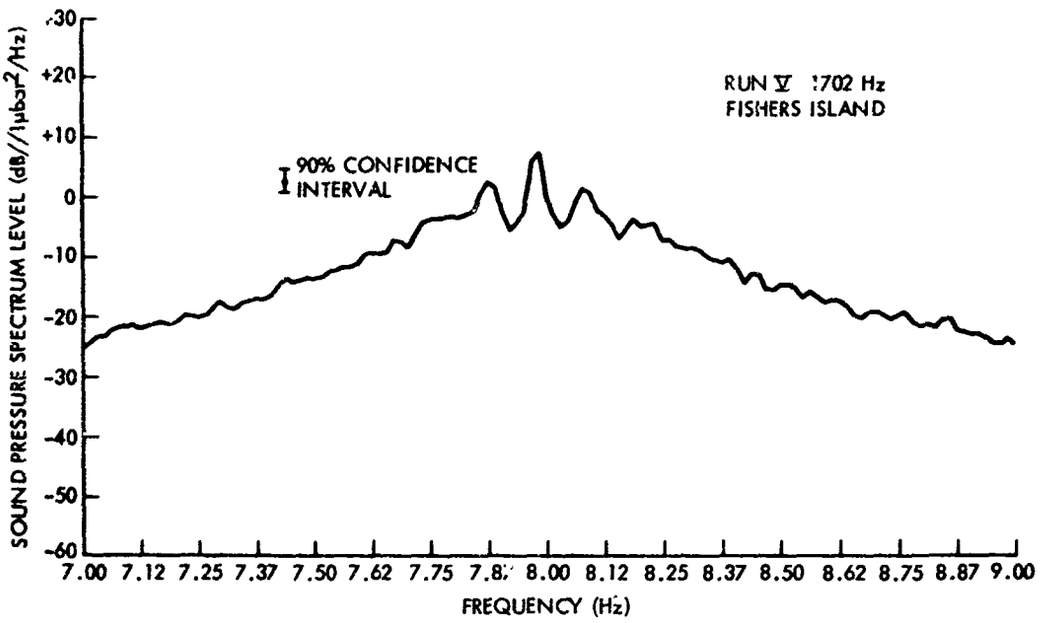

Figure 24. Spectrum level of acoustic signal at Fishers Island for Run V

are still evident at 6 dB below the first-order peaks. Between 0.5 Hz and 0.75 Hz, the slope of this spectrum is very close to that for the spectrum at Position C, i.e., 24 dB/Hz. Samples of the data recorded during Run V are presented in Figure 25.

Run VI was made approximately 1 hour after Run V. These runs illustrate the difference in scattering between the high-frequency (1702 Hz) and the low-frequency (127 Hz) acoustic signals. The acoustic spectrum at Position C (Figure 26B) exhibits first-order sidebands at $\pm$.09 Hz and 21 dB below the carrier, as compared with 3 dB for the 1702-Hz case. The sidebands are narrower and exhibit no possible second-order peaks. The acoustic sidebands are narrower than the wave-height spectrum, having a width at the half-power point of about 0.06 Hz as compared with about 0.1 Hz for the wave-height spectrum. The spectrum at Fishers Island is shown in Figure 27.

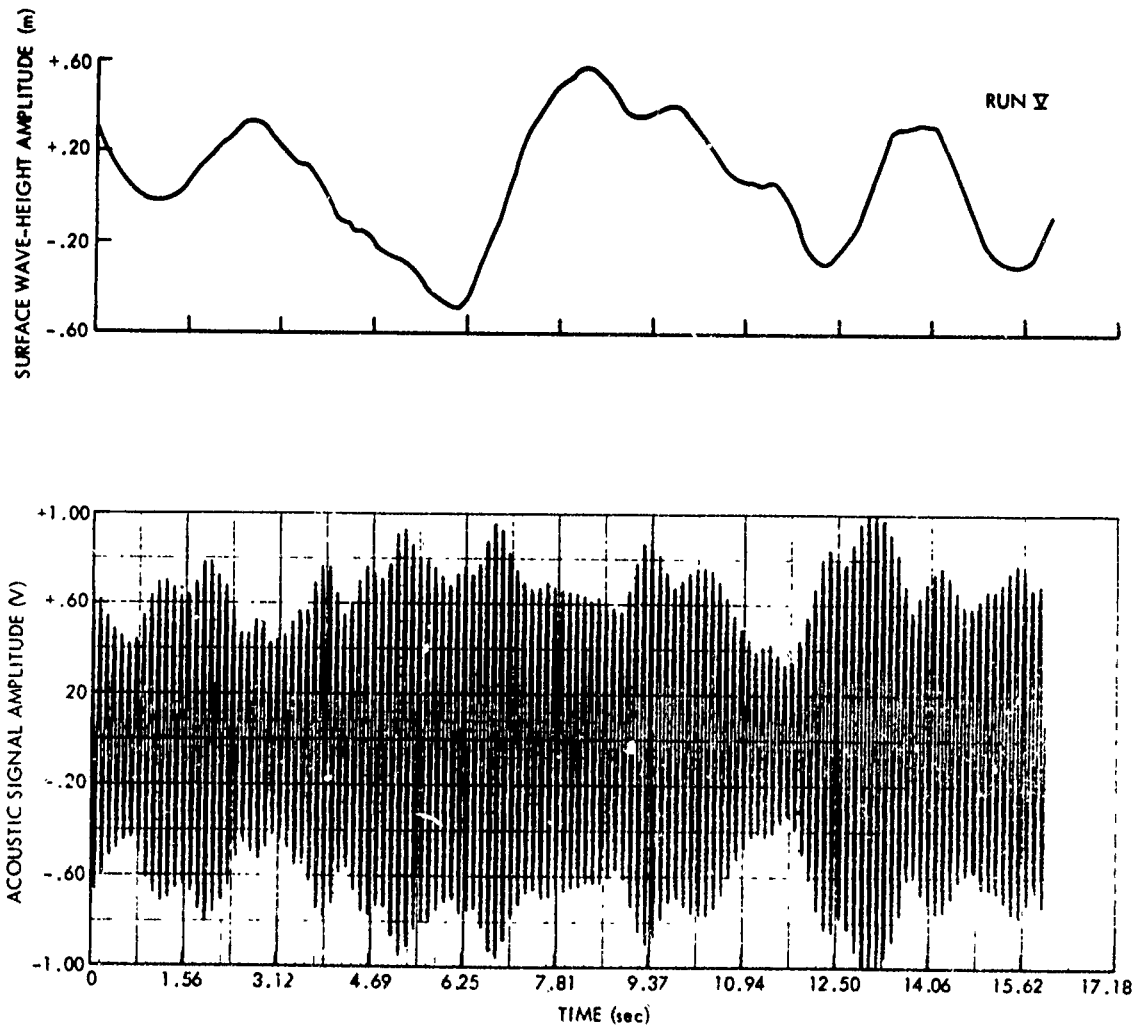

Figure 25. Sample record of ocean wave height and acoustic signal at Position C for Run V

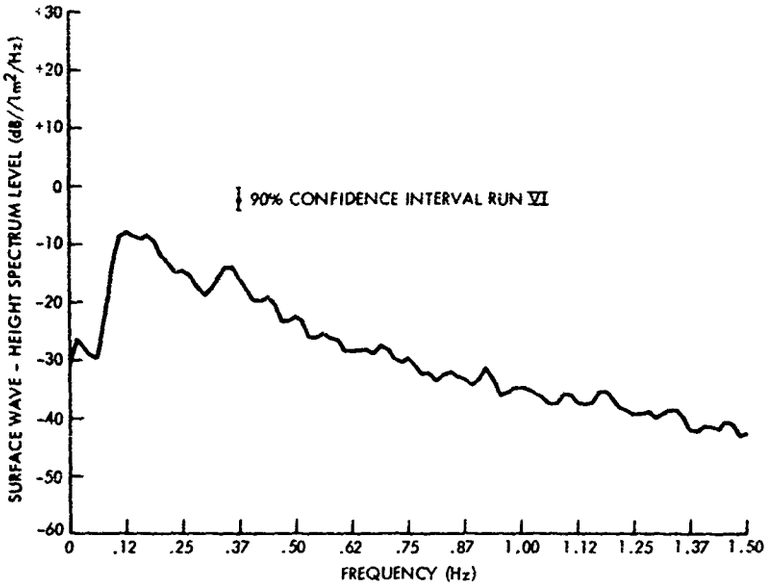

Figure 26A. Spectrum level of ocean wave height at Position C for Run VI

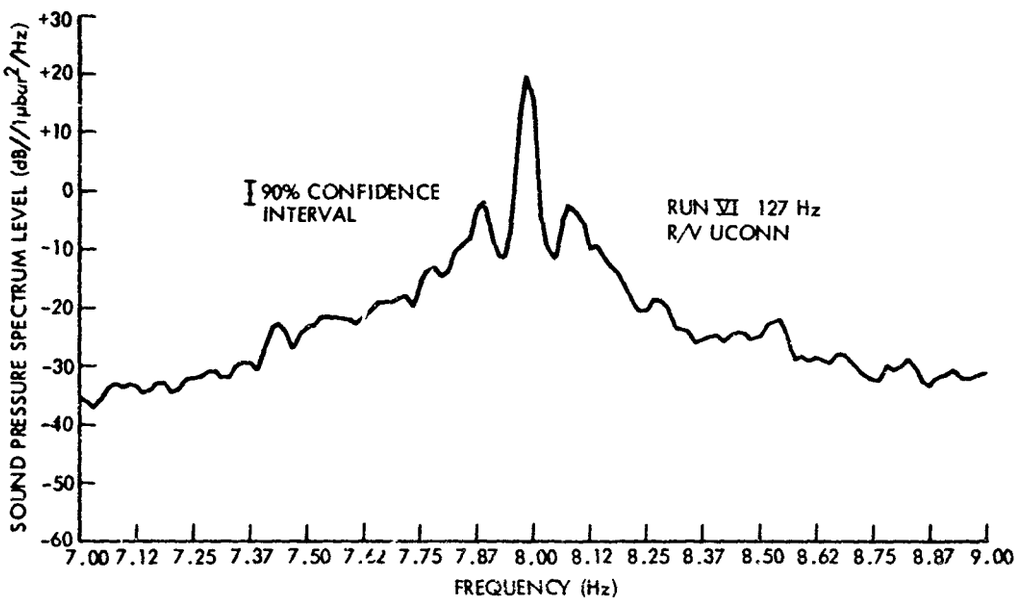

Figure 26B. Spectrum level of acoustic signal at Position C for Run VI

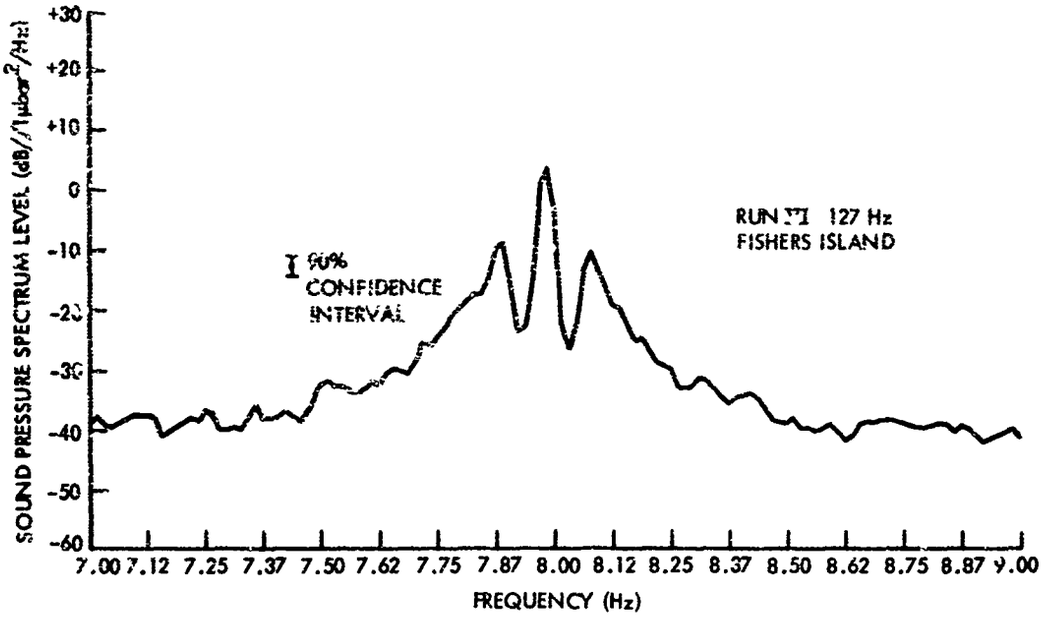

Figure 27. Spectrum level of acoustic signal at Fishers Island for Run VI

Run VII took place at Position A (Figure 6) following the passage of a cold front late on the previous day.[64] The wind direction had shifted from northeast to northwest prior to the run (Appendix B). The wave-height spectrum (Figure 28) exhibits considerable energy at the swell band (0.08 - 0.14 Hz), plus a well-developed wind wave spectrum from 0.24 Hz. The swell direction was opposite to that of the local sea (Table 1). The very low-frequency peak at about 0.03 Hz is due not to the wave motion but rather to a slow oscillation in the spar buoy induced by the extremely strong current (greater than 4 knots). Low-frequency sidebands about 23 dB below the carrier occur in the acoustic spectrum at close to $\pm$0.10 Hz or close to the swell frequency. The wind peak at 0.27 Hz, which is 1 dB higher than the swell peak, occurs in the acoustic spectrum as a small peak in the down-Doppler sideband 8 dB below the first-order peak. (This small peak could also

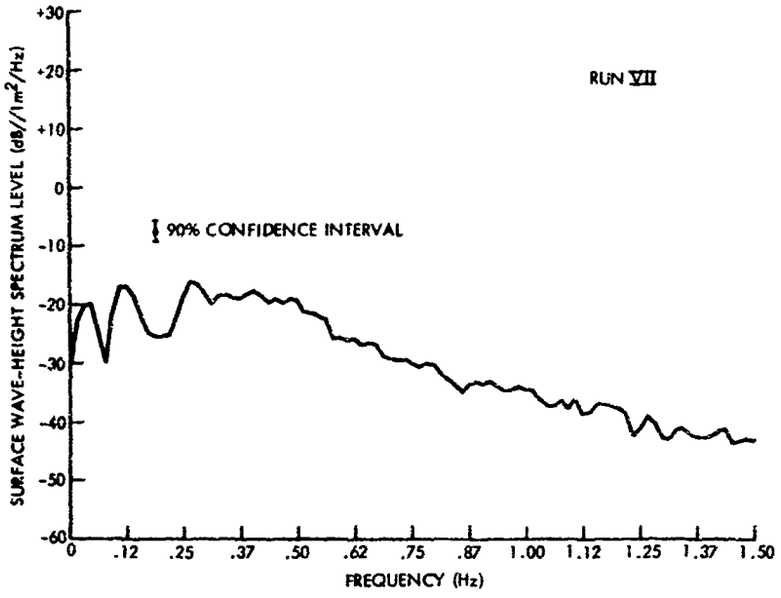

Figure 28A. Spectrum level of ocean wave height at Position A for Run VII

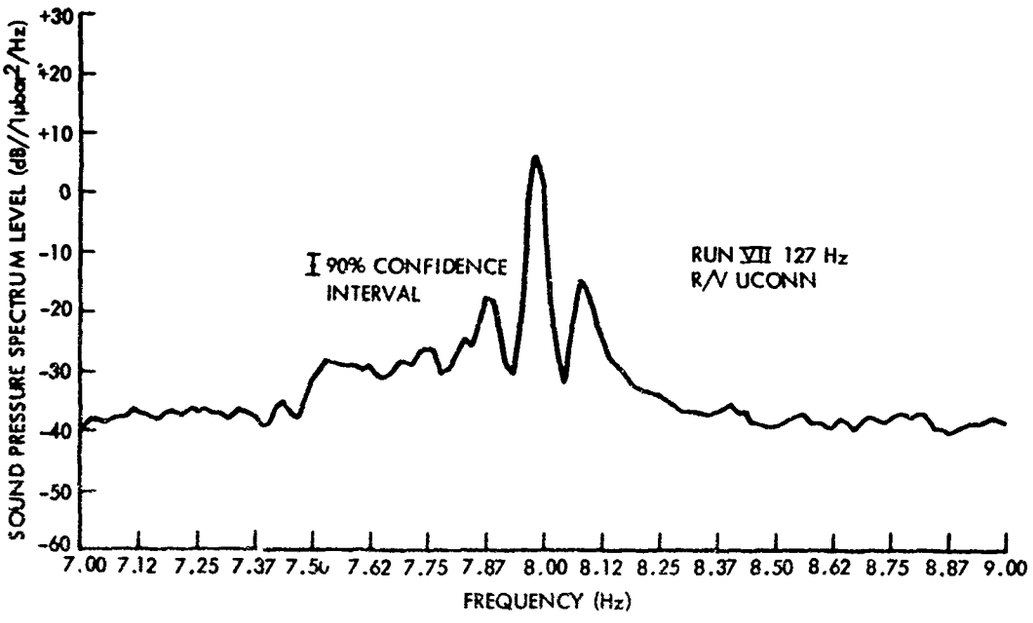

Figure 28B. Spectrum level of acoustic signal at Position A for Run VII

represent second-order scatter; however, second-order scattering at this frequency is not a likely possibility.) The Fishers Island spectrum for Run VII, which is presented in Figure 29, exhibits most of the same features as the spectrum at Position A.

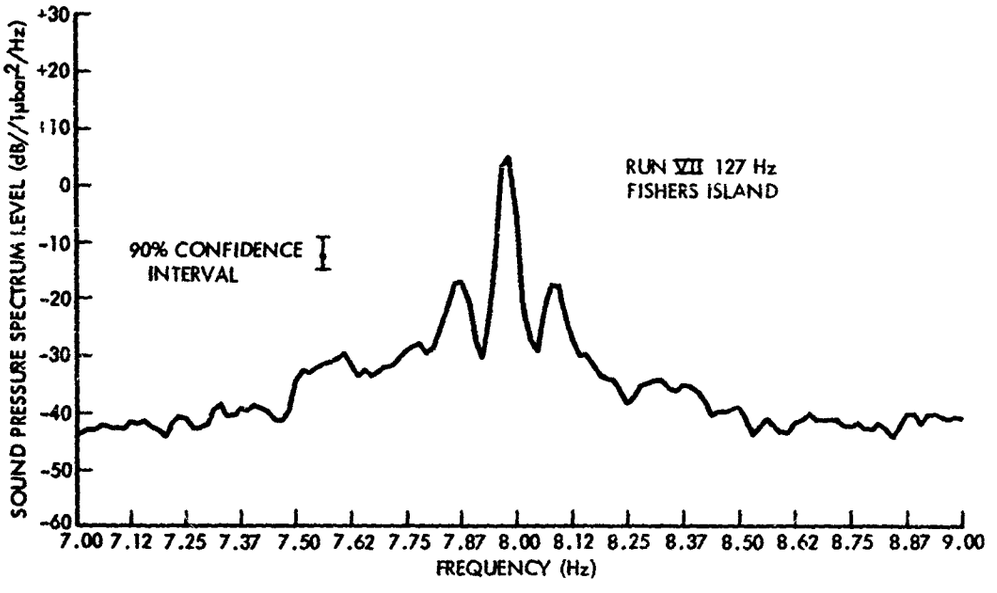

Figure 29. Spectrum level of acoustic signal at Fishers Island for Run VII

4.8 CORRELATION ANALYSIS OF THE SPECTRA

A quantitative measure of the degree of similarity in the acoustic scattered spectrum A(f) and the ocean wave-height spectrum S(f) can be obtained by computing the coefficients of correlation $\hat{\rho}$ as follows:

$$\hat{\rho} = \frac{\left[\sum_{i=1}^{N}\left(S_i(f)\, A_{i+\hat{k}}(f)\right)\right]^2}{\left[\sum_{i=1}^{N}\left(S_i(f)\right)\right]^2 \left[\sum_{i=1}^{N}\left(A_i(f)\right)\right]^2}, \qquad (70)$$

where

N = total points in the sum

i = index of summation

$\hat{k}$ = starting point to begin the computations in the A array. (This index is used to align the scattered part of the acoustic spectrum with the ocean wave-height spectrum.)

The results of the analysis are presented in Table 3.

Table 3

CORRELATION OF ACOUSTIC AND OCEAN WAVE-HEIGHT SPECTRA BETWEEN FREQUENCY INTERVALS

Run Number	Frequency Interval	
	0 - 0.5 Hz	0.5 - 1 Hz
I	0.97	0.93
II	0.89	0.96
III	0.97	0.91
IV	0.75	0.97
V	0.96	0.94
VI	0.93	0.19
VII	0.63*	0.73

* $\hat{\rho}$ = 0.98 between 0.0 - 0.15 Hz

$\hat{\rho}$ = 0.78 between 0.15 - 0.3 Hz

5.0 COMPARISON OF THEORY AND EXPERIMENT

In this chapter, the results from the physical optics, long-crested theoretical model, as expressed by Eqs. (67) and (69), are compared with the experimental measurements presented in Chapter 4. In many ways, the theory is incomplete, in that it does not account for many of the dynamic processes taking place in the ocean or for the multiple reflections from the boundaries of the sea. Nevertheless, the acoustic scattering processes predicted by the theory are occurring in the ocean, although other processes not taken into account by the theory are also taking place.

The luxury of the controlled laboratory experiment is not usually available to the geophysicist in the field. Uncontrolled conditions that are not accounted for by theory can always occur during the experiment. However, the lack of an all-inclusive theory should not be a deterrent to the application of a simplified theory if useful results can be obtained. The results presented below show that underwater acoustics can indeed be a useful remote probe of the ocean surface, if the proper precautions are taken in the interpretation of the measurements.

5.1 THE SUITABILITY OF THE PHYSICAL OPTICS, LONG-CRESTED MODEL TO THE BIFI SCATTERING GEOMETRY

The acoustic experiments in Block Island Sound are modeled by the geometry shown in Figure 5. This idealized model neglects acoustic bottom reflections, as well as multiple reflections from the surface. However, under surface-duct

propagation conditions. i.e., during winter, the effects of the bottom are not very significant at the higher acoustic frequency (1702 Hz).[65] The effects of multiple surface reflections of the acoustic waves propagating from Block Island to Fishers Island were reduced by taking measurements close to the sound source at Position C (Figure 6). Thus, the single-reflection model was made more reasonable. Examination of the data in Chapter 4, however, indicates that the received signal spectra at Position C and at Fishers Island are quite similar. The major difference seems to be that the bandwidth of the received signal spectrum is narrower at Fishers Island. From the "resonance" relation of this theory, $\omega^2/g = (a_m + a_n)/2$, higher frequencies in the received signal spectrum correspond to steep angles of scatter that, from normal mode theory,[38] suffer high attenuation. Thus, a succession of surface-bottom reflections would attenuate the high-frequency Doppler. March and Kuo[31] have shown qualitatively that the spectrum of a signal scattered many times from the sea surface should not differ significantly from a signal scattered only once.

The use of the two-dimensional, long-crested scattering model can be justified as follows:

1. For a source and receiver at long range and shallow depth, the Fresnel zones on the surface become very long and narrow[29]; hence, the most important scattering takes place along a relatively narrow strip above the source-receiver line.

2. The predominant wave directions in Block Island Sound (west to west-northwest for wind waves, and southeast to south for swell) make relatively small

angles with the source-receiver lines (Figure 6).*

3. The most important forward scatterers of underwater acoustic waves are the long swell waves; these tend to be more nearly long-crested than the short gravity waves.

Perhaps the most serious criticism that can be leveled against the application of Eq. (50) to the Block Island Sound data is that the long swell waves in the area of the acoustic range are not in infinitely deep water. Strictly speaking, one should use the following equation in place of Eq. (50)[42]:

$$\Omega^2 = gK \tanh (Kh) \quad , \tag{71}$$

where

h = water depth in meters

$\Omega = 2\pi f$.

However, the ensuing mathematical complications would greatly reduce the usefulness of the model. Therefore, as an alternative procedure, Eq. (50) will be retained, and the extent of error examined. Equation (71) was used to obtain the computer-generated plot shown in Figure 30, where frequency versus wavelength curves are presented for water depths of 10,000 m (in effect, infinitely deep), 40 m, 30 m, 20 m, 10 m, and 5 m.

---

*Long swells from the southeast or south into Block Island Sound are defocused by the Block Island Channel so that the directions of propagation make reasonably small angles with the lines "C" - "P" and "H" - "P" in Figure 6.

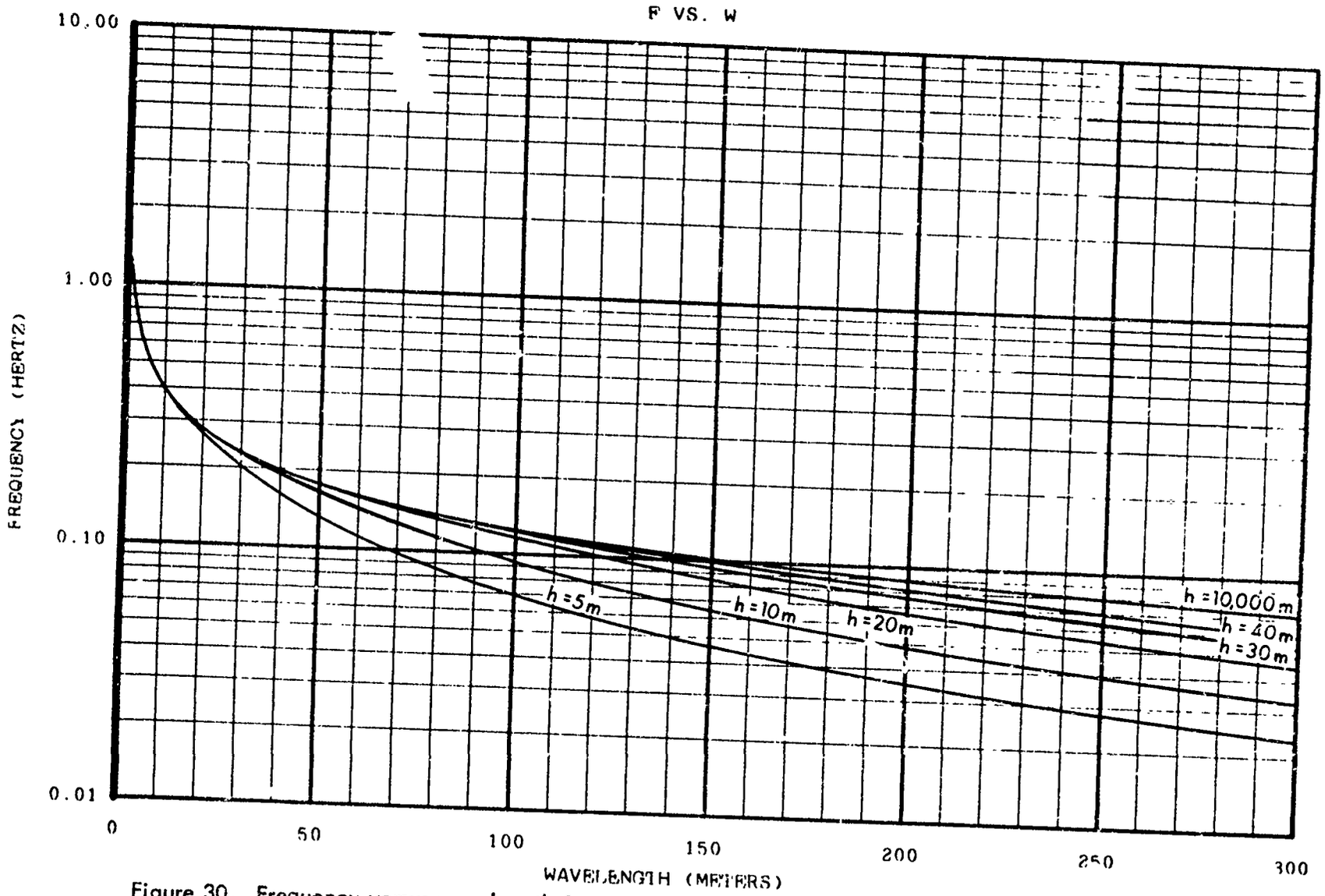

Figure 30. Frequency versus wavelength for ocean gravity (Airy) waves determined from the relation $4\pi^2 f^2 = g K \tanh(Kh)$

The periods of swell in Block Island Sound are typically on the order of 10 sec (0.1 Hz in frequency). The mean water depth is about 40 m. Figure 30 shows that a 10-sec component wave (i.e., a mathematical Airy wave, not a real wave) has a length of approximately 150 m in deep water and a length of 146 m in water 40 m deep. More importantly, for component waves of a given length, e.g., 150 m, there is a 2% error in frequency if the wave is assumed to be in deep water when it is really in water 40 m deep. This error, which has been calculated from Figure 30, increases as water depth decreases and as wavelength increases. For wavelengths of 100 m or less, there is a very small error. Figure 31 presents a computer-generated plot of the phase speed squared versus the water wavelength. There is a 3% error in phase speed if a 150-m wave is assumed to be in deep water when it really is in water 40 m deep.

Since the primary purpose of this study is to investigate a general method rather than to obtain the best possible fit to a particular set of data, the deep water dispersion relation $\Omega^2 = gK$ will be retained (Figure 32) with the knowledge that there is some error present in the modeling of the low-frequency swells, the extent of which can be estimated from Figures 30 and 31.

In this study, the small roughness approximation, i.e., $\exp\left[2c_m c_n \sigma^2 \rho(u,\tau)\right] \approx 1 + 2c_m c_n \sigma^2 \rho(u,\tau)$, was utilized because all the data cases studied were within its limits of validity; the largest error encountered (for the region on the surface closest to the source and receiver) was 3%, which seems reasonable for a field experiment. The other reason for using the small roughness approximation is that it allows the ocean surface correlation function to be brought out of the exponent and

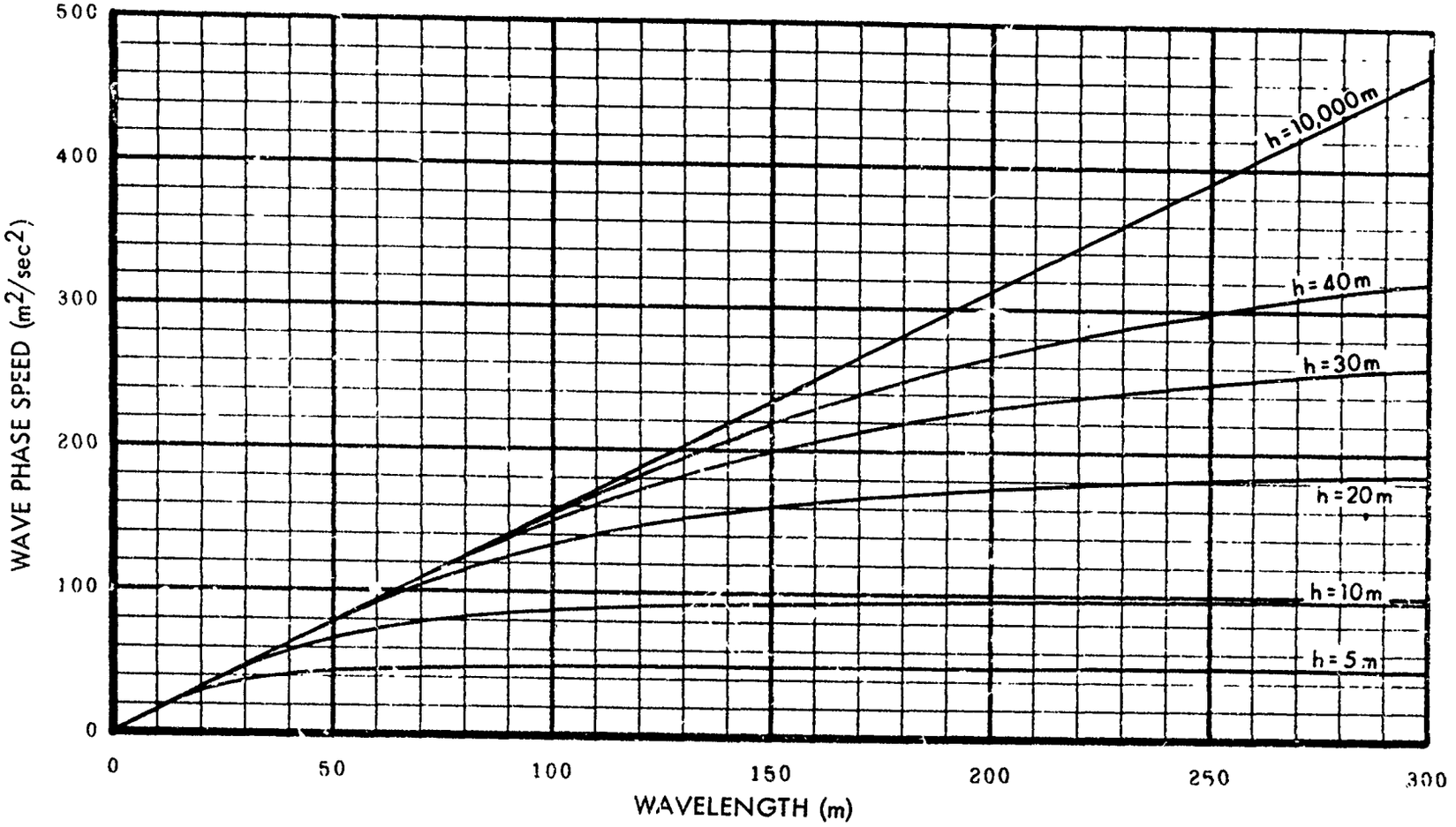

Figure 31. Water wave phase speed squared versus wavelength for ocean gravity (Airy) waves determined from the relation $v^2 = (g/K) \tanh (Kh)$

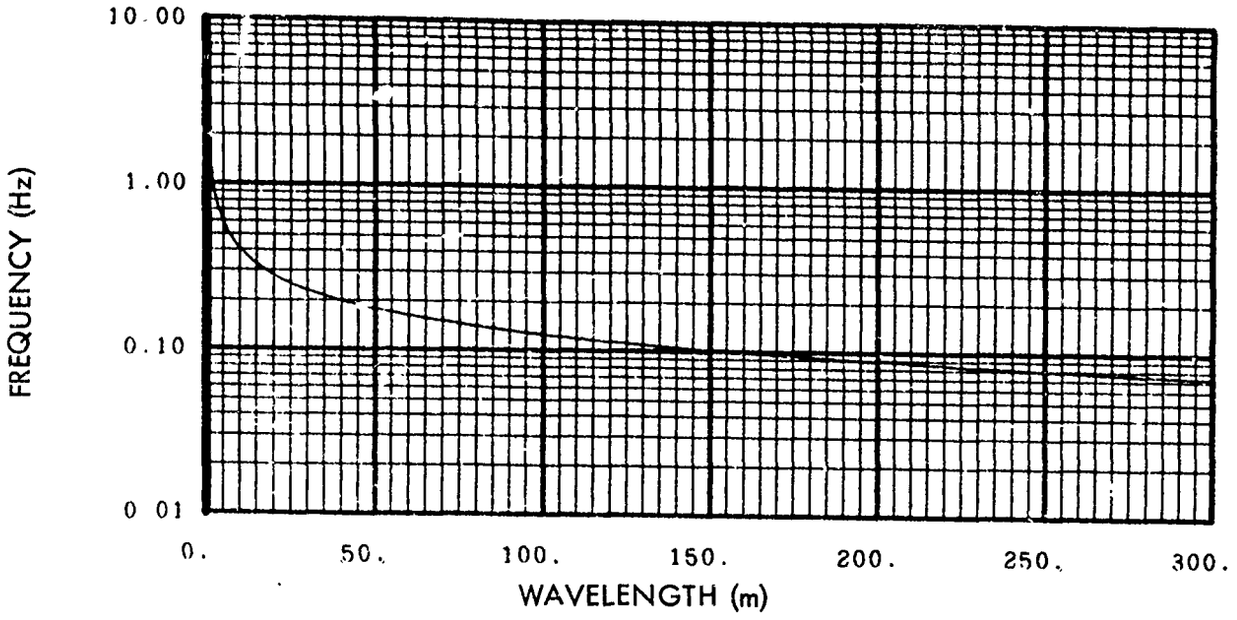

Figure 32. Frequency versus wavelength computed from the classic dispersion relation for deep water (Airy) gravity waves, $4\pi^2 f^2 = gK$

into a linear relationship with the acoustic covariance. When Fourier transformed, this relationship permits a solution for the ocean wave-height spectrum directly in terms of the acoustic scattered spectrum, which is the primary objective of this study. An alternative approach would have been to attempt to fit an assumed form for the spectrum (such as Pierson-Moskowitz[66]) to the acoustic data and minimize the error between the computed and measured spectra by adjusting the parameters in the spectral form (i.e., the A and the B of the Pierson-Moskowitz[66] spectrum). This procedure was not followed here because a direct solution was desired and because, in shallow coastal waters, the spectral shape is not readily predicted by any of the standard theoretical ocean wave spectra models.

It is difficult to assess the importance of tidal currents and internal waves in Block Island Sound on the received signal spectrum. As Clark and Yarnall[4] have shown, such phenomena produce a low-frequency modulation of the acoustic signal. This modulation could appear as a broadening of the coherent component of the received signal, since a 20-min record could not resolve these low-frequency components.

5.2 THE NUMERICAL EVALUATION OF THE ACOUSTIC AND SEA SURFACE SPECTRA

Equations (67) and (69) were programmed for numerical evaluation on the NUSC UNIVAC 1108 digital computer. A listing of the program is given in Appendix E. The first problem to be overcome in the evaluation of these equations is the determination of the following parameters: P^2, the illumination function shape control; L, the length of the subsections on the surface; and M, the number of subsections used in the evaluation.

The choice for P is fairly straightforward in that the acoustic "illumination" at the boundaries between subsections should not be very different from that at the centers of the subsections. If the value of P is not chosen properly, a "ripple" will appear in the illumination and thus cause unwanted interference effects. When $P^2 = 1/2$, the intensities obtained by adding the overlapped portions of the segment illumination functions produce a reasonably smooth total surface illumination. The selection of L and M is more difficult, however. Application of Beckmann's[29] formulas (9) and (10) to the BIFI geometry yielded a Fresnel zone 4,066 m long. Additional discussions in Beckmann and Spizzichino[29] point out that, for weakly directional antennas, a very large area on the scattering surface is involved in scattering the incident radiation. Clay[8] and Medwin and Clay[30] show that in underwater sound experiments, a very large area on the surface is involved if all significant scattered contributions are considered. On the basis of these considerations, the scattering area for this model was made as large as possible without violating the criterion for the "small roughness approximation."* It was arbitrarily decided to keep the error due to the approximation to less than 3%. The 3% error limitation on the small roughness approximation permits, for the roughest surface encountered (Run VI, $\sigma^2 \approx 0.06\ m^2$), a scattering area 4,503 m long.

---

*An easy solution to the determination of the size of the scattering area on the surface would be to include all the area on the surface between the source and receiver. However, for those regions on the surface very close to the source and receiver, the c_m in the small roughness approximation are large. Hence, for the high-frequency case, this criterion would be violated.

For the case of the 1702-Hz measurements, this region comes within 89 m of the source and receiver. In the case of the 127-Hz measurements, it is possible to consider areas much closer to the source and receiver because the c_m are very small as a result of the small wave number ($k = 0.55$). However, because of the long wavelength (11.4 m), one cannot consider scattering areas very near the source and receiver without violating the farfield assumption. Hence, a compromise is again necessary and a scattering area of 4,470 m is used for the data at this wavelength.

The choice of L is limited by the criterion that the wavefront be essentially plane over the subsection length, i.e., the sums of the direction cosines should be essentially constant over the length L. Clay and Medwin[20] used the additional assumption that the size of the subareas should be large compared with the correlation distance on the water surface. This assumption was necessary in order to integrate their expression for the scattered covariance using a theoretical form for the surface space-time correlation function. Their model tank experiments did not quite satisfy this assumption,[30] but agreement between theory and experiment was still good. In the present study, this assumption was not necessary in developing the theory because the scattering equations, Eqs. (56) and (57), could be integrated by means of the long-crested surface correlation function, Eq. (51), and by transforming from the time to the frequency domain. However, by averaging Eqs. (37) and (62) over phase, one finds that the cross-product terms between subsections are equal to zero. This is tantamount to assuming that the contributions from adjacent subsections are incoherent. In a strict sense, the reradiated signals from adjacent subsections can be incoherent only if the surface correlation distance is small in

comparison to the length of each subsection L. However, in the evaluation of the numerical model, Eq. (67), good results are obtained when L is small because, in reality, the coherence between contributions from small adjacent subsections is low as a result of "jitter" in the receiver location and of nonstationary conditions in the ocean.

Marsh[67] has argued that, in numerical models of this type, the mesh (subarea) size should be made very small. The basis for this agreement is that the double summation, Eq. (64), in three-dimensional form would approach an integral if the mesh size is made arbitrarily small. If the integration were performed over all directions, the plane waves would add and thus synthesize spherical waves radiating from a point source and converging on a point receiver. However, in this particular numerical model, Eq. (67), there is a lower bound on the size of L, which is determined by the requirement that the phase terms in Eq. (64) average to zero to a good order of approximation. This means that L must not be so small that contributions from adjacent subsections are coherent. In order to prevent this from happening, the lower bound on L has been set by requiring that the length of the subsections be equal to several radiation wavelengths.

The criterion that the sums of the direction cosines be relatively constant over each subsection was interpreted to mean that the change in the value of a_m or c_m from one subsection to the next should be less than 10%. This constraint limits the size of L to about 5 m at 1702 Hz. For the 1702-Hz data, a value of L = 3 m was adopted, which is almost four times the acoustic wavelength.

For the 127-Hz case, the wavelength is 11.4 m and the criterion that the a_m differ from section to section by less than 10% cannot be met without making L the

size of a wavelength or less, which introduces some conceptual problems in applying the theory. In an attempt to keep the ratio of section length to wavelength constant for both data cases, a value of $L = 30$ m was selected for the 127-Hz data, although the applicability of the theory to this case is marginal. Values of L equal to 15, 20, 25, 30, and 50 m were tried for this case without much change in result. For the 1702-Hz case, several values of L were also tried up to 50 m. The numerical results at 1702 Hz were reasonably consistent for values of L below 10 m.

The numerical results for the 1702-Hz and 127-Hz data will now be presented. In this chapter, all formulas expressed in Chapter 3 in terms of radian frequency have been converted to frequency f. The mirror image of the down-Doppler measured acoustic spectrum is used in the calculations.

The weighting or "transfer" function B(f), in Eqs. (67) and (69), depends on the mean-square wave height σ^2. In this study, σ^2 was measured directly by wave staff, although in principle it could be determined from the acoustic measurements from the coherent component by means of Eq. (42). Through an iteration procedure, σ^2 could be adjusted until the error between the computed and measured coherent components is a minimum in the least-squares sense.

The function B(f) normalized to the peak value is shown in Figure 33. This particular B function has been computed from the data for Run III, but no detectable differences in the plots can be seen in the B's computed from the other runs. The B function has also been estimated by dividing the measured acoustic spectrum $A_1(f)$ by the measured wave-height spectrum S(f). Thus, from Eq. (67), B(f) is

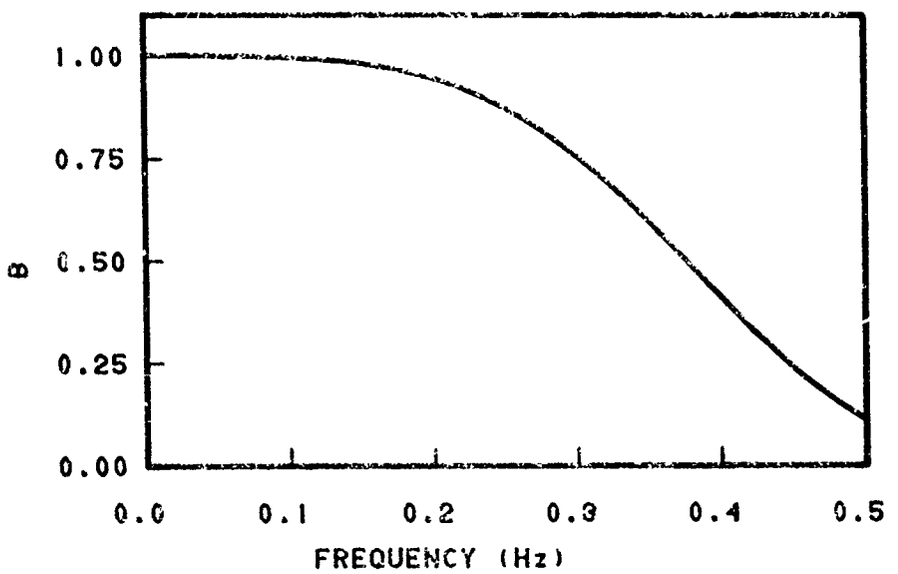

Figure 33. Normalized B function for acoustic wave number k =7.38/m; Block Island Sound. This function was computed using data from Run III

$$B(f) = A_1(f)/S(f) \quad . \tag{72}$$

Since the individual measured B's are quotients of two random processes and thus tend to be very noisy, the average B has been obtained for each wavelength. The B for the 1702-Hz case is presented in Figure 34, where the function begins at about 0.1 Hz because, below 0.1 Hz, energy from the broadened "specular" component can be found which invalidates this calculation. The general form of the measured and computed B's is similar; however, above 0.3 Hz the computed B falls off much more rapidly than does the measured B.

The first example to be considered is Run II. The acoustic scattered spectra, normalized to the peak values, are shown in Figure 35A. The measured spectrum is shown only above 0.05 Hz because the coherent component is encountered below that frequency. The computed spectrum has been evaluated from Eq. (67).

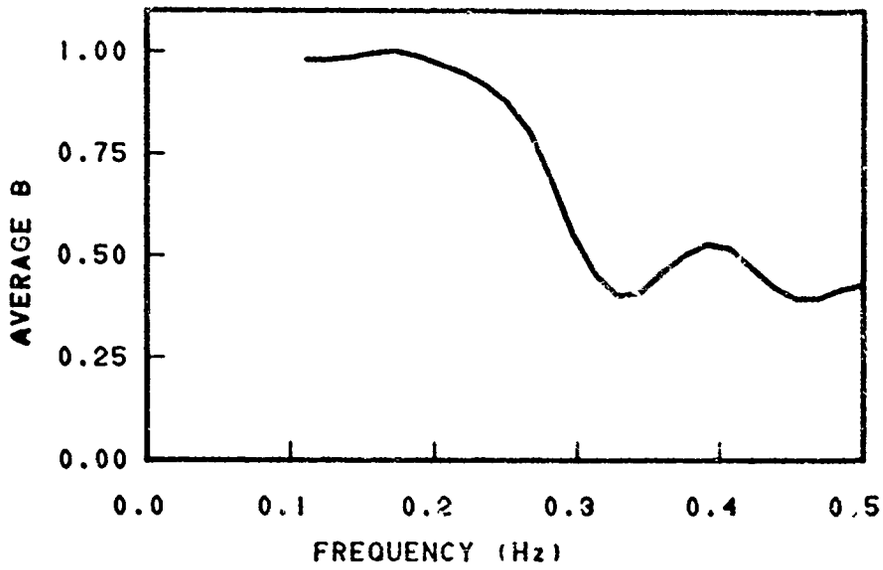

Figure 34. Normalized average measured B function for acoustic wave number k = 7.38/m; Block Island Sound

The normalized ocean wave-height spectra, measured and computed by means of Eq. (69), are compared in Figure 35B. The computed ocean wave-height spectrum is bandlimited because the B function approaches zero as 0.5 Hz is approached (Figure 33). Hence, in this case and in the following cases, the $A_1(f)/B(f)$ computation is truncated at the point where it starts to increase rapidly. The agreement between peak values is generally good. Since both the measured curves and the computed curves are estimates from random processes, the alignment is not expected to be perfect. The measured acoustic spectrum does not reflect the small peak at 0.34 Hz in the computed acoustic spectrum. Consequently, the peak at 0.34 Hz in the wave-height spectrum is not detected in the computed spectrum.

The spectra for Run ill are shown in Figure 36. There is generally good agreement out to 0.44 Hz. This is an interesting case in that the ocean wave-height spectrum peaks at an unusually high frequency for Block Island Sound.

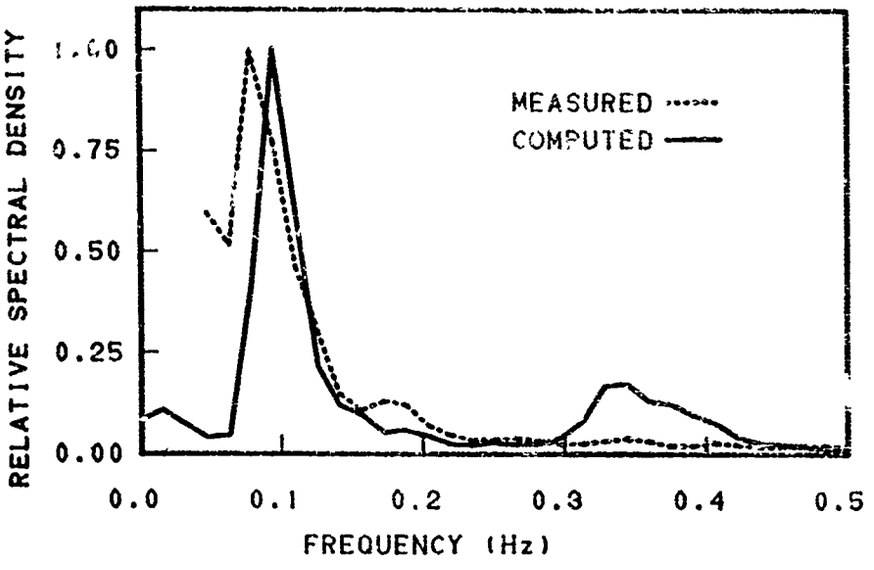

Figure 35A. Normalized acoustic spectra for Run II, 1702 Hz

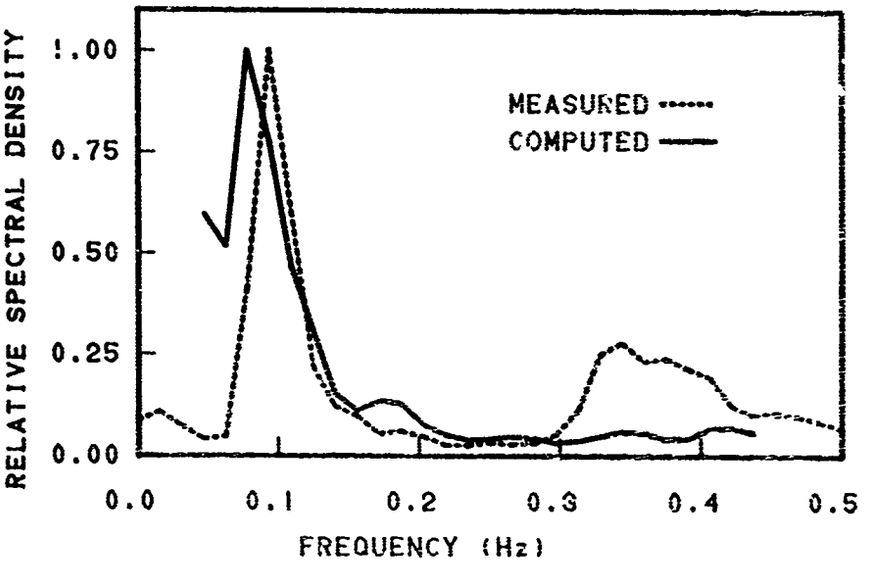

Figure 35B. Normalized ocean wave-height spectra for Run II

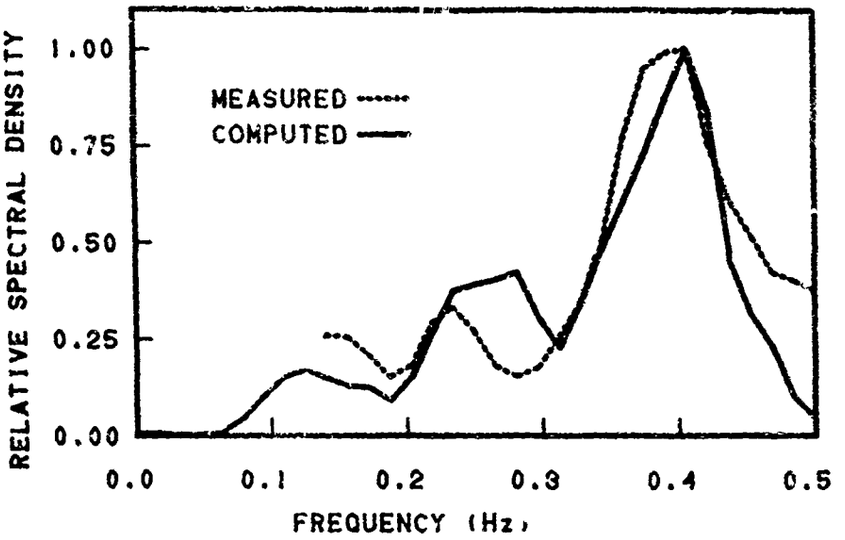

Figure 36A. Normalized acoustic spectra for Run III, 1702 Hz

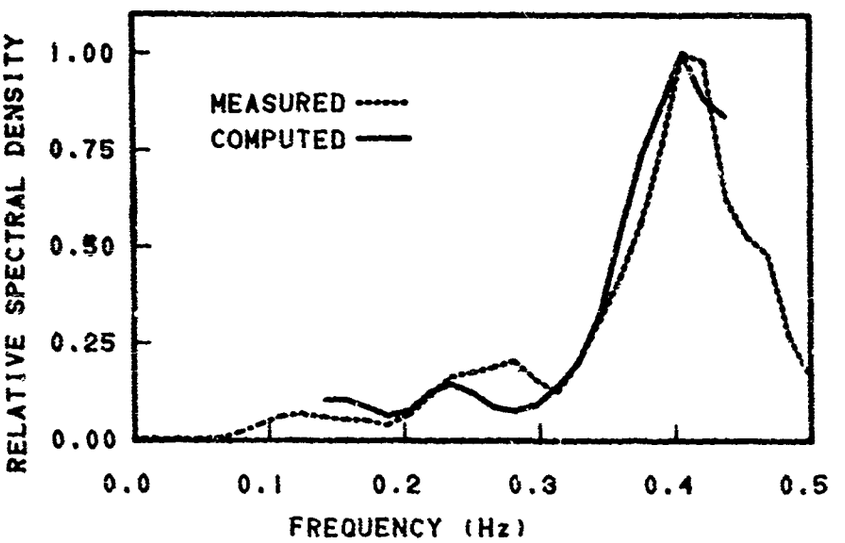

Figure 36B. Normalized ocean wave-height spectra for Run III

The results of Run IV are given in Figure 37. Agreement between theory and experiment is good between 0.1 Hz and 0.35 Hz. However, the double peak below 0.1 Hz in the measured acoustic spectrum may be due to either statistical noise or low-frequency modulation by infragravity waves. This lower peak is falsely predicted in the computed ocean wave-height spectrum.

A relatively rough surface case is shown in Figure 38. (Before this run began, a number of improvements had been made in the electronics to increase the signal-to-noise ratio (Appendix B) of the measured data.) There is good agreement between the ocean wave-height spectra out to 0.46 Hz, where the $A_1(f)/B(f)$ computation is starting to increase rapidly.

The B function for the 127-Hz data is shown in Figure 39. It is much narrower than the 1702-Hz B function and indicates that only ocean waves below 0.2 Hz are effective in modulating the acoustic signal. The narrowness of the B function at 127 Hz implies that information about the sea surface obtained by acoustic scatter measurements is bandlimited to 0.2 Hz for the BIFI geometry. The measured average B function is shown in Fig. 40. Again, the computed B falls off more rapidly than the measured B.

The first 127-Hz data case to be considered is Run I (Figure 41). Agreement between theory and experiment is very poor. During this run, the sea surface was characterized by a high incidence of whitecaps, foam, flying spray, and turbulence, which may have acted in concert to invalidate the assumptions of the theory.

The situation for Run VI is somewhat better (Figure 42). The measured acoustic spectrum is severely bandlimited as compared with the ocean wave-height spectrum. This result, which would be expected from the B function (Figure 39), limits the usefulness of this frequency in measuring the ocean wave-height spectrum, as can

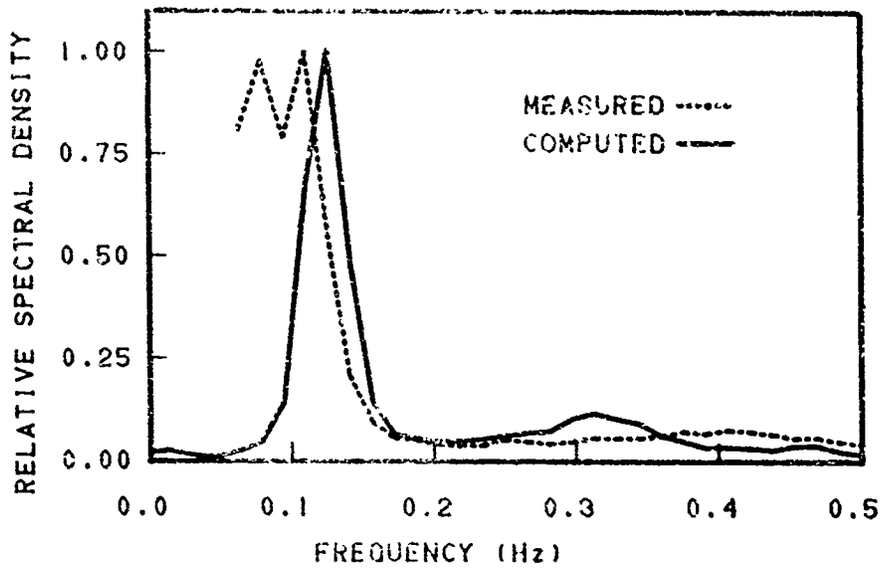

Figure 37A. Normalized acoustic spectra for Run IV, 1702 Hz

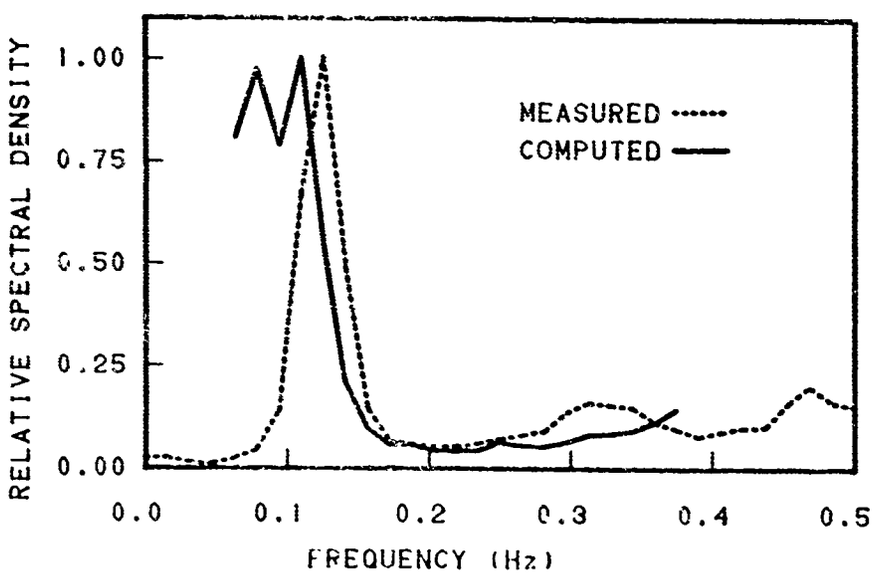

Figure 37B. Normalized ocean wave-height spectra for Run IV

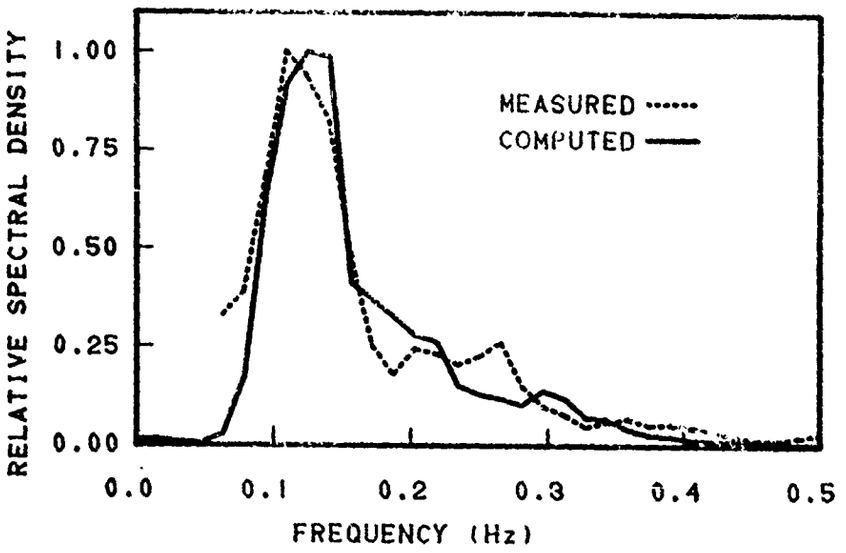

Figure 38A. Normalized acoustic spectra for Run V, 1702 Hz

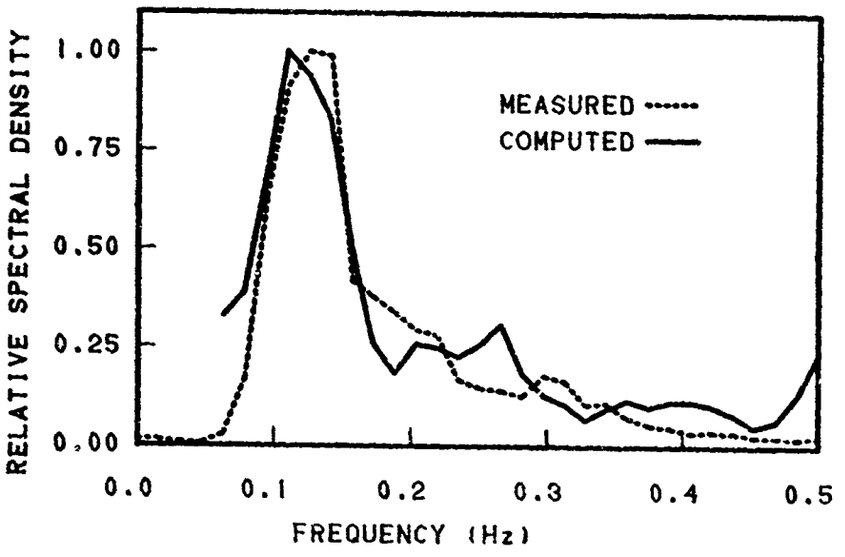

Figure 38B. Normalized ocean wave-height spectra for Run V

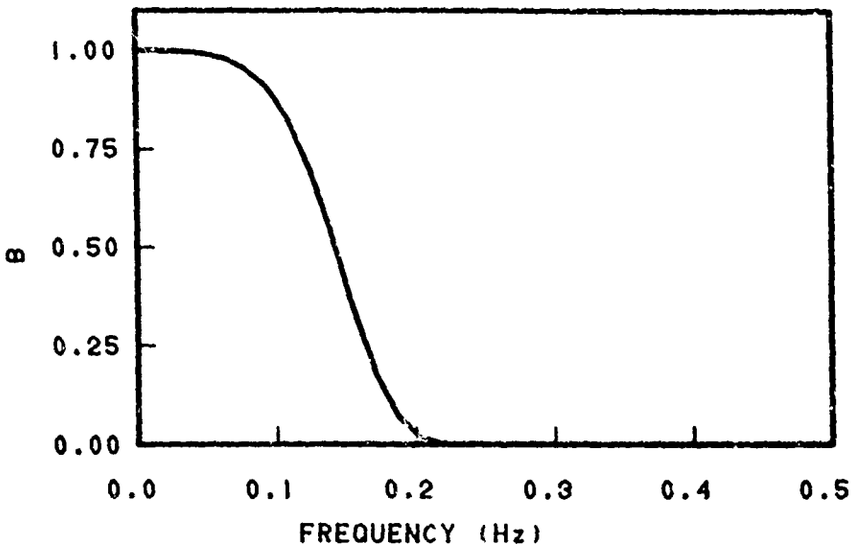

Figure 39. Normalized B function for acoustic wave number k = 0.55/m; Block Island Sound. This function was computed using data from Run VI

be seen in Figure 41B. The low-frequency end of the peak is well reproduced, but no information above 0.18 Hz can be recovered. This effect is more dramatically illustrated in Run VII (Figure 43), where the false peak in the ocean wave-height spectrum at 0.03 Hz in the measured spectrum has been filtered out. The low-frequency swell peak at 0.1 Hz is predicted almost perfectly by the acoustic method, but the wind wave peak at 0.25 Hz is completely absent.

5.3 DISCUSSION

There is better agreement between theory and experiment at 1702 Hz than at 127 Hz. This result is to be expected since the applicability of the physical optics theory to the 127-Hz BIFI scattering experiments is marginal. At 127 Hz, the acoustic wavelength of greater than 11 m is about one-fourth of the depth of the water, and bottom effects become very significant even under positive gradient conditions. For this low frequency, a normal mode model in which the scattering

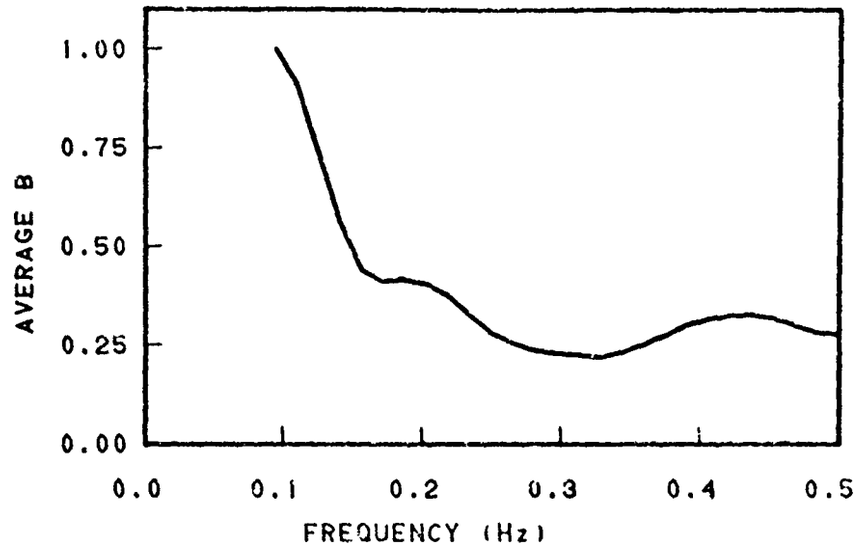

Figure 40. Normalized average measured B function for acoustic wave number k = 0.55/m; Block Island Sound

effects enter the problem through the boundary conditions would most probably yield better results.

However, from both the measured and computed weighting functions B(f) (Figures 39 and 40), it seems clear that this low acoustic frequency discriminates strongly against the high-frequency components on the sea surface, as would be expected from the Rayleigh criterion. Another factor that significantly reduces the usefulness of this low-frequency sound in wind wave studies is that the strength of the surface wave modulation is frequency dependent (Eq. 68) and decreases with increasing acoustic wavelength. This effect is graphically illustrated in Figures 22B and 26B. For a very similar sea surface condition, the scattered acoustic spectrum was 3 dB below the specular component at 1702 Hz but 21 dB below the specular component at 127 Hz. For processing systems with limited dynamic range, the 127-Hz sidebands would be in the noise level of the system and, hence, of no use.

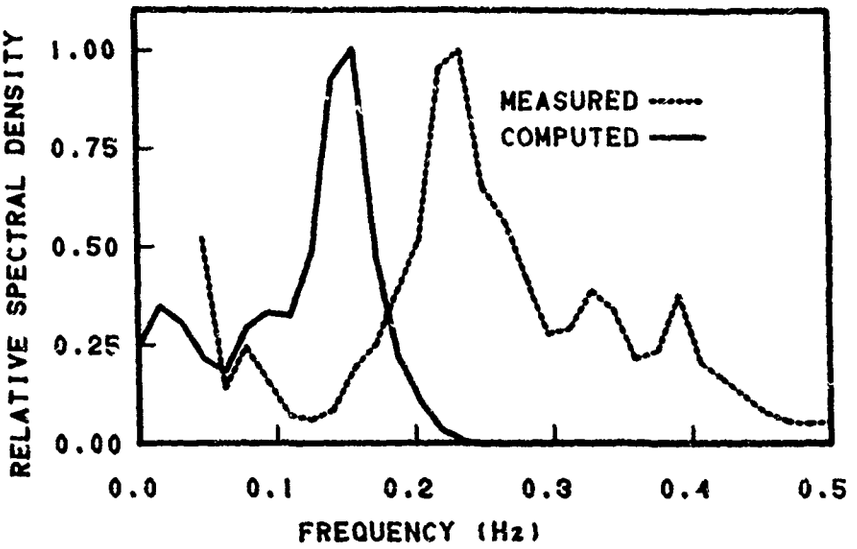

Figure 41A. Normalized acoustic spectra for Run I, 127 Hz

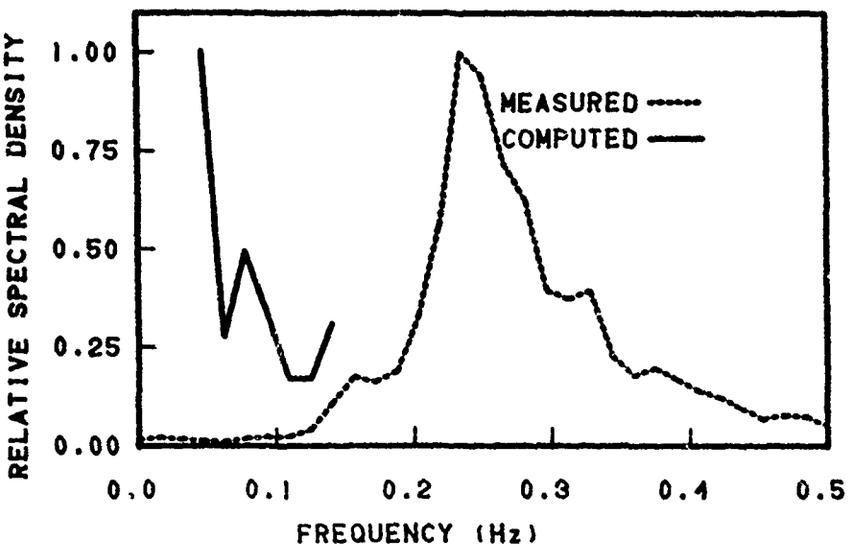

Figure 41B. Normalized ocean wave-height spectra for Run I

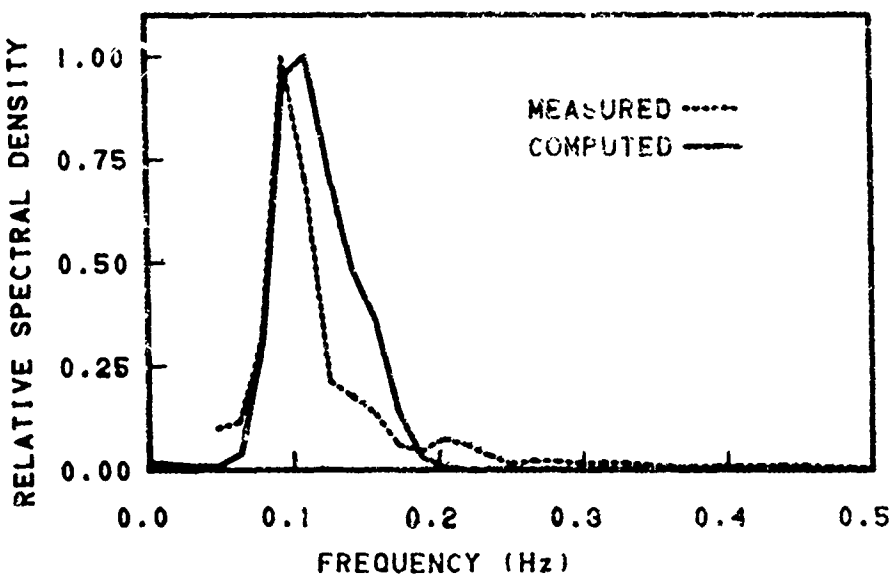

Figure 42A. Normalized acoustic spectra for Run VI, 127 Hz

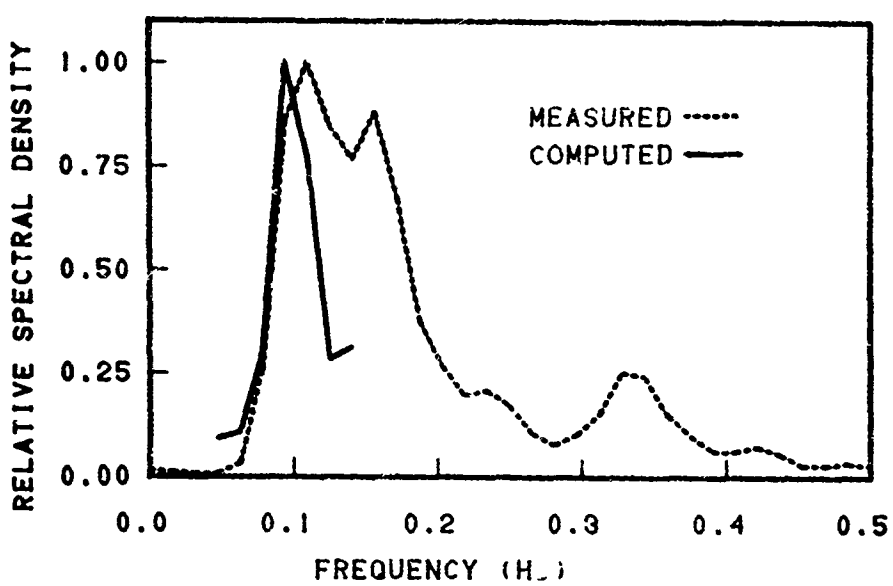

Figure 42B. Normalized ocean wave-height spectra for Run VI

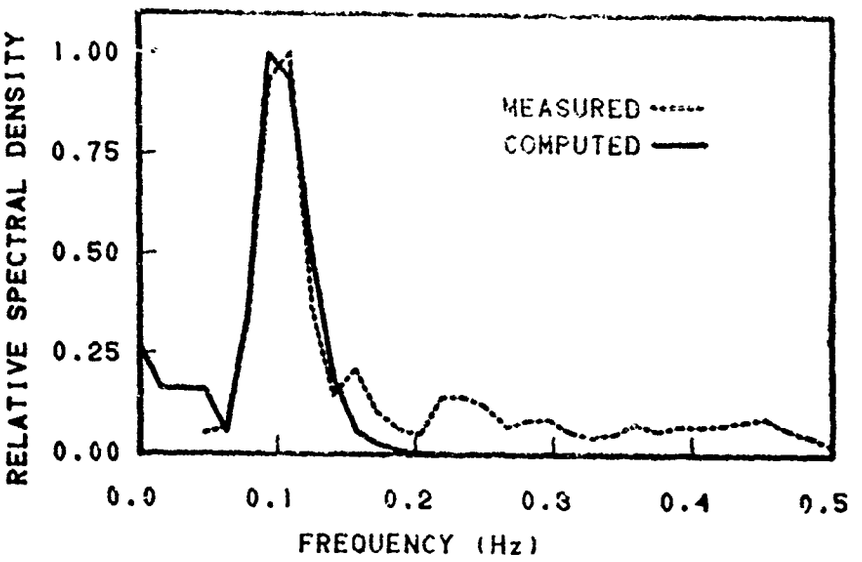

Figure 43A. Normalized acoustic spectra for Run VII, 127 Hz

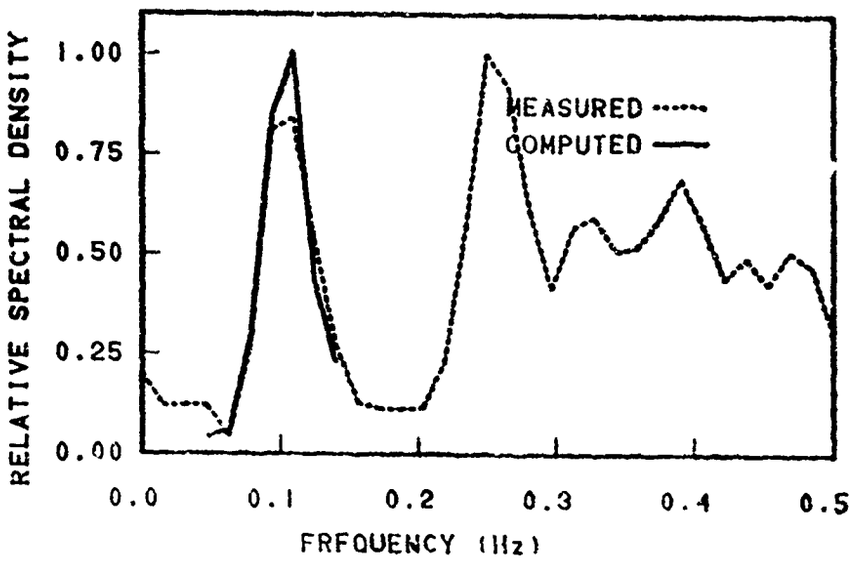

Figure 43B. Normalized ocean wave-height spectra for Run VII

Comparison of the computed and measured B functions for both 1702-Hz and 127-Hz signals reveal that the computed B function falls off with frequency more rapidly than does the measured B. The narrowness of the computed B function is most probably due to the fact that a long-crested surface wave model was used to predict the field scattered from a sea surface that is, in reality, short-crested. The long-crested wave model Eq. (51) has interpreted all the waves "seen" by the wave staff to be propagating in a direction parallel to the source-receiver line. Hence, wave trains propagating at some angle to the source-receiver line would be modeled as having greater wavelengths than they actually have (greater by $\Lambda/\cos\theta_s$, where θ_s is the angle of the waves with the source-receiver line and Λ is the surface wavelength). Thus, it follows that the surface long-crested covariance function Eq. (51) overemphasizes the long wavelengths at the expense of the short wavelengths. Therefore, the long-crested scattering model does not adequately represent the effects of the higher frequency surface waves. Hence, since the B(f) function is calculated by assuming that all the waves are propagating in a direction parallel to the source-receiver line when they really are not, it follows that B(f) will be deficient at high frequencies to an extent controlled by the deviation of the real sea surface from the ideal long-crested sea surface.

In addition, the long-crested scattering model does not take into account scattered contributions from outside the plane of incidence. These contributions may be characterized by large scattering angles, which correspond to high frequencies.

On the basis of these considerations, it is highly probable that, when this physical optics model is generalized to include the short-crested sea surface model (Pierson[40]), the slope in the B function (Figures 33 and 39) will be reduced. The deficiency of the model at high frequencies offers a possible explanation for the poor results of Run I and the reasonably good results of Run VI. This effect is illustrated by comparing the 127-Hz acoustic spectra for Runs I and VI (Figures 41A and 42A). During Run I, the sea surface was wind driven and consisted primarily of short, choppy waves. During Run VI, the sea surface was dominated by incoming swells. Since a much better approximation of a long-crested sea[45] is provided by swells than by short wind waves, the results from Run VI are significantly better than those for Run I. Thus, the agreement between measured and predicted acoustic spectra is partially a measure of how nearly long-crested is the sea surface.

This effect is not so pronounced for the 1702-Hz experiments since the shorter acoustic wavelength used gives greater weight to the short gravity waves on the sea surface. Hence, good results were obtained for Run III even though the wave-height spectral peak occurred at 0.4 Hz.

When the physical optics short-crested model is developed, the B function (Figures 33 and 39) will probably approach unity for the case of an omnidirectional source and receiver located far from land boundaries. Therefore, it is reasonable to conclude that, when all angles of incidence and reflection are taken into account and a short-crested model for the sea surface is employed, the generalized physical optics model will be in agreement with Marsh's prediction that the first-order sidebands are the

uniformly weighted sea surface height spectrum. Hence, the use of an omnidirectional or wide-beam source, combined with the generalized physical optics theory, greatly increases our ability to obtain sea surface information by acoustic means.

5.4 PHYSICAL OPTICS THEORY AS AN AID TO OCEAN WAVE STUDIES

Parkins' single-area scatter theory[16] predicts that the reradiated spectrum consists of a line at the carrier frequency plus two delta functions that depend on the acoustic wavelength, the surface wave-height spectrum, and the angle of incidence and observation. Hence, for the low roughness case, Parkins' theory could yield information about only one frequency component in the sea surface. The generalized physical optics theory, as presented here for the omnidirectional source, considers contributions from many subsections where each subsection corresponds to a Parkins' type model. When the contributions from all the subsections are summed by the method of Clay and Medwin,[20] the result is not three delta functions but a spectral band with contributions coming from each elementary section. Each section contains information about a particular frequency component of the sea surface so that, in theory, a wide band of surface frequencies can be measured.

The nature of the transfer function B of the acoustic experiment is that of a low-pass filter that is relatively flat out to a certain point and then begins to fall off. It appears that the rate of fall predicted by the physical optics long-crested

model is too high and would be decreased by employing the short-crested model.[40,41]

These considerations from the physical optics method indicate that the most practical way to measure the wave-height spectrum acoustically is to spectrally analyze the surface reradiated signal from an omnidirectional source. If the surface is not too rough, the distribution of variance in first-order sidebands in the acoustic spectrum will be similar to the sea surface spectrum out to a given point on the frequency axis when the weighting function begins to fall. When it is near zero, no information about the wave-height spectrum can be obtained. The location of this cutoff point and the slope must be determined for each new experimental situation by the methods described above. The total variance in the wave-height spectrum can be determined in principle from the coherent component in the received signal spectrum.

5.5 SPECIAL PRECAUTIONS

In Runs II, III, V, VI and VII, there was reasonably good agreement between theory and experiment. Run IV on the other hand showed a peak in the acoustic spectrum not predicted by theory, whereas Run I diverged completely from theory. When the sound spectrum level plots (Chapter 4) for these runs are examined and compared with the computed curves of this chapter, it is seen that the best results are obtained when the level of the sidebands is high compared with the level of the carrier. For example, in Run V, the sidebands are only about 3 dB below the carrier and excellent agreement was obtained. In Run I, the sidebands were on the order of 35 dB below the carrier, and in Run IV the sidebands were 30 dB below the carrier. At 127 Hz, the coherent component dominates the spectrum, and it is very difficult to retrieve useful information. At this frequency,

the surface modulation is very weak and may be distorted by background noise. In addition, on very calm days, such as the day Run IV was made, mixing may be reduced in the water column and density gradients that would invalidate the assumption of an isovelocity medium can develop.

It can therefore be inferred that the conditions for obtaining the maximum information possible from the acoustic experiment are as follows:

1. High acoustic frequency (within the constraints of the small roughness approximation).

2. Sufficiently rough surface to produce vigorous modulation of the acoustic waves, but not so rough as to violate the small roughness approximation.

3. Good signal-to-noise ratios in the recording and processing electronics.

4. The water column must be well mixed.

6.0 CONCLUSIONS

The surface reradiated signal spectra estimated from acoustic measurements in Block Island Sound during isovelocity or positive gradient conditions are spread in frequency and have two primary features:

1. A specular component exists at the transmitted frequency and some scattered energy exists immediately adjacent to the specular component. The scattered energy effectively broadens the specular component. This broadening could be the result of second-order scattering or modulation by infragravity waves, internal waves, or tides.

2. When either sea or swell (but not both) are present on the sea surface, energy is contained in the first-order sidebands of the acoustic spectrum close to the peak frequency in the surface wave-height spectrum. When sea and swell occur simultaneously, the modulation effect of the swell tends to mask the modulation effects of the sea.

Second-order sidebands were present in only one measurement, which was taken at 1702 Hz when the mean-square wave height was 0.06 m^2. In all other cases, the mean-square wave height was less than 0.06 m^2 and no second-order sidebands could be positively identified.

The acoustic spectra measured simultaneously at 4.5 km and 31 km from the sound source are remarkably similar with regard to peak location of first-order sidebands. Both the specular component and the sidebands are generally narrower for the data at long range. This occurs because the high-frequency Doppler,

which corresponds to steep angles of scatter, is more heavily attenuated by successive reflections than is the low-frequency Doppler, which corresponds to small angles of scatter.

The scattering is much stronger at 1702 Hz than at 127 Hz. For one experiment during nearly similar sea conditions, the level of the first-order sidebands was 3 dB below the carrier level at 1702 Hz but 21 dB below the carrier level at 127 Hz.

The generalized physical optics, long-crested scattering theory predicts that the spectrum of an incident sinusoidal signal reradiated by the rough, moving surface of the sea consists of the following:

1. A specular (coherent) component that is free from Doppler spreading and that occurs at the transmitted (carrier) frequency.

2. A scattered component that is symmetrical about the carrier; this component is the weighted sea surface height spectrum. The weighting function depends on the signal frequency, the experimental geometry, and the mean-square wave height; it applies only to conditions of low surface roughness, i.e.,

$$2c_m c_n \sigma^2 \rho < 1 \ .$$

The generalized physical optics, long-crested model developed in this study provides reasonably good agreement with field measurements, if the level of the acoustic sidebands are not more than 25 dB below the level of the carrier.

Agreement between theory and experiment was significantly better at 1702 Hz than it was at 127 Hz. This follows because at 127 Hz, the effects of the bottom are significant and cannot be neglected. A normal mode model, in which the surface roughness entered through the boundary conditions, would provide better

results at this frequency.

The mean-square wave height can be determined, according to theory, from the strength of the coherent component (Eq. 42) or from the ratio of the power in the sidebands to the power in the coherent component. The ocean wave-height frequency spectrum can be determined within a limited frequency band by using measurements of forward-scattered acoustic signals reradiated from the sea surface. The bandwidth in which information can be obtained is determined from the width of the B function, which depends upon the geometry of the experiment and the source frequency. More information can be obtained from high-frequency sound than from low-frequency sound if the small roughness criterion is not violated. This follows by noting that the modulation is wavelength dependent and decreases with increasing acoustic wavelength; i.e., the surface as seen by long acoustic wavelengths is smoother than the surface as seen by short acoustic wavelengths.

The weighting function B behaves like a low-pass filter that is relatively flat out to a certain point and then begins to slope down to higher frequencies to a near-zero or "cutoff" value. The rate of slope of the B function computed by means of the theoretical model is greater than the corresponding slope of the B function computed by means of field data. This discrepancy results from the fact that the long-crested ocean wave model does not contain sufficient energy at high frequencies, when the ocean is really short-crested.

When the generalized physical optics theory is extended to include the short-crested sea surface model (Pierson[40]), the slope in the B (weighting) function will be decreased. For unrestricted experimental geometry, the B function will probably approach

unity over the gravity wave band. Hence, the generalized physical optics theory approaches Marsh's prediction that the spectral density of the first-order sidebands in the received, reradiated signal spectrum is identical, within a constant, to the spectral density of the ocean wave height.

As a remote analytical probe for studying the dynamics of the ocean surface, the acoustic test range offers exciting possibilities, but much further study is still required. One feature of the acoustic method is that the acoustically measured wave-height spectrum contains information about a very large area of the sea surface (up to many thousands of square meters), whereas the wave staff is a point measurement. Hence, it cannot be expected that the spectra estimated from acoustic and wave-staff methods should be identical. It appears that the acoustic forward-scattered spectrum can provide an effective means of studying the distribution of water wave phase velocities and the limits of applicability of the dispersion relation. The forward-scattered spectrum can also be used to determine the suitability of various sea surface models (such as the long-crested, the short-crested, and the isotropic) that predict the effects of the sea surface on reradiated acoustic and electromagnetic waves. Before such analytical studies can be made, however, much further research is indicated. Some topics for future research are presented in the next chapter.

7.0 SUGGESTIONS FOR FURTHER STUDY

Among the most difficult problems in the present study are the choice of size for the effective scattering area on the ocean surface and the selection of the length of the subsection (L). The long-range experimental results are also complicated by the fact that Block Island Sound is a shallow coastal area with strong tidal currents; hence, one is forced to deal with data that have been contaminated to at least some degree by multipath interference effects.

Since the surface scattering problem is rather difficult to begin with and has not been completely solved for even the single-reflection case, it does not appear wise at this time to attempt to create an all-inclusive theoretical model that could predict the forward-scatter spectrum resulting from multiple scattering in a stratified medium with a rough, moving boundary and a boundary with a variable acoustic impedance. Therefore, with the main purpose of this thesis always in mind (i.e., to study the ocean surface by means of reflected and scattered underwater sound and, hopefully, to show that new things can be learned about the ocean surface spectrum and the distribution of phase velocities by means of the remote acoustic probe), a new experiment is proposed, along with additional theoretical work.

7.1 THE IDEAL OCEAN WAVE/ACOUSTIC SCATTERING EXPERIMENT

Although the omnidirectional source provides the maximum information about the sea surface in the received signal spectrum, interpretation is difficult. A

better means of obtaining this information, in which much greater control over the experiment could be achieved, would involve a multifrequency array and one or more remote receiving arrays in which the beam shape and the angles of incidence on the surface could be controlled. With such an array, the size of the scattering area could be easily determined, both theoretically and by measurements in the field. When the shape of the illuminated area is known, the other parameters in the model, P and L, could be precisely determined. In addition, the array should be in deep water to eliminate the multipath effects at low acoustic frequencies, which are inevitable in shallow water. The ocean in the test area should be as nearly homogeneous as possible or should show a slight increase of temperature with depth from the surface to the bottom. The Arctic Ocean offers suitable locations for the array. However, if the theoretical model is expanded to include refraction effects, the area off Bermuda could be used and suitable arrays have been installed there. Roderick and Cron[18] have already reported on a surface scattering experiment conducted in this area.

With such a setup, it would be possible to vary the size of the illuminated area on the surface, to change the angles of incidence (with more than one receiving array), and to determine the coherence between elements of the receiving array so that spatial information on the scattering surface could be obtained.

In addition, much rougher sea states are possible in the open ocean, and the wave-height spectrum is more readily predictable and is free from land mass refraction, reflection, and diffraction effects that render basic physical studies very difficult. In deep water, of course, the dispersion relation is more nearly satisfied.

The ocean wave-height spectrum should be determined by means of Stillwell's[68] optical technique or by stereo photography, as in the Stereo Wave Observation Project (SWOP)[69] experiments.

7.2 ADDITIONAL THEORETICAL STUDY

Two extensions of the generalized physical optics theory are evident:

1. Include the short-crested ocean wave model (Pierson[40]) to determine directional effects and to compute a more accurate weighting (B) function.

2. Extend the theory to allow for larger surface roughness. An initial way to do this would be to take more terms in the power series expansion for $\exp\left\{2c_m c_n \sigma^2 \rho\right\}$ and solve the resulting algebraic (but no longer linear) equation for $S(\omega)$ by numerical means, if necessary. As a starting point for this generalization, it would be better to start with the physical optics theory as formulated by Nuttall and Cron.[19]

3. Include the effects of sound speed gradients in the scattering model.

Appendix A

THE ILLUMINATION FUNCTION

The illumination function in acoustic scattering theory describes how the acoustic intensity is distributed over the reflecting surface. The simplest illumination function is the box car (rectangular) function, which is 1 inside the illuminated area and zero outside. Beckmann and Spizzichino[29] and Parkins[16] use this illumination function.

Clay and Medwin[20] point out, however, that this function leads to undesirable diffraction sidelobes, which would be a serious problem when acoustic intensities from many subsections are summed. To avoid this, they use a Gaussian Illumination Function of the form

$$\exp\left\{-\left[(x - X_m)^2/L + (y - y_m)^2/L_1\right]\right\},$$

where

(X_m, Y_m) = center of the subarea

L and L_1 = lengths of the subsections.

When the summation is made, one subarea can be smoothed into the next by the proper choice of parameters.

In this study a more general method (due to Nuttall[44]) is used in which it is possible to use any reasonable illumination function. The Gaussian function is

chosen in this work for the reasons given by Clay and Medwin.[20]

The function $H(\beta, u)$, from Eq. (28) in the main text, has been defined as

$$H(\beta, u) \equiv \int_{-\infty}^{+\infty} dx \exp(i\beta x)\, I\left(\frac{x - \frac{u}{2}}{PL}\right) I\left(\frac{x + \frac{u}{2}}{PL}\right) . \qquad (A\text{-}1)$$

For the Gaussian Illumination Function, this becomes

$$H(\beta, u) = \int_{-\infty}^{+\infty} dx \exp(i\beta x) \exp\left\{ - \left(\frac{x - \frac{u}{2}}{PL}\right)^2 - \left(\frac{x + \frac{u}{2}}{PL}\right)^2 \right\} . \qquad (A\text{-}2)$$

Expanding the exponents and collecting terms yields

$$H(\beta, u) = \int_{-\infty}^{+\infty} dx \exp(-2\ x^2 + i\beta x)\ \exp(-u^2/2) . \qquad (A\text{-}3)$$

This integral can be evaluated (Kinsman[70]) and the result is

$$H(\beta, u)\, PL\, (\pi/2)^{1/2} \exp\left\{ - \beta^2 P^2 L^2/8 - u^2/2p^2 L^2 \right\} . \qquad (A\text{-}4)$$

Now, the functions $\bar{H}\left(\beta, \alpha - \frac{\omega^2}{g}\right)$ and $\bar{H}\left(\beta, \alpha + \frac{\omega^2}{g}\right)$, from Eq. (58) in the main text, are evaluated. Define the Fourier Transform $\mathcal{I}(r)$ of the illumination function $I(x)$:

$$\mathcal{I}(r) \equiv \frac{1}{2\pi} \int_{-\infty}^{+\infty} dx \exp(-irx)\, I(x) \ ; \qquad (A\text{-}5)$$

therefore,

$$I(x) = \int_{-\infty}^{+\infty} dr \exp(irv)\, \mathcal{L}(r) \quad . \tag{A-6}$$

Substituting Eq. (A-6) into Eq. (54) of the main text yields

$$\bar{H}\left(\beta, \alpha - \frac{\omega^2}{g}\right) = \frac{1}{2\pi} \int_{-\infty}^{+\infty} du \left[\exp\left\{ -i \left(\alpha - \frac{\omega^2}{g}\right) u \right\} \int_{-\infty}^{+\infty} dx \exp(i\beta x) \right.$$

$$\cdot \int_{-\infty}^{+\infty} \int da'\, db' \exp\left\{ i \left[a' \left(\frac{x - \frac{u}{2}}{PL} \right) + b' \left(\frac{x + \frac{u}{2}}{PL} \right) \right] \right\}$$

$$\left. \cdot \mathcal{L}(a')\, \mathcal{L}(b') \right] . \tag{A-7}$$

Factoring the terms in Eq. (A-7), interchanging the order of integration, and collecting terms in u and x result in

$$\bar{H}\left(\beta, \alpha - \frac{\omega^2}{g}\right) = \frac{1}{2\pi} \int_{-\infty}^{+\infty} du \left[\exp\left\{ -i \left[\left(\alpha - \frac{\omega^2}{g}\right) + \frac{a' - b'}{2PL} \right] u \right\} \right.$$

$$\left. \cdot \int_{-\infty}^{+\infty} dx \exp\left\{ i \left[\beta + \frac{a' + b'}{PL} \right] x \right\} \cdot \int_{-\infty}^{+\infty} da'\, \mathcal{L}(a') \int_{-\infty}^{+\infty} db'\, \mathcal{L}(b') \right] . \tag{A-8}$$

The result of integrating Eq. (A-8) with respect to v and x is

$$\bar{H}\left(\beta,\ \alpha-\frac{\omega^2}{g}\right)=\frac{1}{2\pi}\int_{-\infty}^{+\infty}da'\left[\mathcal{I}(a')\int_{-\infty}^{+\infty}db'\ \mathcal{I}(b')\,2\pi\delta\left[\left(\alpha-\frac{\omega^2}{g}\right)+\frac{a'-b'}{2PL}\right]\right.$$

$$\left.\cdot\,2\pi\delta\left[\beta+\frac{a'+b'}{PL}\right]\right]. \qquad \text{(A-9)}$$

Collecting terms and integrating with respect to b yield

$$\bar{H}\left(\beta,\ \alpha-\frac{\omega^2}{g}\right)=\frac{1}{2\pi}\int_{-\infty}^{+\infty}da'\left[\mathcal{I}(a')\,\mathcal{I}\left[a'+2PL\left(\alpha-\frac{\omega^2}{g}\right)\right](2\pi)^2P^2L^2\right.$$

$$\left.\cdot\,2\delta\left[2a'+PL\beta+2PL\left(\alpha-\frac{\omega^2}{g}\right)\right]\right]. \qquad \text{(A-10)}$$

Integrating Eq. (A-10) with respect to a yields

$$\bar{H}\left(\beta,\ \alpha-\frac{\omega^2}{g}\right)=4\pi P^2L^2\,\mathcal{I}\left[-PL\beta/2-PL\left(\alpha-\frac{\omega^2}{g}\right)\right]$$

$$\mathcal{I}\left[-PL\beta/2+PL\left(\alpha-\frac{\omega^2}{g}\right)\right]. \qquad \text{(A-11)}$$

For the Gaussian Illumination Function the result is

$$\left.\begin{aligned}
\mathcal{L}\left[-PL\beta/2 - PL\left(\alpha - \frac{\omega^2}{g}\right)\right] &= \frac{1}{2\pi}\int_{-\infty}^{+\infty} dx \exp\left\{-i\left[-PL\left(\alpha - \frac{\omega^2}{g}\right) - PL\beta/2\right]x - x^2\right\} \\
\mathcal{L}\left[-PL\beta/2 + PL\left(\alpha - \frac{\omega^2}{g}\right)\right] &= \frac{1}{2\pi}\int_{-\infty}^{+\infty} dx \exp\left\{-i\left[PL\left(\alpha - \frac{\omega^2}{g}\right) - PL\beta/2\right]x - x^2\right\}
\end{aligned}\right\} \quad \text{(A-12)}$$

When Eq. (A-12) is integrated using the method of Kinsman,[70] the result is

$$\left.\begin{aligned}
\mathcal{L}\left[-PL\beta/2 - PL\left(\alpha - \frac{\omega^2}{g}\right)\right] &= \frac{1}{2\pi}(\pi)^{1/2}\exp\left\{-\frac{1}{4}\left[P^2L^2\left(\alpha - \frac{\omega^2}{g}\right)^2 + P^2L^2\left(\alpha - \frac{\omega^2}{g}\right)\beta + P^2L^2\beta^2/4\right]\right\} \\
\mathcal{L}\left[-PL\beta/2 + PL\left(\alpha - \frac{\omega^2}{g}\right)\right] &= \frac{1}{2\pi}(\pi)^{1/2}\exp\left\{-\frac{1}{4}\left[P^2L^2\left(\alpha - \frac{\omega^2}{g}\right)^2 - P^2L^2\left(\alpha - \frac{\omega^2}{g}\right)\beta + P^2L^2\beta^2/4\right]\right\}
\end{aligned}\right\} \quad \text{(A-13)}$$

Substituting Eq. (A-13) into Eq. (A-11) yields the final result for the function $\bar{H}\left(\beta, \alpha - \frac{\omega^2}{g}\right)$ in the case of the Gaussian Illumination Function:

$$\bar{H}\left(\beta,\ \alpha-\frac{\omega^2}{g}\right)=P^2L^2\exp\left\{-\frac{P^2L^2}{2}\left[\left(\alpha-\frac{\omega^2}{g}\right)^2+\beta^2/4\right]\right\}\ . \qquad \text{(A-14)}$$

A similar procedure is followed to obtain $\bar{H}\left(\beta,\ \alpha+\frac{\omega^2}{g}\right)$.

Appendix B

OCEANOGRAPHIC OBSERVATIONS DURING THE BLOCK ISLAND SOUND TESTS

Hourly weather observations for the time period covering the acoustic/oceanographic experiments in Block Island Sound were furnished by William B. Phelan, of the U. S. Weather Bureau. The data were taken at Block Island Airport and are presented in Figure B-1.

Sound speed versus depth data obtained during the measurements are given in Table B-1. The values were computed from temperature and salinity data by means of Wilson's equation.[25]

TABLE B-1*

SOUND SPEED VERSUS DEPTH

Date	Site	Time (hr)	Depth (ft)	Sound Speed (m/sec)
29 December 1969	Station B	1025	5	1470.10
			40	1469.90
			80	1470.10
			114	1469.80
	Station C	1150	5	1469.20
			40	1469.00
			80	1469.20
			113	1469.40
	Station A	1717	5	1466.15
			54	1466.40
			107	1467.40
			160	1467.65
8 January 1970	Station B	1005	5	1464.75
			40	1465.35
			80	1466.05
			114	1466.25
	Station C	1107	5	1465.35
			35	1465.25
			72	1463.60
			110	1464.20
	Station A	1640	5	1459.80
			35	1460.00
			75	1459.70
			110	1459.50

*From Nalwalk, Rathbun, Robinson, and Riley.[53]

TABLE B-1 (Cont'd)

SOUND SPEED VERSUS DEPTH

Date	Site	Time (hr)	Depth (ft)	Sound Speed (m/sec)
16 January 1970	Station B	0945	5	1455.25
			39	1455.45
			78	1456.15
			113	1459.45
	Station C	1035	5	1455.75
			40	1456.75
			80	1457.65
			114	1460.65
	Station A	1515	5	1456.15
			43	1456.65
			86	1456.85
			124	1457.25
26 January 1970	Station B	1000	5	1452.20
			40	1454.65
			80	1457.35
			120	1457.65
	Station C	1102	5	1453.80
			37	1455.65
			75	1456.65
			115	1456.85
	Station A	1710	5	1451.20
			33	1452.60
			66	1452.40
			97	1452.80

TABLE B-1 (Cont'd)

SOUND SPEED VERSUS DEPTH

Date	Site	Time (hr)	Depth (ft)	Sound Speed (m/sec)
30 January 1970	Station B	0955	5	1452.60
			40	1453.60
			80	1449.85
			116	1457.60
	Station C	1110	5	1453.50
			39	1453.80
			78	1455.20
			113	1455.40
	Station A	1346	5	1453.30
			34	1453.50
			68	1454.10
			97	1454.80

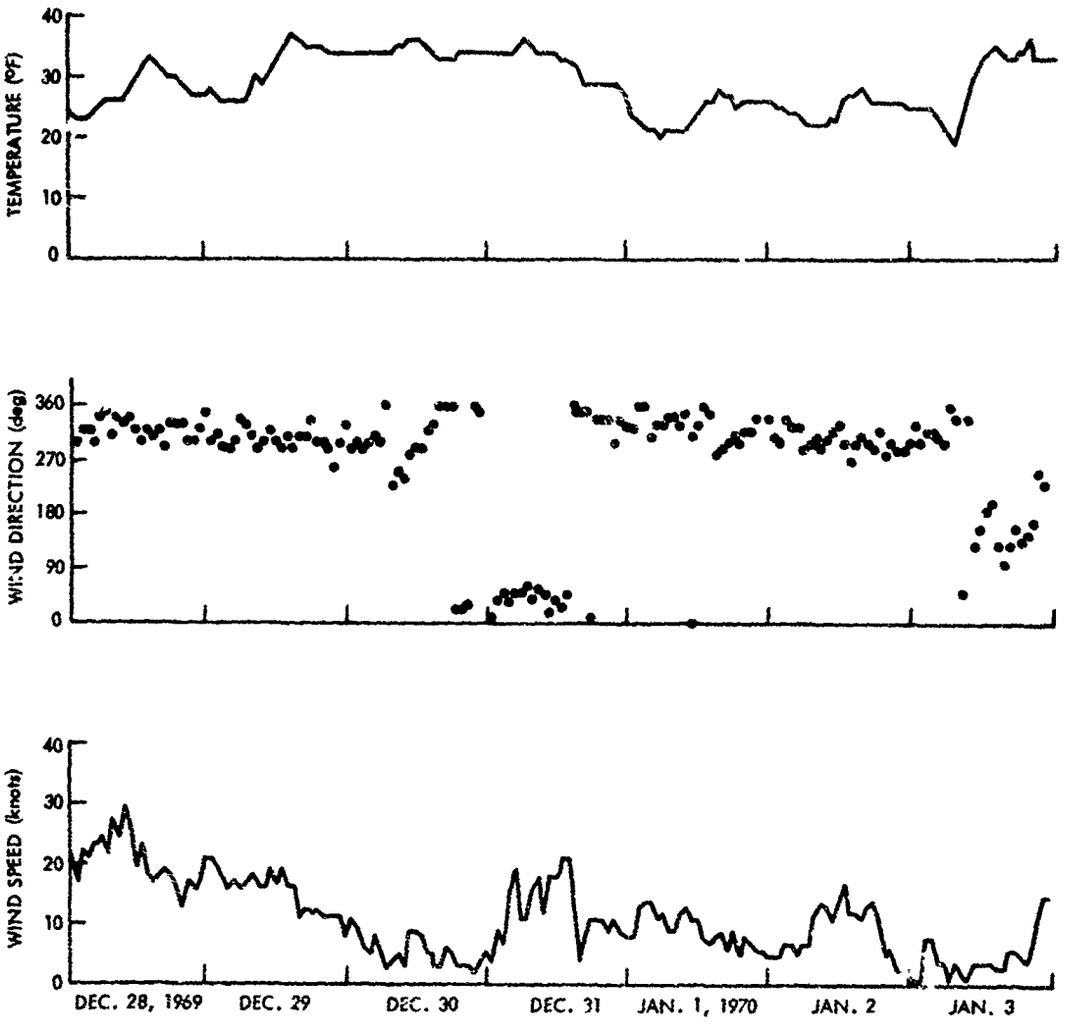

Figure B-1. Hourly weather observations at the Block Island Airport

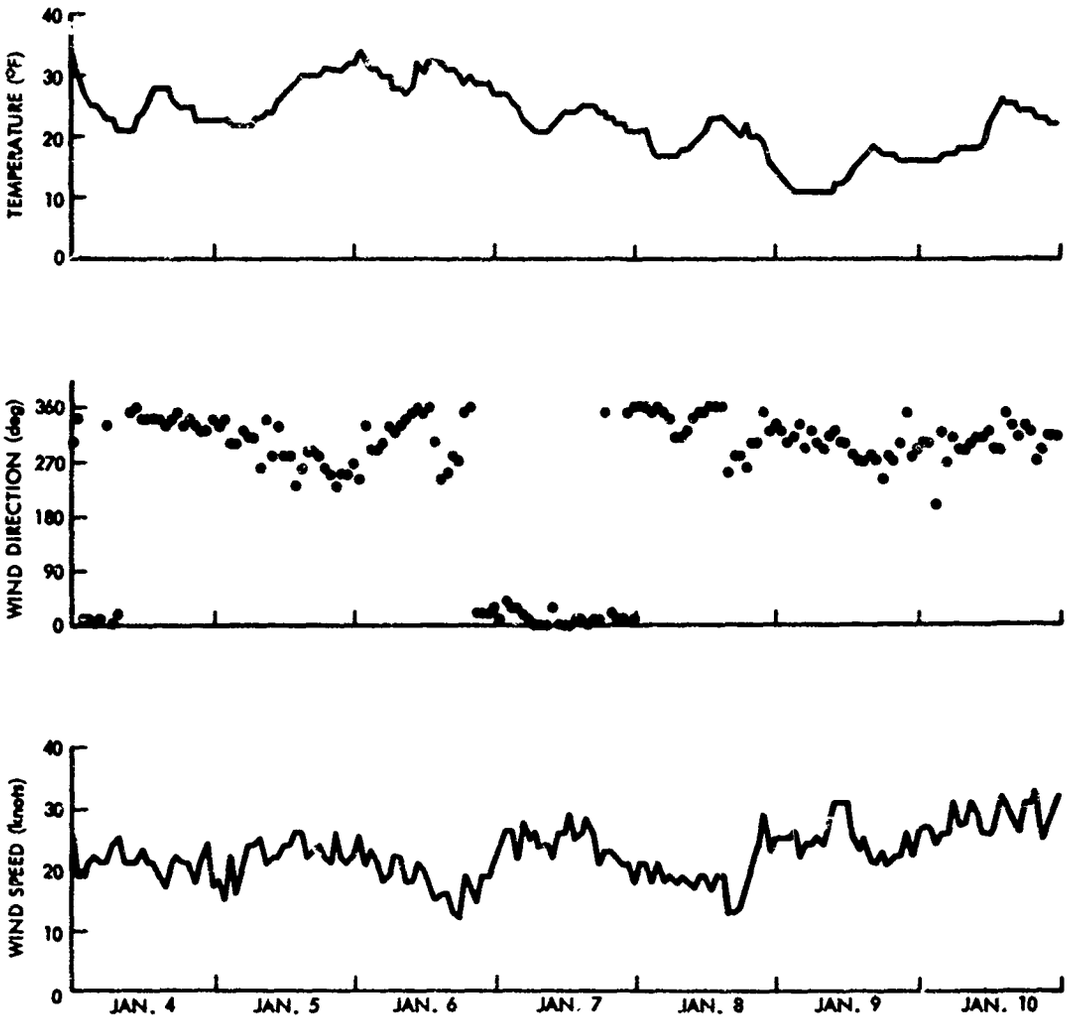

Figure B-1. (Cont'd) Hourly weather observations at the Block Island Airport

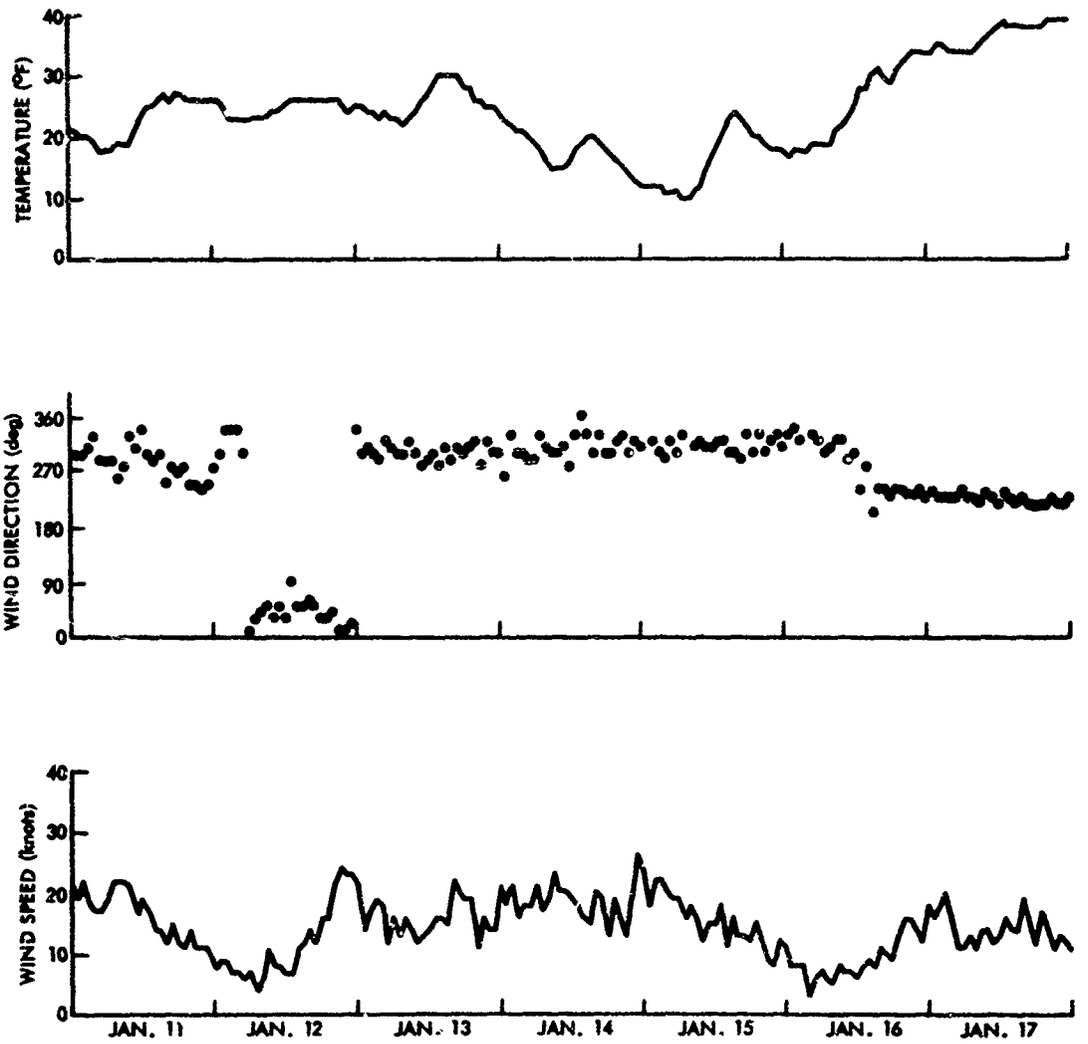

Figure B-1. (Cont'd) Hourly weather observations at the Block Island Airport

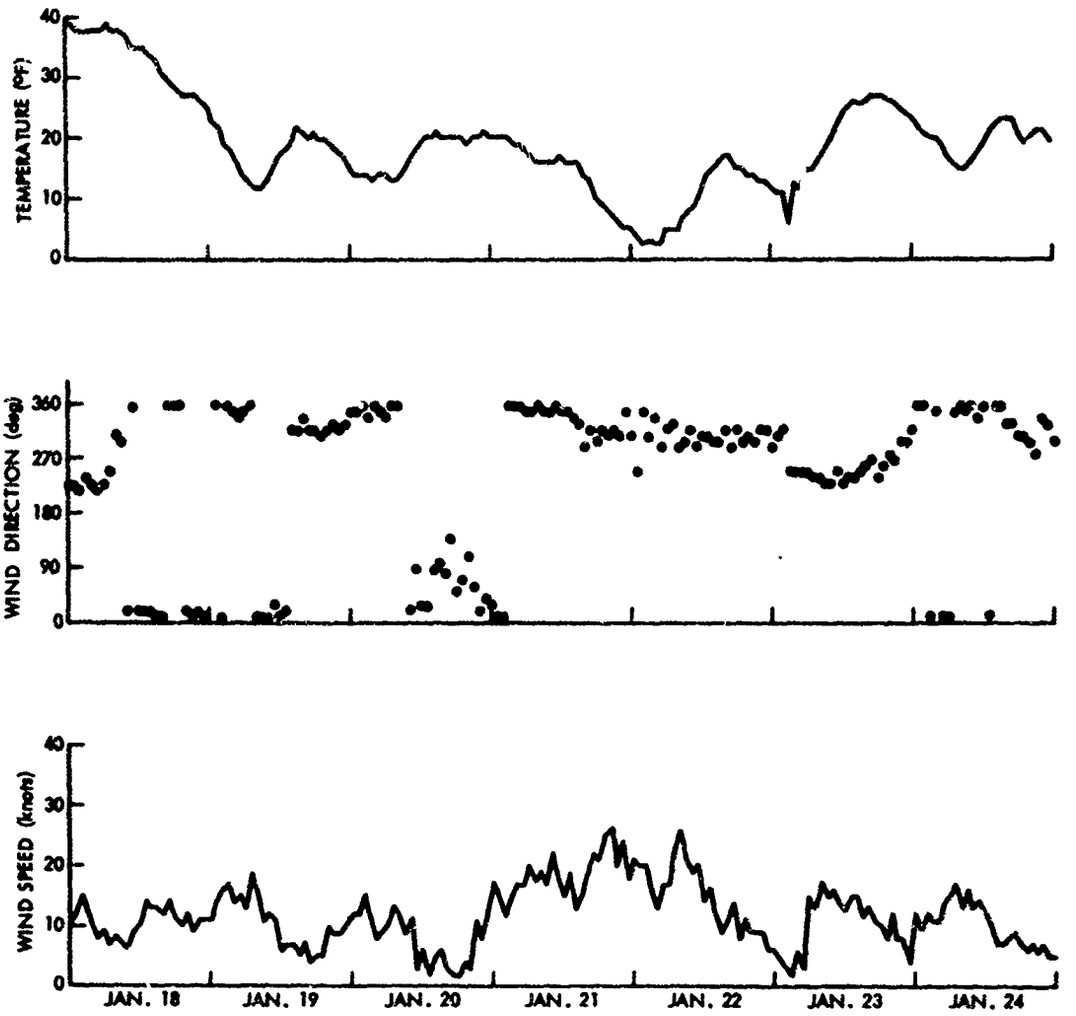

Figure B-1. (Cont'd) Hourly weather observations at the Block Island Airport

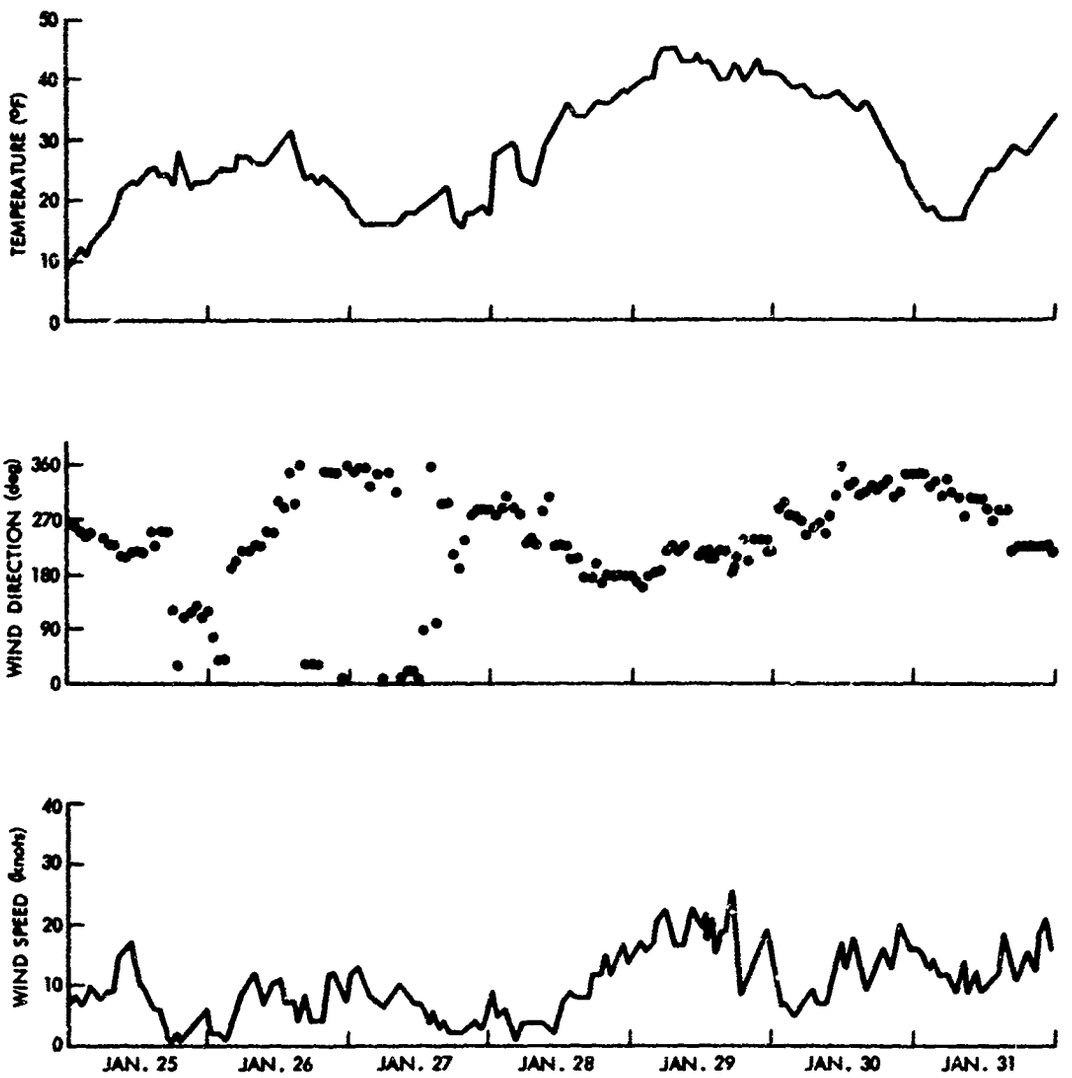

Figure B-1. (Cont'd) Hourly weather observations at the Block Island Airport

APPENDIX C

INSTRUMENTATION

The following major instrumentation was used in this study:

1. An XU-1378 magnetostrictive scroll transducer. —The XU-1378 has a resonance frequency of 1700 Hz, a bandwidth of 200 Hz, and a source level of +97.6 dB//1 μbar. It is connected to shore via cables that terminate at the Block Island field station.

2. A 127-Hz Minneapolis-Honeywell source. —This projector has a bandwidth of 25 Hz and a source level of +106.2 dB//1 μbar and consists of one stave of an HX-37 ceramic bender-bar projector. During these experiments, one of the three stages of the projector failed; consequently, the source level was somewhat less than the output specified for three stages.

3. Two bottom-mounted DT-55 hydrophones. —The hydrophones were implanted about 1-m above the bottom south of Fishers Island and were connected by cable to shore. Each of the hydrophones has a self-contained preamplifier.

4. An NUS LM-3 hydrophone.—The LM-3 contains preamplifier and calibration circuitry. It is omnidirectional and completely flat in response from 10 Hz to 100 kHz. The sensitivity is -90.4 dBV//1 μbar. This hydrophone was connected by cable to the ship's laboratory.

5. A standard Navy model Bendix anemometer. —This device was mounted on top of the Block Island field station.

6. A Braincon Type 474 wave measuring system. — This system consists of a free-floating accelerometer wave buoy, Model 231-2, tethered to a toroid mooring buoy containing a transmitter and batteries. The buoy can be turned on from shore. The data are received at the Fishers Island field station. The shape of the buoy is a truncated cone with a small cylinder extending down from its base. In the normal position, this configuration provides a flat undersurface with good wave-following characteristics. The buoy is made of fiberglass-reinforced plastic and is self-righting.

The principle employed in the accelerometer is that of measuring the rise and fall time of a moving body (a coil), which is given an upward impulse of fixed momentum relative to a reference frame. The coil is located in an annular air gap in a permanent magnet. When contacts close at the base of the gap, a monostable multivibrator circuit supplies a current pulse of fixed amplitude and duration. The system is essentially pulse-code modulated, i.e., the varying acceleration due to the ocean waves modulates the basic pulse repetition rate.

7. A 12-m aluminum spar buoy. — The buoy was designed and built by Kirk Patton, of the Naval Underwater Systems Center (NUSC).

8. An Interstate Electronics Model 438-2000 wave staff. — The staff was constructed from 1/2-in. PVC pipe and 28-gauge tophat-A resistance wire, which served as the active element. The connection to the end of the resistance wire, which is normally in the sea water, is a length of 20-gauge, vinyl-insulated wire. This insulated wire is recessed into a longitudinal slot in the PVC pipe and is held in place by the resistance wire, which is spirally wound in grooves in the PVC. The 15-ft wave staff has a standard resistance of 44 ohms/linear foot and is

clamped at both ends to the aluminum spar buoy so that the staff proper is 6 in. away from the buoy.

The staff was powered by a stable, dc power supply at 12 V and 20 mA. The staff output (0-5 Vdc) is proportional to wave height. The calibration accuracy is 1% of the dynamic range, and the linearity is 1% over 90% of the dynamic range. The voltage to the sensor unit is 5 VRMS at 500 Hz. The electronics package contains fully transistorized circuitry and is housed in a PVC cylinder. A calibration check performed at the NUSC Millstone Pond facility, along with a block diagram of the system, is shown in Figure C-1. A system calibration was performed in the field before and after each run.

9. An NUS TR-4 velocimeter. —The NUS TR-4 consists of a pair of piezoelectric ceramic transducers and an acoustic reflector rigidly mounted to form a sound path of known geometry. The sound path is folded to minimize Doppler error due to fluid flow along the acoustic path. The on-deck equipment consists of an amplifier, a frequency doubler, and an electronic counter. The frequency of the counter was read at 3-m depth intervals and was converted to sound speed by an equation of the form $C = Kf$, where C is the sound speed, f is the frequency, and K is the constant. The accuracy of this instrument is 0.15 m/sec with a stability of 0.01 m/sec.

10. General-Radio, coherent decade frequency synthesizers (Type 1161). —One synthesizer was used to control the output frequency of the sound source. The other synthesizers were used to generate the reference signals that were recorded on the magnetic tape with the data signal to provide for tape speed control and band shifting. This instrument is a tunable quartz-crystal-controlled oscillator

with resolution to nine significant figures. It has an rms fractional frequency deviation on the order of 3 parts in 10^9.

Although these instruments provide an extremely accurate and stable output, it was not always possible to set the frequency difference between the transmitted signal and the center frequency of the received signal to exactly 8 Hz. This difficulty occurred because, on some occasions, frequency counters with sufficient accuracy to check the output of the synthesizers were not available. Hence, although no drift occurred in the synthesizer output, the absolute frequency was slightly in error. A central timing control system could have been used to lock all synthesizers at the desired frequency, but none was available. As indicated in the text, this error is corrected by measuring frequency shifts in the received signal from the peak observed carrier frequency, rather than from 8 Hz.

11. A Montronics frequency synthesizer. — This synthesizer was used to record a stable frequency on the magnetic tape for use in analog-to-digital conversion of the R/V UCONN data.

12. An Ampex Model FR-1200, 14-track, analog tape recorder.—The signals from the Fishers Island hydrophone were FM recorded at 7 1/2 IPS. At this tape speed, the frequency response to within 1 dB is 0 to 2500 Hz, with a signal-to-noise ratio of 42 dB (broad band) and a total harmonic distortion of 1.5%. The record-reproduce voltage linearity is 1.0% of full band.

13. An Ampex Model CP 100D, 7 track, analog tape recorder on R/V UCONN. — The data were FM recorded at 7 1/2 IPS. At this tape speed, the frequency response to within 1 dB is 0 to 2500 Hz, with a broad-band signal-to-noise ratio of 42 dB and a 1-Hz band signal-to-noise ratio of 60 dB. Tape flutter

is rated at less than 0.25%.

14. Two Intronics Model M502 wideband analog multipliers.—The multipliers were employed to bandshift the acoustic and radio signals to 8 Hz prior to recording. These instruments feature four quadrant dc operation on both inputs and employ variable transconductance to maintain a smooth linearity. The full-scale accuracy is ±0.5% in amplitude. Maximum deviation from linearity is ±.3%.

The instrumentation used during the accelerometer buoy experiments is shown in Figure C-2. The acoustic signal was recorded on tape and later bandshifted to 2 Hz for computer processing. The accelerometer buoy signal was played into a frequency-to-voltage converter, the output of which was digitized for computer analysis.

For Runs 1 through 7, the acoustic signal was bandshifted to 8 Hz before it was recorded on magnetic tape. Extreme care was taken to eliminate the effects of tape flutter. A 12.5 kHz signal generated by a quartz-crystal, frequency synthesizer (Montronics) was recorded[71] and later used in a servocontrol phase lock system on playback during analog-to-digital conversion. In addition, a 256-Hz sampling frequency from a stable oscillator, as well as voice and time code, was recorded. Block diagrams of the electronics aboard R/V UCONN and at the NUSC laboratory are shown in Figures C-3 and C-4, respectively.

In a later version of these experiments, performed in late January 1970, the acoustic signal was transmitted over a radio link and the bandshifted radio frequency was recorded simultaneously with the bandshifted acoustic signal and the wave staff output, as shown in Figure C-5. The purpose of this modification was to prove that none of the sideband structure seen around the acoustic signal spectrum was

due to instrumentation. Some other minor changes were also made to improve the quality of the recording, such as using a bucking voltage to eliminate the dc component of the wave staff. In addition, the internal 13.5-kHz FM subcarrier was recorded and used on playback in a new flutter compensation system, which improved the signal-to-noise ratio by 6 dB.[71]

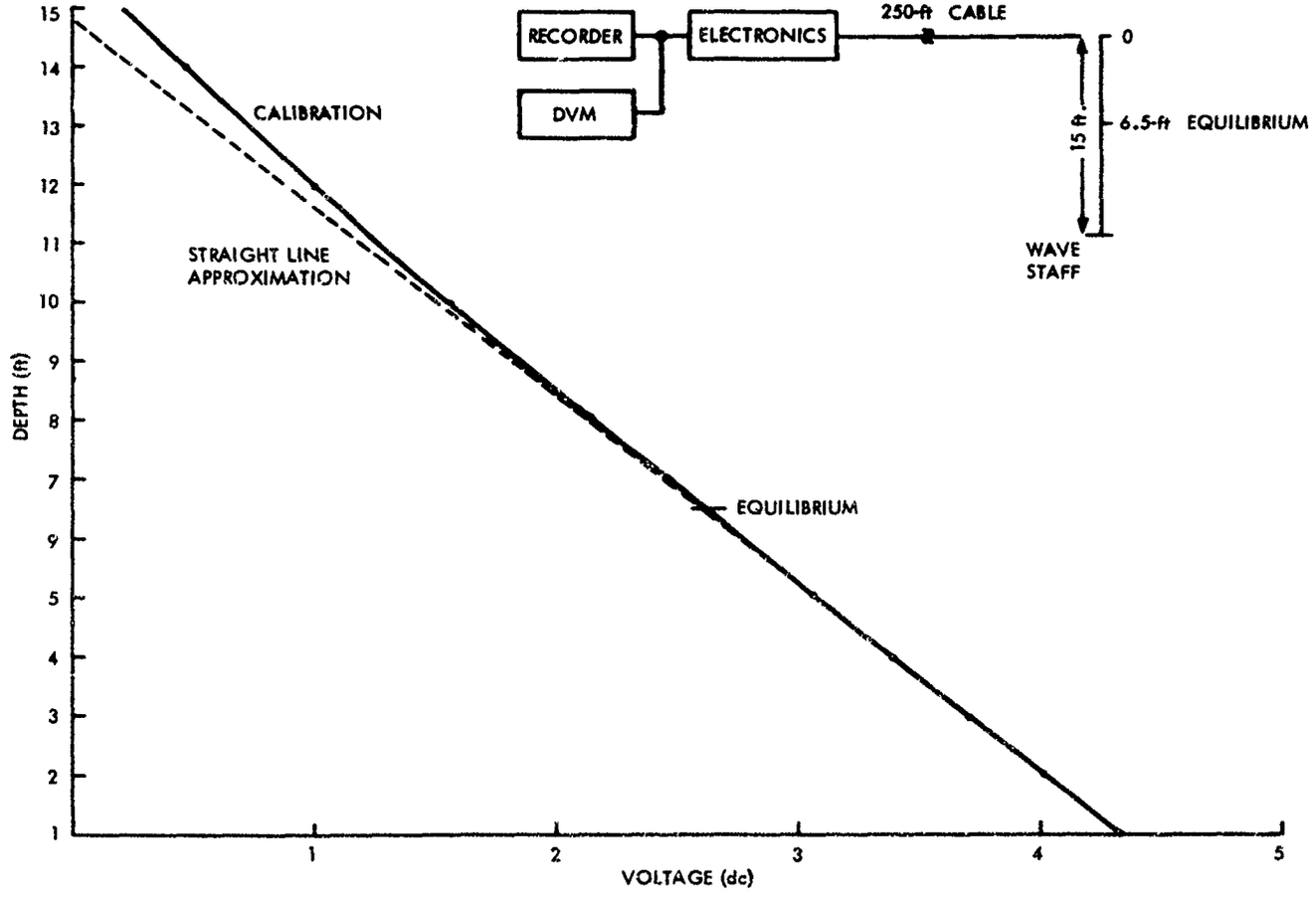

Figure C-1. Wave-staff calibration at Millstone Pond

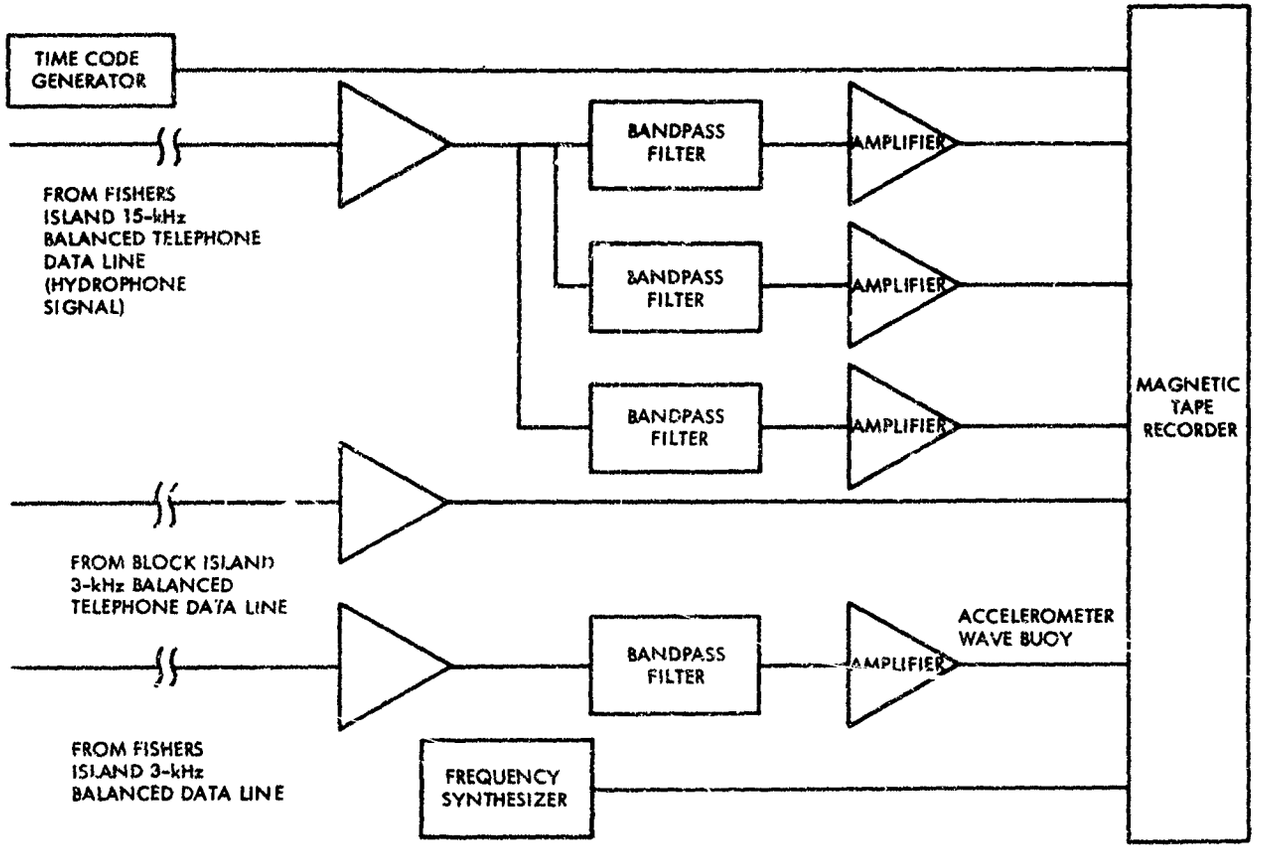

Figure C-2. Recording electronics for the accelerometer buoy experiment

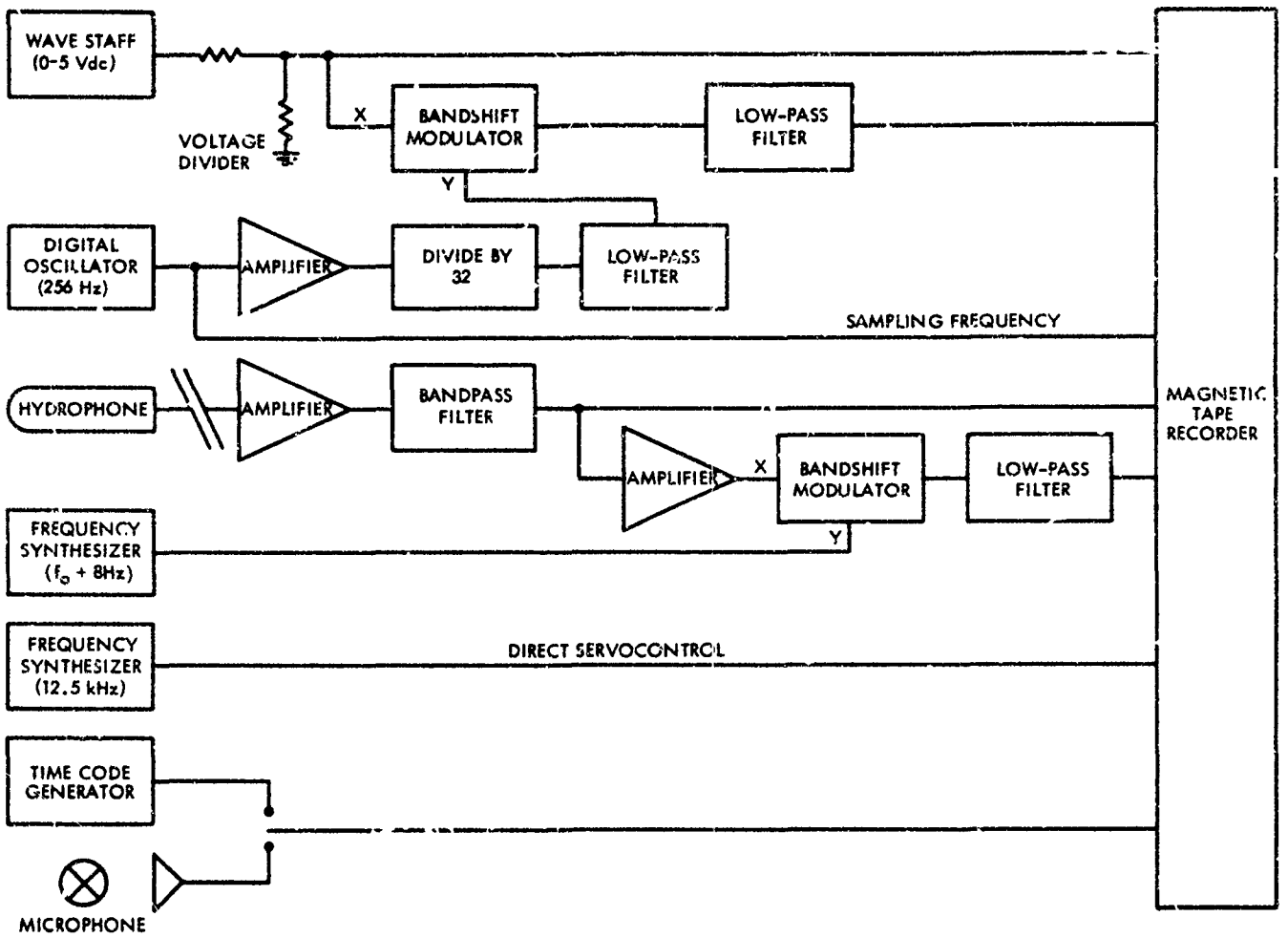

Figure C-3. Receiving and recording electronics aboard R/V UCONN
(29 December 1969 - 25 January 1970)

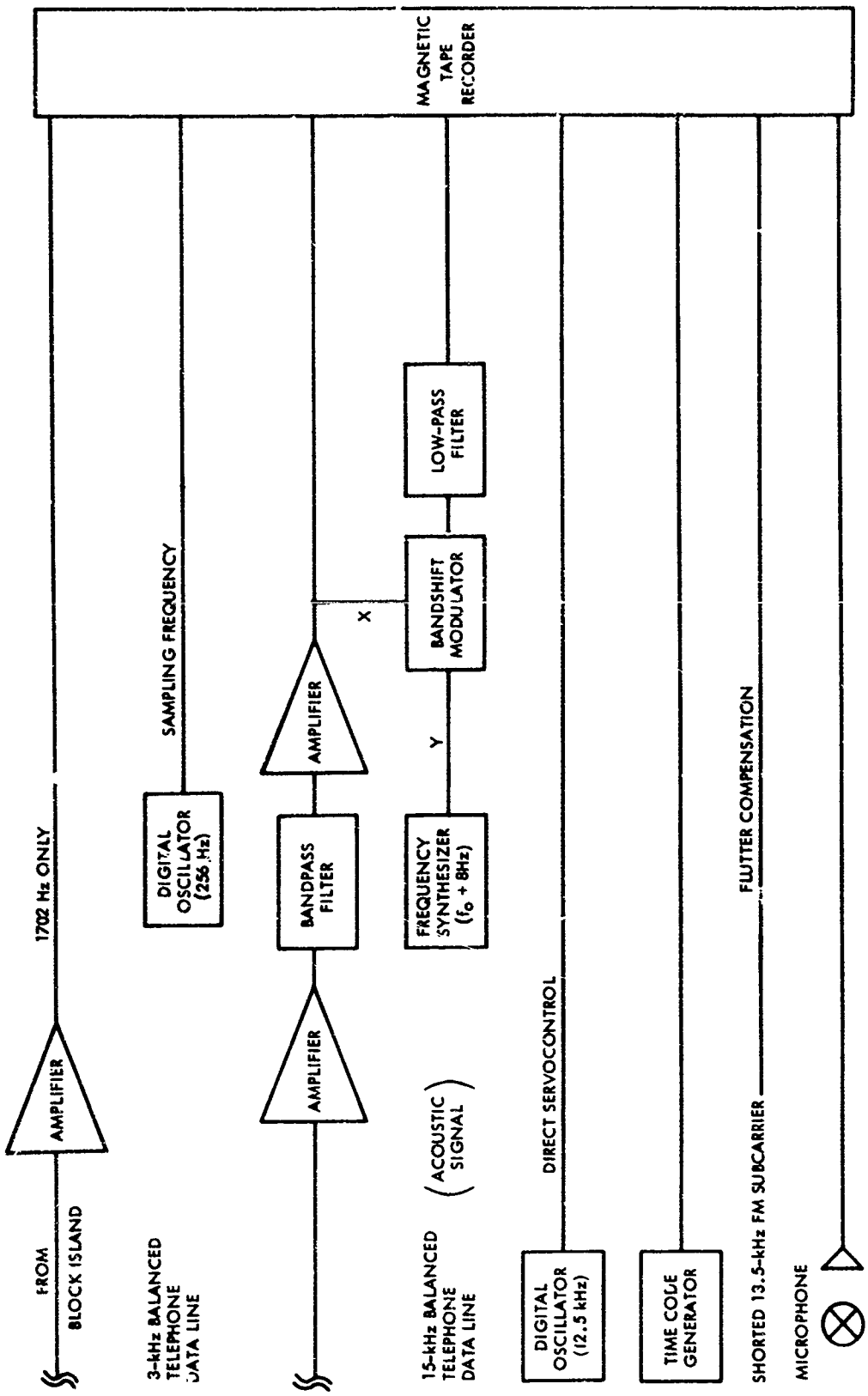

Figure C-4. Recording electronics at the Naval Underwater Systems Center (29 December - 30 January 1970)

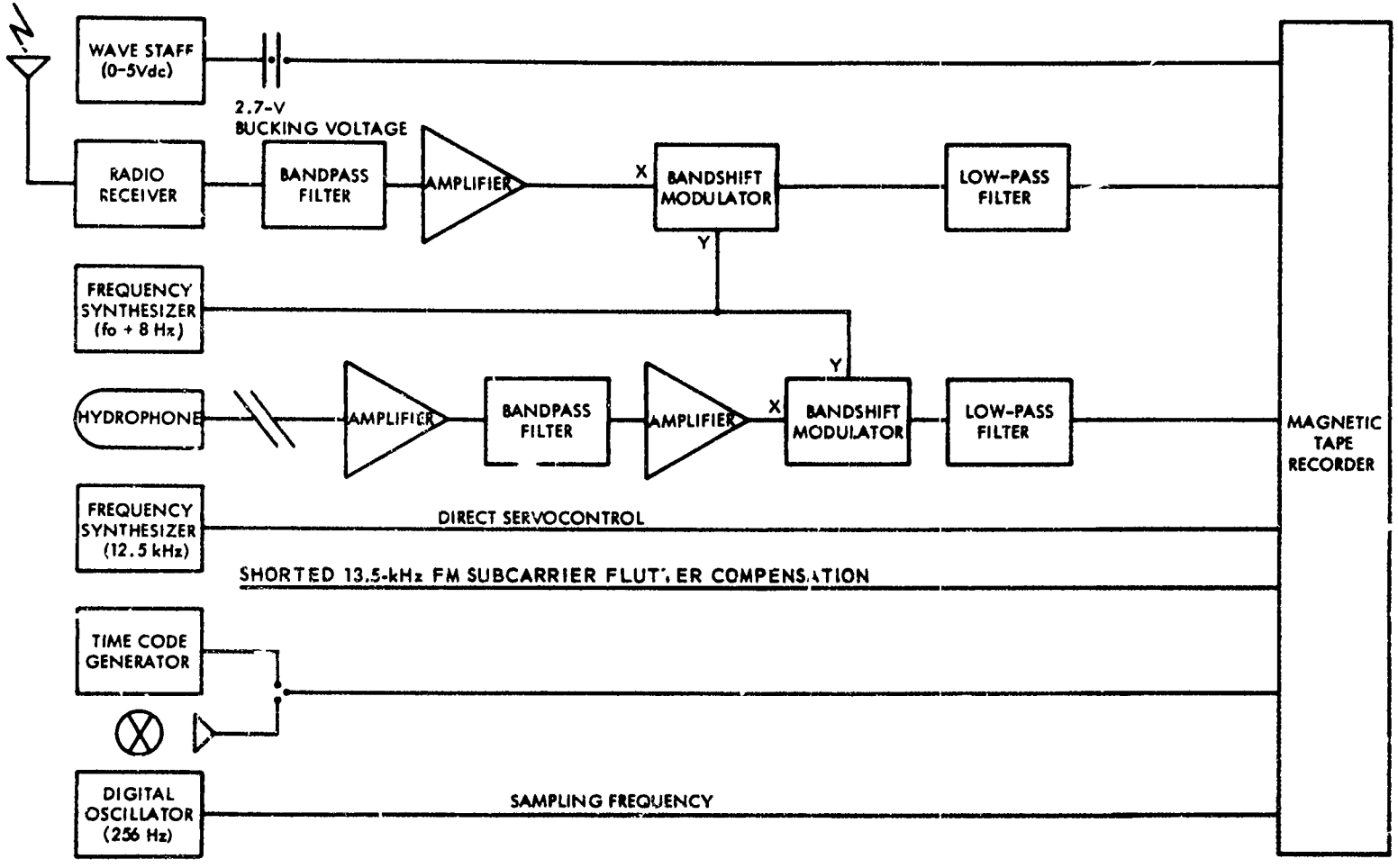

Figure C-5. Modified receiving and recording electronics aboard R/V UCONN (26 January - 30 January 1970)

Appendix D

DATA PROCESSING AND ANALYSIS

ANALOG PROCESSING AND ANALOG-TO-DIGITAL CONVERSION

Data taken in the field were FM recorded on analog magnetic tape, and Krohn-Hite low-pass and band-pass filters were used to suppress the high-frequency content out of the band of interest. On playback during analog-to-digital (A-D) conversion, additional low-pass filtering prevented future aliasing of the spectra. A Control Data Corporation (CDC) A-D converter digitized the wave-staff and the bandshifted acoustic data at a rate of 64 samples per second, whereas the ambient noise data and calibration signals were digitized at a rate of 8192 samples per second.

The control signals from the frequency synthesizers, the 256-Hz sampling frequency, and the FM subcarrier shorted input were recorded on magnetic tape; during playback, these signals were used to eliminate the effects of tape flutter from the recorded data (P. Stahl[71]). Digital data were recorded on digital computer tapes in CDC format for further computer processing.

METHODS OF ANALYSIS

In studies involving spectrum analysis of digital data, resolution and stability are primary considerations. Resolution determines the ability to observe fine detail in the spectrum, whereas stability is a measure of the variance of the smoothed spectral estimator. Resolution and stability determine the length of the

data record required to answer, with confidence, the questions being asked about the spectrum.

In general, it is always an advantage to obtain as long a data record as possible. However, the process being observed must be reasonably stationary over the length of time of the observations. For wind waves in Block Island Sound, this time is on the order of 20 min, which provides an upper bound on the length of data recorded for subsequent processing to determine spectral content.

In addition to considerations of resolution and stability, Bingham, Godfrey, and Tukey[58] and Welch[57] point out that, prior to spectrum analysis, the linear trend and dc component of the data should be removed. Spectral leakage must be minimized prior to squaring and adding the Fourier coefficients. An appropriate spectral window must be chosen for this purpose. Statistical stability in the estimates computed by means of the Fast Fourier Transform (FFT) can be obtained only by averaging several estimates of the spectrum. Welch[57] has developed a method of averaging that employs overlapped sections of data to achieve maximum variance reduction for a given resolution and record length.

These considerations have been utilized by Nuttall[72] to develop an optimum FFT spectral analysis procedure, which has been used to process the data presented in Chapter 4.

In order to obtain the data presented in Chapter 4, the following essential steps were followed:

1. Determine the resolution desired. This specifies the length of each piece of record to be used in computing the average spectrum.

2. Remove the dc component and the linear trend from each piece.

3. Window the data in the time domain. The window used on Runs I-VII is the cosine window, which reduces the maximum sidelobe level to -31.5 dB. The recommended overlap for the cosine window is 60%. However, computational convenience dictated an overlap of 50%. For the cosine window, the resolution B_{3dB} (-3 dB bandwidth) is[72]

$$B_{3dB} = 1.44/\text{segment length} \quad . \tag{D-1}$$

4. Compute the FFT on each piece. Square and add to determine the "power" and then form the average. The result is a stable estimate of the spectrum if a sufficient number of pieces have been employed in the average.

The equivalent degrees of freedom (EDF) is defined[60] as

$$EDF \cong \frac{E^2\left\{\hat{S}_p(f)\right\}}{Var\left\{\hat{S}_p(f)\right\}} \quad , \tag{D-2}$$

where

$E\left\{\hat{S}_p(f)\right\}$ = expected value of the estimate of the true spectrum $S(f)$ at frequency f, based on p pieces.

Var = variance.

For the cosine window for 50% overlap, Nuttall[72] has shown that

$$EDF = 2.76(B_{3dB}) \quad , \tag{D-3}$$

where T = total record length. The number of pieces into which the record must be sectioned to obtain this number of EDF is

$$EDF = 1.39\, B_{3dB}\, T - 1 \quad . \tag{D-4}$$

The data discussed in Chapter 4 were spectrally analyzed by means of NUSC Computer Program S1086/W (Arnold, Nuttall, Ferrie, and Carter[59]) in order to accomplish the above procedures. Several resolutions were used in the analysis, as suggested by Jenkins and Watts.[61] The resolutions were 0.0056 Hz, 0.0112 Hz, 0.0225 Hz, and 0.0450 Hz. These resolutions correspond to transform sizes of 8192, 4096, 2048, and 1024 data points, respectively. The 90% confidence intervals were computed by means of the approximating chi-square distribution, as given by Blackman.[73] The 90% confidence limits are approximately equal to

$$10 \left(\frac{1}{3\,EDF - 1} \pm \frac{1}{(EDF - 1)^{1/2}} \right) \text{dB for EDF} > 3 \quad . \tag{D-5}$$

AN EXAMPLE OF A SPECTRUM ANALYSIS

In the main text, the acoustic signal record for Run V, at Position C was nearly 20 min long. The sampling rate during A-D conversion was 64 Hz. Only every other data point was used in the spectrum analysis in order to permit finer resolution than would be possible if every data point were utilized. This results in a time increment between data samples of 0.03125 sec.

Since high resolution was desired, the maximum transform size permitted by the Cooley-Tukey algorithm[56] on the UNIVAC 1108 was tried first. Figure D-1 shows the result of the calculations. The -3 dB equivalent resolution bandwidth for this case is 0.0056 Hz. However, with only 10 degrees of freedom, the 90% confidence

intervals are very large and thus result in poor statistical stability. Clearly, this record has been over-resolved.

Consequently, the transform size was halved, and the spectrum analysis was repeated (Figure D-2). Almost twice as many pieces were averaged, and the number of degrees of freedom increased to 21. However, the bandwidth increased to 0.0112 Hz. The confidence interval was still too large, and it appears that this spectrum was also over-resolved.

Figure D-3 shows the results on the same record calculated for a transform size of 2048 data points, which permits twice as much averaging as in the previous case. The bandwidth is still satisfactory (0.0225 Hz), whereas the confidence interval is reasonably small. This estimate of the spectrum has 45 degrees of freedom.

The analysis was carried one step further, i.e., a transform size of 1024 points was used to generate an average spectrum with 91 degrees of freedom (Figure D-4). This estimate of the spectrum has excellent stability but does not reveal much detail. The bandwidth is 0.0450 Hz, which is too coarse since ocean swell peaks can occur at 0.08 Hz. From this and other examples, it is concluded that a resolution of 0.0225 Hz (a transform size of 2048 points) provides the optimum estimate of the spectrum for the purposes of this study.

Program S1086/T was written by J. F. Ferrie, of NUSC, to compute the acoustic and wave-height spectra by means of S1086/W and output the result on magnetic tape. These tapes were used as input to the theoretical Program S1731.

Since the wave staff is not precisely linear (Figure D-1), the spline interpolation routine of E. Mehr (New York University, Department of Meteorology and Oceanography) was used to convert from wave-staff voltage to wave height.

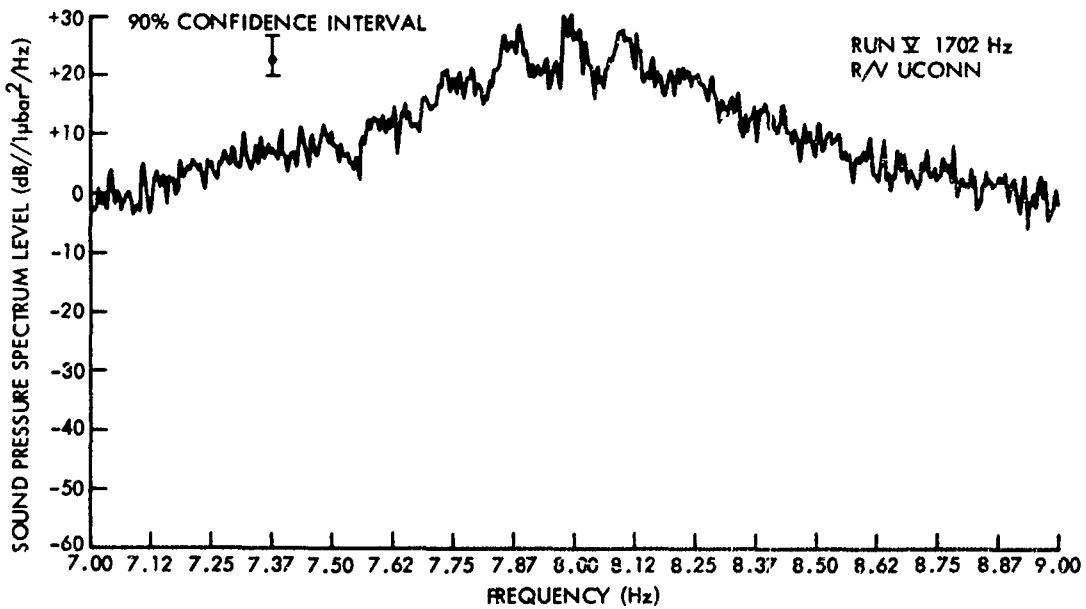

Figure D-1. Spectrum level of acoustic signal at Position C
(resolution = 0.0056 Hz, EDF = 10)

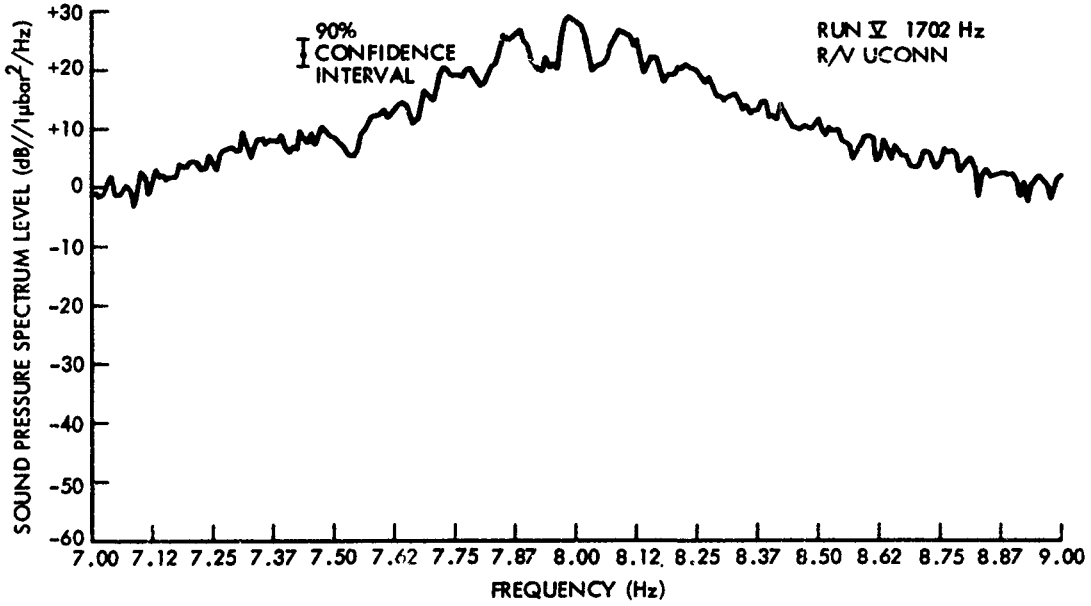

Figure D-2. Spectrum level of acoustic signal at Position C (resolution = 0.0112 Hz, EDF = 21)

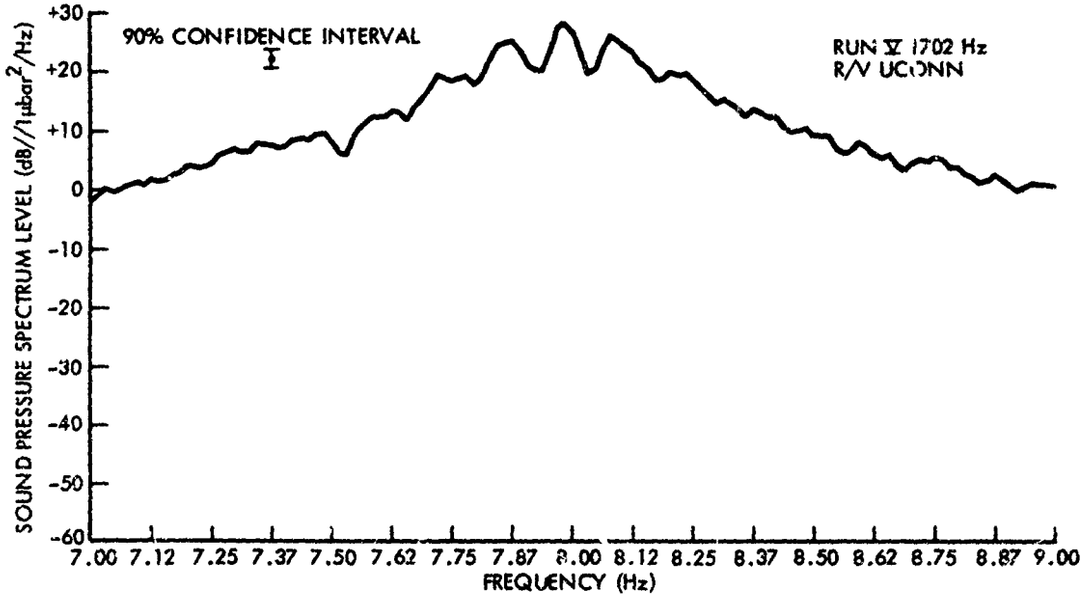

Figure D-3. Spectrum level of acoustic signal at Position C (resolution = 0.0225 Hz, EDF = 45)

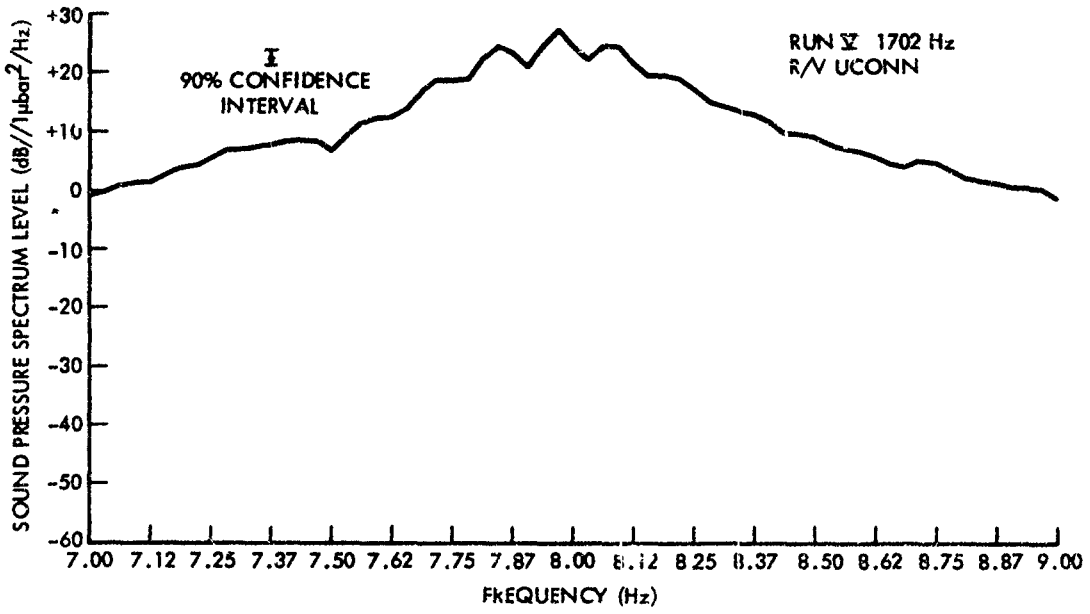

Figure D-4. Spectrum level of acoustic signal at Position C (resolution = 0.0550 Hz, EDF = 91)

Appendix E

COMPUTER PROGRAM FOR CALCULATING THE SPECTRA FROM THE PHYSICAL OPTICS MODEL

Computer Program S1731, which is included in the following pages, was written by R. C. Jennings, of NUSC, to calculate the acoustic and ocean wave-height spectra by means of Eqs. (67) and (69), respectively. The program is written in the FORTRAN V language for the UNIVAC 1108 Computer and the Stromberg-Carlson 406 Plotter. The input to this program is the tape output from the Spectral Analysis Program S1086/1 (Appendix D).

The output of Program S1731 includes the following computer-generated plots:

1. The computed weighting function B(f) versus f.
2. Measured B(f) versus f.
3. A_1 (f) measured and A_1(f) calculated versus f.
4. S(f) measured and S(f) calculated versus f.

Figures 33 through 43, in Chapter 5 of the main text, are outputs of this program.

```
000001       PARAMETER NPTS=33
000002       DIMENSION F(NPTS), B(NPTS), S(NPTS), AMEAS(NPTS), ASCAT(NPTS),
000003      1     ADB(NPTS), BMEAS(NPTS)
000004       DIMENSION SDB(NPTS), ADBDB(NPTS), AMESDB(NPTS), ASCTDB(NPTS)
000005       DIMENSION A(10000), GHAT(10000)
000006       DIMENSION AMODES(200), YLABEL(4), XPNT(4), YPNT(4)
000007       DOUBLE PRECISION XCAPDP, D1DP, D2DP, D1SQ, D2SQ, SQSQDP, PDP, LDP,
000008      1     KDP, X, RSSQ, RS, RASQ, RA, C, ARG, D1D2MX, ARG1, ARG2,
000009      2     XEXPDP, TERM, RARSSQ, PLSQD4, PL2SQ2, SUM, TERM2, PLSQ2G,
000010      3     DELF, PL22G2, ARG3
000011       DOUBLE PRECISION DENOM, TERM1, ACOH
000012       DOUBLE PRECISION PAMES1, PAMES2, PAMES3, PASCT1, PASCT2, PASCT3,
000013      1     TRPINT, SMPINT, NC5INT
000014       DOUBLE PRECISION PI /3.14159265358979324D0/, G /9.80665D0/
000015       REAL L, K
000016       EXTERNAL FONT2
000017       DATA YLABEL/'0.000.250.500.751.00'/
000018       DATA P/0.5/
```

```
000019          12 CONTINUE
000020             READ(1,100) (S(I),I=1,NPTS)
000021         100 FORMAT(8012)
000022             CALL NTRAN(1,8,1)
000023           9 READ(1,100) (AMEAS(I),I=1,NPTS)
000024             CALL NTRAN(1,10)
000025             SCALES = 0.0
000026             SMAX = -1.0E38
000027             SMIN = 1.0E38
000028             DELF = 0.01562500
000029             DO 10 I=1,NPTS
000030             F(I) = FLOAT(I-1) * DELF
000031             BMEAS(I) = AMEAS(I)/S(I)
000032             SDB(I) = 10.0 * ALOG10(S(I))
000033             AMESDB(I) = 10.0 * ALOG10(AMEAS(I))
000034             SCALES = AMAX1(SCALES,S(I))
000035             SMAX = AMAX1(SMAX,SDB(I))
000036             SMIN = AMIN1(SMIN,SDB(I))
```

```
C00037            10 CONTINUE
C00038               SMIN = SMIN - SMAX
000039               READ(3,105) NBEGIN, NB1, NSTOP, N
000040            105 FORMAT(4I5)
000041               READ(3,101) XCAP, D1, D2
000042            101 FORMAT(5E15.8)
000043               READ(3,101) L, K, SGMASQ, ESQ
C00044               NCOPY = N
000045               WRITE(4,103) (F(I),S(I),SDB(I),AMEAS(I),AMESDB(I),BMEAS(I),I=1,
000046              :     NPTS)
000047            103 FORMAT(//T11,'F',16X,'S',14X,'AMEAS',10X,'BMEAS=AMEAS/S'/(6E17.8))
C00048               WRITE(4,102) XCAP, D1, XCAP, D2, NCOPY, L, K, SGMASQ, P, NBEGIN,
000049              1     NB1, NSTOP, ESQ
C00050            102 FORMAT(//T11,'PT. S IS AT ( -',F9.3,',',F7.3,')'//T11,
000051              1     'PT. A IS AT (',F9.3,',',F7.3,')'//T11,'THERE ARE ',I5,
000052              2     ' PARTITIONS, EACH OF LENGTH',F10.5//T11,'ACOUSTIC WAVE ',
000053              3     'NUMBER  K = ',E15.8//T11,'SIGMA SQUARED = ',E15.8//T11,
000054              4     'P = ',E15.8//T11,'NBEGIN =',I4,5X,'NB1 =',I4,5X,'NSTOP =',
```

```
000055          5     I4//T11,'POWER FACTOR & SQUARED =',E13.6)
000056           D1DP = DBLE(D1)
000057           D1SQ = D1DP**2
000058           D2DP = DBLE(D2)
000059           D2SQ = D2DP**2
000060           XCAPDP = DBLE(XCAP)
000061           D1D2MX = D1DP*D2DP - XCAPDP**2
000062           SGSQDP = DBLE(SGMASQ)
000063           PDP = DBLE(P)
000064           LDP = DBLE(L)
000065           KDP = DBLE(K)
000066           PLSQD4= PDP * LDP**2 / 4.0D0
000067           WRITE(4,502)
000068         502 FORMAT(//T10,'I',9X,'X',16X,'RS',15X,'RA',17X,'A',16X,'C',12X,
000069            1     'RARSSQ'/T31,'ARG1',13X,'ARG2',12X,'XEXPDP',9X,'TERM',12X,
000070            2     'GMAT')
000071           INDEX1 = N/2 + 1
000072           ACOM = 0.0D0
000073           DO 1 I=1,N
```

```
C00074                X = DBLE(FLOAT(I-INDEX1)) * LDP
C00075                RSSQ = D1SQ + (XCAPDP+X)**2
C00076                RS = DSQRT(RSSQ)
C00077                RASQ = D2SQ + (XCAPDP-X)**2
C00078                RA = DSQRT(RASQ)
C00079                A(I) = KDP * ((XCAPDP+X)/RS - (XCAPDP-X)/RA)
C00080                C = -KDP * (D1DP/RS + D2DP/RA)
C00081                ARG1 = -SGSQDP * C**2
C00082                ARG2 = -PLSQD4 * A(I)**2
C00083                ARG = ARG1 + ARG2
C00084                XEXPDP = DEXP(ARG)
C00085                RARSSQ = RASQ*RSSQ
C00086                TERM = D1D2MX + RA*RS + X**2
C00087                DENOM = RS * RA * (D1DP*RA + D2DP*RS)
C00088                TERM1 = TERM * XEXPDP / DENOM
C00089                ACOM = ACOM + TERM1**2
C00090                GHAT(I) = TERM * XEXPDP  /  RARSSQ
C00091              1 CONTINUE
```

```
C00092            ACOH = 0.5D0 * PDP * (LDP*KDP)**2 * DBLE(ESQ) * ACOH
C00093            WRITE(4,106) ACOH
C00094        106 FORMAT(//T11,'COHERENT COMPONENT OF A',D14.8)
C00095            PL2SQG = 2.0D0 * PDP * (LDP * PI)**2  /  G
C00096            PL22G2 = -8.0D0 * PDP * LDP**2 * PI**4  /  G**2
C00097            SCALE = 0.0
C00098            SCALE1 = 0.0
C00099            ASCTMX = -1.0E38
C00100            ASCTMN = 1.0E38
C00101            CNSCAT = PDP * LDP**2 * KDP**4 * ESQ
C00102            WRITE(4,504) CNSCAT
C00103        504 FORMAT(//T11,'CNSCAT = ',E15.8)
C00104            DO 2 I=1,NPTS
C00105            PL2G02 = PL2SQG * F(I)**2
C00106            SUM = 0.0D0
C00107            DO 3 J=1,N
C00108            TERM2 = DEXP(PL2G02*A(J))
C00109            SUM = SUM + (GHAT(J)*TERM2)**2
```

```
000110          3 CONTINUE
C00111            ARG3 = PL2262 * F(I)**4
000112            IF (ARG3 .LT. -709.0D0)  GO TO 4
000113            B(I) = CNSCAT * DEXP(ARG3) * SUM
000114            ASCAT(I) = B(I) * S(I)
000115            ASCTDB(I) = 10.0 * ALOG10(ASCAT(I))
C00116            ADB(I) = AMEAS(I)/B(I)
000117            ADBDB(I) = 10.0 * ALOG10(ADB(I))
000118            SCALE = AMAX1(SCALE,B(I))
000119            SCALE1 = AMAX1(SCALE1,ASCAT(I))
C00120            ASCTMX = AMAX1(ASCTMX,ASCTDB(I))
C00121            ASCTMN = AMIN1(ASCTMN,ASCTDB(I))
000122          2 CONTINUE
C00123            ASCTMN = ASCTMN - ASCTMX
000124            NCPY = NPTS
000125            GO TO 5
000126          4 NCPY = 1
000127          5 CONTINUE
000128            SCALEB = 0.0
```

```
000129              DO 14 I=NB1,NPTS
000130              SCALEB = AMAX1(SCALEB,BMEAS(I))
000131           14 CONTINUE
000132              ADBMAX = -1.0E38
000133              ADBMIN = 1.0E38
000134              SCALE2 = 0.0
000135              DO 11 I=NBEGIN,NSTOP
000136              SCALE2 = AMAX1(SCALE2,ADB(I))
000137              ADBMAX = AMAX1(ADBMAX,ADBDB(I))
000138              ADBMIN = AMIN1(ADBMIN,ADBDB(I))
000139           11 CONTINUE
000140              ADBMIN = ADBMIN - ADBMAX
000141              SCALEA = 0.0
000142              AMAX = -1.0E38
000143              AMIN = 1.0E38
000144              DO 13 I=NBEGIN,NPTS
000145              SCALEA = AMAX1(AMEAS(I),SCALEA)
000146              AMAX = AMAX1(AMAX,AMESDB(I))
```

```
000147            AMIN = AMIN1(AMIN,AMESDB(I))
000148         13 CONTINUE
000149            AMIN = AMIN - AMAX
000150            DO 15 I=1,NPTS
000151            SDB(I) = SDB(I) - SMAX
000152            ADBDB(I) = ADBDB(I) - ADBMAX
000153            AMESDB(I) = AMESDB(I) - AMAX
000154            ASCTDB(I) = ASCTDB(I) - ASCTMX
000155         15 CONTINUE
000156            WRITE(4,503) (F(I),B(I),ASCAT(I),ASCTDB(I),ADB(I),ADBDB(I),S(I),
000157           1     I=1,NPTS)
000158        503 FORMAT(//T11,'F',16X,'B'15X,'B*S',14X,'A/B',15X,'S'/(7E17.8))
000159            PAMES1 = 2.0D0 * TRPINT(DELF,AMEAS(NBEGIN),NCPY-NBEGIN+1)
000160            PAMES2 = 2.0D0 * SMPINT(DELF,AMEAS(NBEGIN),NCPY-NBEGIN+1)
000161            PAMES3 = 2.0D0 * NCSINT(DELF,AMEAS(NBEGIN),NCPY-NBEGIN+1)
000162            PASCT1 = 2.0D0 * TRPINT(DELF,ASCAT(NBEGIN),NCPY-NBEGIN+1)
000163            PASCT2 = 2.0D0 * SMPINT(DELF,ASCAT(NBEGIN),NCPY-NBEGIN+1)
000164            PASCT3 = 2.0D0 * NCSINT(DELF,ASCAT(NBEGIN),NCPY-NBEGIN+1)
```

```
000165              WRITE(4,107) PAMES1, PAMES2, PAMES3
000166          107 FORMAT(//T11,'POWER IN SCATTERED COMPONENT OF MEASURED A',5X,
000167             1     3D20.8)
000168              WRITE(4,108) PASCT1, PASCT2, PASCT3
000169          108 FORMAT(//T11,'POWER IN SCATTERED COMPONENT OF COMPUTED A',5X,
000170             1     3D20.8)
000171              YMINA = AMIN1(AMIN,ASCTMN)
000172              YMINS = AMIN1(SMIN,ADBMIN)
000173              CALL MODESG(AMODES,0)
000174              XPNT(1)=2.9
000175              XPNT(2)=3.2
000176              YPNT(1)=1.9
000177              YPNT(2)=1.9
000178              YPNT(3)=1.7
000179              YPNT(4)=1.7
000180              CALL SETSMG(AMODES,90,2.0)
000181              CALL OBJCTG(AMODES,500.0,2100.0,1725.0,2850.0)
000182              CALL SUBJEG(AMODES,0.0,0.0,0.5,1.1*SCALE1)
000183              CALL GRIDG(AMODES,0.0,0.0,0.0,0)
```

```
000184                CALL SETSMG(AMODES,51,1,0)
000185                CALL VECIG(AMODES,FONT2,0)
000186                CALL SETSMG(AMODES,102,30,0)
000187                CALL SETSMG(AMODES,103,30,0)
000188                CALL LABELG(AMODES,0,0.1,0,3,1)
000189                CALL LABELG(AMODES,1,0.25*SCALE1,4,YLABEL)
000190                CALL TITLEG(AMODES,18,'FREQUENCY (H$LZ$U)',25,'RELATIVE SPECTRAL D
000191               1ENSITY',0,0)
000192                CALL SETSMG(AMODES,30,2,0)
000193                CALL LINESG(AMODES,NCPY,F,ASCAT)
000194                CALL SUBJEG(AMODES,0.0,0.0,0.5,1.1*SCALEA)
000195                CALL SETSMG(AMODES,31,1,0)
000196                CALL LINESG(AMODES,NPTS-NBEGIN+1,F(NBEGIN),AMEAS(NBEGIN))
000197                CALL SETSMG(AMODES,30,1,0)
000198                CALL SETSMG(AMODES,31,0,0)
000199                CALL SUBJEG(AMODES,0.0,0.0,3.9,2.4)
000200                CALL LEGNDG(AMODES,2.1,1.9,6,'MEASURED')
000201                CALL LEGNDG(AMODES,2.1,1.7,6,'COMPUTED')
```

```
000202                CALL SETSMG(AMODES,30,2.0)
000203                CALL SETSMG(AMODES,31,1.0)
000204                CALL LINESG(AMODES,2,XPNT,YPNT)
000205                CALL SETSMG(AMODES,31,0.0)
000206                CALL LINESG(AMODES,2,XPNT,YPNT(3))
000207                CALL SETSMG(AMODES,30,1.0)
000208                CALL OBJCTG(AMODES,500.0,850.0,1725.0,1600.0)
000209                CALL SUBJEG(AMODES,0.0,0.0,0.5,1.1*SCALE2)
000210                CALL GRIDG(AMODES,0.0,0.0,0,0)
000211                CALL LABELG(AMODES,1,0.25*SCALE2,4,YLABEL)
000212                CALL LABELG(AMODES,0,0.1,0,0.1)
000213                CALL TITLEG(AMODES,18,'FREQUENCY (HSLZSU)',25,'RELATIVE SPECTRAL D
000214               1ENSITY',0,0)
000215                CALL SETSMG(AMODES,30,2.0)
000216                CALL LINESG(AMODES,NSTOP-NBEGIN+1,F(NBEGIN),ADB(NBEGIN))
000217                CALL SUBJEG(AMODES,0.0,0.0,0.5,1.1*SCALES)
000218                CALL SETSMG(AMODES,31,1.0)
000219                CALL LINESG(AMODES,NPTS,F,S)
```

```
000220          CALL SETSMG(AMODES,31,0.0)
000221          CALL SETSMG(AMODES,30,1.0)
000222          CALL SUBJEG(AMODES,0.0,0.0,3.9,2.4)
000223          CALL LEGNDG(AMODES,2.1,1.9,8,'MEASURED')
000224          CALL LEGNDG(AMODES,2.1,1.7,8,'COMPUTED')
000225          CALL SETSMG(AMODES,30,2.0)
000226          CALL SETSMG(AMODES,31,1.0)
000227          CALL LINESG(AMODES,2,XPNT,YPNT)
000228          CALL SETSMG(AMODES,31,0.0)
000229          CALL LINESG(AMODES,2,XPNT,YPNT(3))
000230          CALL SETSMG(AMODES,30,1.0)
000231          CALL SETSMG(AMODES,93,0.0)
000232          CALL PAGEG(AMODES,0,1,1)
000233          CALL OBJCTG(AMODES,500.0,2100.0,1725.0,2850.0)
000234          CALL SUBJEG(AMODES,0.0,0.0,0.5,1.1*SCALE)
000235          CALL GRIDG(AMODES,0.0,0.0,0.0,0.0)
000236          CALL LABELG(AMODES,0,0.1,0,3.1)
000237          CALL LABELG(AMODES,1,0.25*SCALE,4,YLABEL)
000238          CALL TITLEG(AMODES,18,'FREQUENCY (HzLZ3U)',10,'COMPUTED B',0,0)
```

```
000239          CALL SETSMG(AMODES,30,2.0)
000240          CALL LINESG(AMODES,NCPY,F,B)
000241          CALL SETSMG(AMODES,30,1.0)
000242          CALL OBJCTG(AMODES,500.0,850.0,1725.0,1600.0)
000243          CALL SUBJEG(AMODES,0.0,0.0,0.5,1.1*SCALEB)
000244          CALL GRIDG(AMODES,0.0,0.0,0.0,0)
000245          CALL LABELG(AMODES,0,0.1,0,0.1)
000246          CALL LABELG(AMODES,1,0.25*SCALEB,4,YLABEL)
000247          CALL TITLEG(AMODES,18,'FREQUENCY (HzLZSU)',10,'MEASURED B',0,0)
000248          CALL SETSMG(AMODES,30,2.0)
000249          CALL LINESG(AMODES,NCPY-NB1+1,F(NB1),BMEAS(NB1))
000250          CALL SETSMG(AMODES,30,1.0)
000251          CALL PAGEG(AMODES,0.1,1)
000252          CALL OBJCTG(AMODES,500.0,2100.0,1725.0,2850.0)
000253          CALL SUBJEG(AMODES,0.0,YMINA,0.5,0.0)
000254          CALL GRIDG(AMODES,0.0,0.0,0.0,0)
000255          CALL LABELG(AMODES,0,0.1,0,0.1)
000256          CALL LABELG(AMODES,1,-YMINA/4.0,0,4.0)
```

```
000257                CALL TITLEG(AMODES,18,'FREQUENCY (HSLZSU)',25,'RELATIVE SPECTRAL D
000258               1ENSITY',0,0)
000259                CALL SETSMG(AMODES,30,2.0)
000260                CALL LINESG(AMODES,NCPY,F,ASCTDB)
000261                CALL SETSMG(AMODES,31,1.0)
000262                CALL LINESG(AMODES,NPTS-NBEGIN+1,F(NBEGIN),AMESDB(NBEGIN))
000263                CALL SETSMG(AMODES,30,1.0)
000264                CALL SETSMG(AMODES,31,0.0)
000265                CALL SUBJEG(AMODES,0.0,0.0,5.9,2.4)
000266                CALL LEGNDG(AMODES,2,1,1.9,8,'MEASURED')
000267                CALL LEGNDG(AMODES,2,1,1.7,8,'COMPUTED')
000268                CALL SETSMG(AMODES,30,2.0)
000269                CALL SETSMG(AMODES,31,1.0)
000270                CALL LINESG(AMODES,2,XPNT,YPNT)
000271                CALL SETSMG(AMODES,31,0.0)
000272                CALL LINESG(AMODES,2,XPNT,YPNT(3))
000273                CALL SETSMG(AMODES,30,1.0)
000274                CALL OBJCTG(AMODES,500.0,850.0,1725.0,1600.0)
```

```
000275                CALL SUBJEG(AMODES,0.0,YMINS,0.5,0.0)
000276                CALL GRIDG(AMODES,0.0,0.0,0.0,0.0,0)
000277                CALL LABELG(AMODES,0,0.1,0,3.1)
000278                CALL LABELG(AMODES,1,-YMINS/4.0,0.0,4.0)
000279                CALL TITLEG(AMODES,18,'FREQUENCY (HSLZSU)',25,'RELATIVE SPECTRAL D
000280               1ENSITY',0,0)
000281                CALL SETSMG(AMODES,30,2.0)
000282                CALL LINESG(AMODES,NSTOP-NBEGIN+1,F(NBEGIN),ADBDB(NBEGIN))
000283                CALL SETSMG(AMODES,31,1.0)
000284                CALL LINESG(AMODES,NPTS,F,SDB)
000285                CALL SETSMG(AMODES,31,0.0)
000286                CALL SETSMG(AMODES,30,1.0)
000287                CALL SUBJEG(AMODES,0.0,0.0,3.9,2.4)
000288                CALL LEGNDG(AMODES,2.1,1.9,8,'MEASURED')
000289                CALL LEGNDG(AMODES,2.1,1.7,8,'COMPUTED')
000290                CALL SETSMG(AMODES,30,2.0)
000291                CALL SETSMG(AMODES,31,1.0)
000292                CALL LINESG(AMODES,2,XPNT,YPNT)
000293                CALL SETSMG(AMODES,31,0.0)
```

```
000294                CALL LINESG(AMODES,2,XPNT,YPNT(3))
000295                CALL SETSMG(AMODES,30,1,0)
000296                CALL PAGEG(AMODES,0,1,1)
000297                CALL EXITG(AMODES)
000298                READ(3,100,END=9999) XINDC
000299                GO TO 12
000300           9999 CALL NTRAN(1,11)
000301                STOP
000302                END

      END COR
```

REFERENCES

1. R. C. Chia, "The Theory of Radar Backscatter From the Sea," Ph. D dissertation, University of Kansas.

2. W. J. Pierson and R. K. Moore, "Surface Weather and Wave Conditions," paper presented at THE OCEAN WORLD, A Joint Oceanographic Assembly of IAPSO, IABO, CMG, and SCOP, 1970.

3. P. Vigoureux and J. B. Hersey, The Sea, vol. 1, pt. I, M. N. Hill, Editor, Interscience Publishers, John Wiley and Sons, N. Y., 1962.

4. J. G. Clark and J. R. Yarnall, Long Range Ocean Acoustics and Synoptic Oceanography — Straits of Florida Results, Institute of Marine Science, University of Miami, Miami, Florida, May 1967, pp. 309-365.

5. C. Eckart, "The Scattering of Sound from the Sea Surface," Journal of the Acoustical Society of America, vol. 25, May 1953, pp. 556-570.

6. B. B. Baker and E. T. Copson, The Mathematical Theory of Huygens' Principle, first edition, The Clarendon Press, Oxford, 1939.

7. J. M. Proud, R. T. Beyer, and P. Tamarkin, "Reflection of Sound from Randomly Rough Surfaces," Journal of Applied Physics, vol. 31, March 1960, pp. 543-552.

8. C. S. Clay, "Fluctuations of Sound Reflected from the Sea Surface," Journal of the Acoustical Society of America, vol. 32, December 1960, pp. 1547-1551.

9. M. V. Brown and J. Ricard, "Fluctuations in Surface-Reflected Pulsed CW Arrivals," Journal of the Acoustical Society of America, vol. 32, December 1960, pp. 1551-1554.

10. H. Medwin, "Specular Scattering of Underwater Sound from a Wind-Driven Surface," Journal of the Acoustical Society of America, vol. 41, June 1967, pp. 1485-1495.

11. L. N. Liebermann, "Analysis of Rough Surfaces by Scattering," Journal of the Acoustical Society of America, vol. 35, June 1963, p. 932 (L).

12. H. W. Marsh, "Exact Solution of Wave Scattering by Irregular Surfaces," Journal of the Acoustical Society of America, vol. 33, March 1961, pp. 334-340.

13. N. Wiener, The Fourier Integral and Certain Applications, Dover Press, 1933.

14. Lord Rayleigh, Theory of Sound, vol. 2, third edition, Macmillian Company, London, 1896.

15. H. W. Marsh and R. H. Mellen, "Boundary Scattering Effects in Underwater Sound Propagation," Radio Science, vol. 1, March 1966, pp. 339-346.

16. B. E. Parkins, "Scattering from the Time-Varying Surface of the Ocean," Journal of the Acoustical Society of America, vol. 42, December 1967, pp. 1262-1267.

17. E. P. Gulin, "Amplitude and Phase Fluctuations of a Sound Wave Reflected from a Sinusoidal Surface," Soviet Physics — Acoustics, vol. 8, January-March 1963, pp. 223-227.

18. W. I. Roderick and B. F. Cron, "Frequency Spectra of Forward-Scattered Sound from the Ocean Surface," Journal of the Acoustical Society of America, vol. 48, October 1970, pp. 759-766.

19. A. H. Nuttall and B. F. Cron, Spectrum of a Signal Reflected from a Time-Varying Random Surface, Naval Underwater Systems Center, New London, Conn., Report No. NL-3013, 25 August 1970.

20. C. S. Clay and H. Medwin, "Dependence of Spatial and Temporal Correlation of Forward Scattered Underwater Sound on the Surface Statistics, I. Theory," Journal of the Acoustical Society of America, vol. 47, May 1970, pp. 1412-1418.

21. K. V. Mackenzie, "Long-Range Shallow-Water Signal-Level Fluctuations and Frequency Spreading," Journal of the Acoustical Society of America, vol. 34, January 1962, pp. 67-75.

22. J. A. Scrimger, "Signal Amplitude and Phase Fluctuations Induced by Surface Waves in Ducted Sound Propagation," Journal of the Acoustical Society of America, vol. 33, February 1961, pp. 239-247.

23. E. P. Gulin and K. I. Malyeshev, "Statistical Characteristics of Sound Signals Reflected from the Undating Sea Surface," Soviet Physics — Acoustics, vol. 10, April-June 1965, pp. 365-368.

24. A. Ellinthorpe, Naval Underwater Systems Center, New London, Conn., private communication.

25. W. D. Wilson, "Speed of Sound in Sea Water as a Function of Temperature, Pressure, and Salinity," Journal of the Acoustical Society of America, vol. 32, June 1960, pp. 641-644.

26. L. E. Kinsler and A. R. Frey, Fundamentals of Acoustics, John Wiley & Sons, Inc., New York, 1962.

27. M. Schulkin, The Propagation of Sound in Imperfect Ocean Surface Ducts, Navy Underwater Sound Laboratory, New London, Conn., Report No. 1013, 22 April 1969.

28. L. C. Huff, "Phase Characteristics of Continuous-Wave Transmission in Shallow Water," Journal of the Acoustical Society of America, vol. 44, August 1968, p. 650 (L).

29. P. Beckmann and A. Spizzichino, The Scattering of Electromagnetic Waves from Rough Surfaces, The Macmillan Co., New York, 1963.

30. H. Medwin and C. S. Clay, "Dependence of Spatial and Temporal Correlation of Forward-Scattered Underwater Sound on the Surface Statistics, II. Experiment," Journal of the Acoustical Society of America, vol. 47, May 1970, pp. 1419-1429.

31. H. W. Marsh and E. Kuo, Further Results on Sound Scattering by the Sea Surface, Avco report, October 1965.

32. J. W. Wright, "Backscattering from Capillary Waves With Application to Sea Clutter," IEEE Transactions on Antennas and Propagation, vol. P-14, November 1966, pp. 749-754.

33. F. J. Kingsbury, An Experimental Model Study of Underwater Acoustic Scattering From a Wind-Driven Surface, Naval Underwater Systems Center, New London, Conn., Report No. NL-3021, 13 August 1970.

34. L. Fortuin, "Survey of Literature on Reflection and Scattering of Sound Waves at the Sea Surface," Journal of the Acoustical Society of America, vol. 47, May 1970, pp. 1209-1228.

35. H. W. Marsh, M. Schulkin, and S. G. Kneale, "Scattering of Underwater Sound by the Sea Surface," Journal of the Acoustical Society of America, vol. 33, March 1961, pp. 334-340.

36. H. W. Marsh, "Non-Specular Scattering of Underwater Sound by the Sea Surface," Underwater Acoustics, V. M. Albers, Editor, Plenum Press, New York, 1962, Lecture 11, pp. 193-197.

37. H. W. Marsh, Sound Reflection and Scattering by the Ocean Boundaries, Avco report, December 1963.

38. I. Tolstoy and C. S. Clay, Ocean Acoustics:Theory and Experiment in Under-Water Sound, McGraw-Hill Book Company, Inc., New York, 1966.

39. W. J. Pierson, Jr., A Unified Mathematical Theory for the Analysis, Propagation and Refraction of Storm Generated Ocean Surface Waves, Parts I and II, New York University, College of Engineering, Research Division, 1952.

40. W. J. Pierson, Jr., "Wind-Generated Gravity Waves," Advances in Geophysics, vol. 2, Academic Press, Inc., New York, 1955, pp. 93-178.

41. G. Neumann and W. J. Pierson, Jr., Principles of Physical Oceanography, Prentice-Hall, Inc., Englewood Cliffs, New Jersey, 1966.

42. B. Kinsman, Wind Waves, Prentice-Hall, Inc. Englewood Cliffs, New Jersey, 1965.

43. H. Medwin, C. S. Clay, J. M. Berkson, and D. L. Jaggard, "Traveling Correlation Function of the Heights of Wind-Driven Water Waves," Journal of Geophysical Research, vol. 75, August 20 1970, pp. 4519-4524.

44. A. H. Nuttall, Naval Underwater Systems Center, New London, Conn., private communication.

45. W. J. Pierson, Jr., G. Neumann, and R. W. James, "Practical Methods for Observing and Forecasting Ocean Waves by Means of Wave Spectra and Statistics," U. S. Hydrographic Office, Pub. No. 603, 1955.

46. B. Gold and C. M. Rader, Digital Processing of Signals, McGraw-Hill Book Company, Inc., New York, 1969.

47. V. Oppenheim, Editor, Papers on Digital Signal Processing, M. I. T. Press, Cambridge, Mass., August 1969.

48. M. V. Brown, Reflections from the Ocean Surface and Bottom, Hudson Laboratories, Columbia University, Technical Report No. 162, October 1968.

49. D. E. Weston, A. A. Horrigan, S. J. L. Thomas, and J. Revie, "Studies of Sound Transmission Fluctuations in Shallow Coastal Waters," Philosophical Transactions of the Royal Society of London, vol. 265, 1969, pp. 567-608.

50. H. De Ferrari, "Measurement of Time-Varying Spectra of Surface Reverberation," paper presented at the 79th Meeting of the Acoustical Society of America, Atlantic City, 21-24 April, 1970.

51. R. G. Williams, Physical Oceanography of Block Island Sound, Navy Underwater Sound Laboratory, New London, Conn., Report No. 966, 9 July 1969.

52. R. G. Williams, T. Azarovitz, and J. J. Lamoureaux, Seasonal Variations of Temperature and Sound Velocity in Block Island Sound, Naval Underwater Systems Center, New London, Conn., report in preparation.

53. A. J. Nalwalk, C. Rathbun, H. G. Robinson, and L. A. Riley, Final Report of Oceanographic Measurements Along the Block Island-Fishers Island (BIFI)

Range in Block Island Sound from January 1969 through June 1970, University of Connecticut Marine Research Laboratory.

54. R. W. Hasse and W. R. Schumacher, "BIFI Shallow Water Program," Navy Underwater Sound Laboratory, New London, Conn., Technical Memorandum No. 2211-281-68, 4 December 1968.

55. R. G. Williams, "Results of Acoustic and Ocean Wave Tests in the BIFI Range in Block Island Sound — April-May 1968," Naval Underwater Systems Center, New London, Conn., ser. ltr. TA131-53, 20 April 1971.

56. J. W. Cooley, P. A. W. Lewis, and P. D. Welch, "Historical Notes on the Fast Fourier Transform," IEEE Transactions on Audio and Electroacoustics, vol. AU-15, June 1967, pp. 76-78.

57. P. D. Welch, "The Use of Fast Fourier Transform for the Estimation of Power Spectra: A Method Based on Time Averaging Over Short, Modified Periodograms," IEEE Transactions on Audio and Electroacoustics, vol. AU-15, June 1957, pp. 70-73.

58. C. Bingham, M. D. Godfrey, and J. W. Tukey, "Modern Techniques of Power Spectrum Estimation," IEEE Transactions on Audio and Electroacoustics, vol. AU-15, June 1967, pp. 56-66.

59. C. Arnold, A. H. Nuttall, J. F. Ferrie, and C. G. Carter, Naval Underwater Systems Center, New London, Conn., unpublished computer programs.

60. R. B. Blackman and J. W. Tukey, The Measurement of Power Spectra from the Point of View of Communications Engineering, Dover Publications, Inc., New York, 1958.

61. F. M. Jenkins and D. G. Watts, Spectral Analysis and its Applications, Holden-Day, San Francisco, Calif., 1969.

62. Daily Weather Maps, January 5-11 1970, U. S. Department of Commerce, Environmental Science Services Administration, Environmental Data Service.

63. Daily Weather Maps, January 19-25 1970, U. S. Department of Commerce, Environmental Science Services Administration, Environmental Data Service.

64. Daily Weather Maps, January 26-February 1 1970, U. S. Department of Commerce, Environmental Science Services Administration, Environmental Data Service.

65. B. Sussman and W. Kanabis, "Propagation of 127, 400 and 1700 Hz Acoustic Energy in the BIFI Range," paper presented at the 80th Meeting of the Acoustical Society of America, Houston, Texas, 3-6 November 1970.

66. W. J. Pierson, Jr. and L. Moskowitz, "A Proposed Spectral Form for Fully Developed Wind Seas, Based on the Similarity Theory of S. A. Kitaigorodskii," Journal of Geophysical Research, vol. 69, December 1964, pp. 5181-5190.

67. H. W. Marsh, Naval Underwater Systems Center, New London, Conn., private communication.

68. D. Stillwell, "Directional Energy Spectra of the Sea from Photographs," Journal of Geophysical Research, vol. 74, April 1969, pp. 1974-1986.

69. L. J. Cote, J. O. Davis, W. Marks, R. J. McGough, E. Mehr, W. J. Pierson, Jr., J. F. Ropek, G. Stephenson, and R. C. Vetter, "The Directional Spectrum of a Wind Generated Sea as Determined from Data Obtained by the Stereo Wave Observation Project," Meteorological Papers, New York University, College of Engineering, vol. 2, 1960.

70. B. Kinsman, Op. cit., p. 194.

71. P. Stahl, "Recording of Analog Data for Most Exact Reproduction," Naval Underwater Systems Center, New London, Conn., Technical Memorandum PL 18371, in preparation.

72. A. H. Nuttall, Spectral Estimation by Means of Overlapped FFT Processing of Windowed Data, Naval Underwater Systems Center, New London, Conn., report in preparation.

73. R. B. Blackman, Linear Data-Smoothing and Prediction in Theory and Practice, Addison — Wesley, Reading, Mass., 1965.